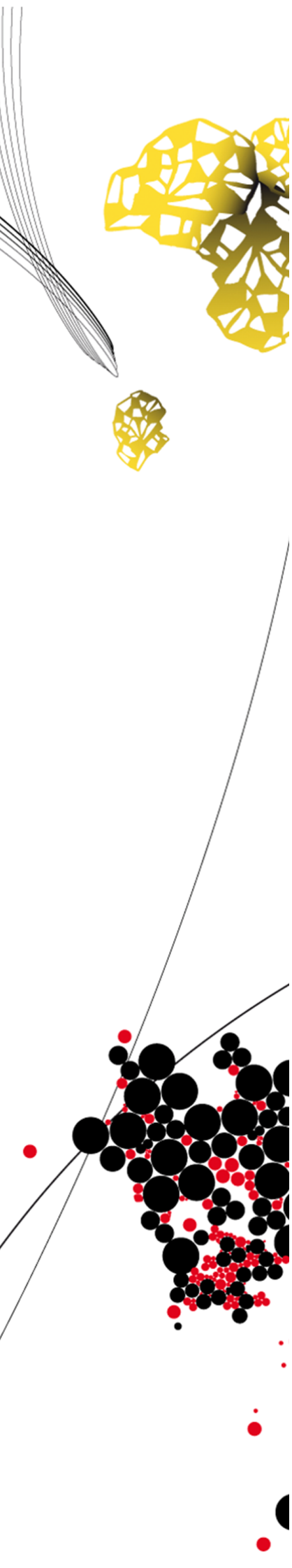

UNIVERSITY OF TWENTE.

Faculty of Engineering Technology

Generalised Fuzzy Logic Control Strategy for Ankle Exoskeleton for Hopping and Walking

Thejas Shankar Srinivas

M.Sc. Thesis

July 2024

Supervisors:
prof. dr. Massimo Sartori
dr. Mahdi Nabipour
Graduation committee:
dr. ir. Arvid Q. L. Keemink

Biomechanical Engineering Group
Faculty of Electrical Technology
University of Twente
P.O. Box 217
7500 AE Enschede
The Netherlands

Summary

This research aims to design and enhance a Fuzzy Logic Controller (FLC) for an ankle exoskeleton, enabling it to automatically adapt to multiple hopping frequencies. The current controller is restricted to a single frequency and requires manual adjustments to operate across various frequencies. The objective is to develop an automated system that allows the exoskeleton to function seamlessly at different frequencies in a hopping scenario. Additionally, the research seeks to extend the controller's capabilities to walking scenarios with varying speeds. This will be achieved by incorporating different excitations tailored to each speed derived from muscle synergy patterns observed during the walking gait.

Contents

Chapter 1

Introduction

Designing closed-loop controllers with musculotendon load for wearable exoskeletons is an evolving study area. The primary challenge is designing controllers that can assist with dynamic activities such as hopping and walking. Exploration of this field can potentially assist individual biological tissues with high precision, such as tendons. Such exoskeleton devices can assist individual muscles and tendons in a closed-loop framework, which considers the mechanical strains and loads, eventually reducing the strain on the muscles and tendons. These controllers could avoid potential injuries related to repetitive and high-impact tasks and assist in rehabilitating tissues specific to the motor tasks. This field of controlling musculotendon loads in a closed-loop with exoskeletons for various locomotion tasks is a relatively recent endeavour. A robot that can limit tendon loads to a predefined value regardless of continuously varying mechanical demands of motor tasks does not exist. The motor tasks include gait speed, frequency, and loads. Additionally, the robot must aid multiple people using a 'one size fits all' strategy.

Researchers have employed various control techniques in robotic exoskeletons to assist with motor tasks related to the human ankle. Some of the basis for these control techniques are heuristics [1], optimisation of energy expenditure with a human in the loop (HIL) [2], muscle's chemical energy expenditure [3] , walking speed [4] and user preference [5]. Some controllers were also designed to generate support profiles proportional to the musculoskeletal mechanics of the subject using a proportional myoelectric controller [6], joint power control [7], and real-time EMG-based joint torque control [8]. Few recent studies have discussed proportional assistance based on force profiles of the Achilles tendon. A recent study discusses Achilles tendon force control using nine predefined plantar flexion assistance profiles [9]. Another study focused on the development of an ankle torque profile for the subject with the help of ultrasound measurements of soleus velocity during walking to reduce metabolic costs [9]. The measurements were analysed offline to process the ultrasound images and generate torque profiles. The processing took approxi-

mately 5 seconds, significantly lower than the fastest HIL system studied by Slade et al. [10]. However, these studies do not explore closed-loop control of Achilles tendon force.

A recent study that addresses this employed the closed-form modelling of the Soleus Musculotendon Unit [11]. A nonlinear model predictive control (NMPC) framework was implemented to integrate this closed-form model with the equations of motion of a human leg [12]. This model maintained the peak tendon force within a target threshold. This ability to maintain tendon force under the target threshold was extended to varying hopping intensities [13]. Further, this has been improved to provide varying levels of assistance suitable to the user and also demonstrate its effectiveness in controlling tendon force of various muscle fiber phenotypes [14].

This project discusses the design of closed-loop tendon force control of the Achilles tendon using a Generalised Fuzzy Logic Control (GFLC) approach. The controller has been designed for two tasks, hopping and walking. The aim of the controller is to offer assistance only when necessary. Essentially, it needs to control the peak Achilles tendon force during the cyclic tasks of hopping and walking.

A Fuzzy Logic Controller (FLC) has been proposed to explore the expert knowledge-based controller design technique for the control of Achilles tendon. This controller is not a model-based approach; thus, a perfectly replicated model is not required to design an FLC. FLC techniques have been used in various robotic prostheses and exoskeletons. A Fuzzy Logic Controller was designed and successfully implemented in a lower extremity exoskeleton for its smooth and fast response [15]. An adaptive Fuzzy PID to control a tendon-driven finger based on position and tendon tension was designed [16]. A Fuzzy Logic Control has been designed to perform gain scheduling for a PID controller with the help of a Fuzzy Logic System (FLS). Another research discussed a similar controller for a lower-extremity exoskeleton for elderly mobility [17]. Unlike these controllers, this project discusses the design of an FLC that interacts with the model directly without a PID control.

This project explores the feasibility of GFLC by simulation. Although FLC is not a model-based controller, a model is still necessary to acquire expert knowledge in this scenario and observe the controller's performance. Thus, an ankle model was inspired by Robertson et al. [18] with added damping modification to the muscle portion of the Musculotendon Unit (MTU) . A Hill-type MTU has been used in this ankle model. The ankle model is discussed in Chapter 4, and the Hill-type muscle model is discussed in detail in Chapter 2.

Further in this thesis, the Muscle Model is discussed in Chapter 2 followed by an introduction to Fuzzy Logic Systems in Chapter 3. In Chapter 4 the methodology is discussed, and the results are discussed in Chapter 5. Chapter 6 has discussions and Chapter 7 has conclusions.

Chapter 2

Muscle Model

In this chapter we discuss how the Hill-type muscle Model can be used to model muscle and tendon. All equations have been referred to from Clay Anderson's manuscript on "Equations for Modelling the Forces Generated by Muscles and Tendons" [19].

In the realm of musculoskeletal modelling for robotics, the most widely adopted modelling strategy for muscle-tendon units is the Hill-type muscle model. Thus, for this project a Pennated Compliant Tendon Model with parallel (to Contractile Element (CE)) Passive Elastic Element (PE) and a parallel Damping Element (D) is chosen. This model is shown in Figure 2.1 This muscle model closely represents

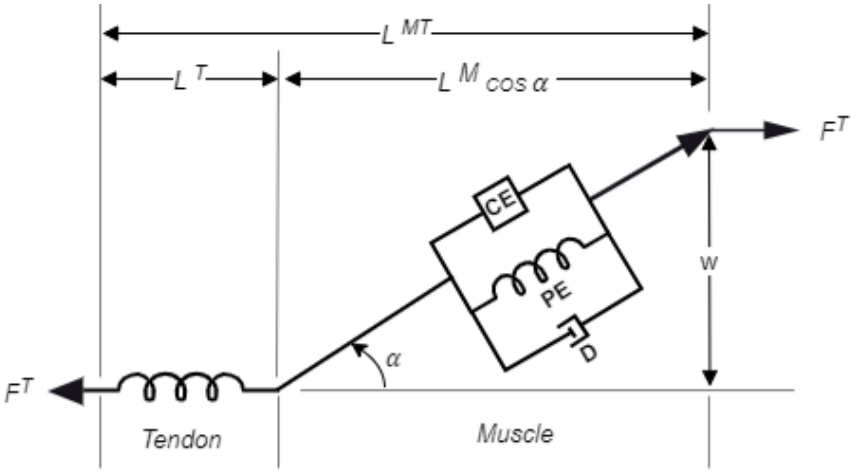

Figure 2.1: Pennated Compliant Tendon model with damping in parallel with PE and CE

a real model. The tendon force (F^T) generated depends non-linearly on the length and velocity of the muscle. Tendon is designed to be elastic with a linear stress-strain relationship. The pennation allows the force to act at an angle to the muscle instead of parallel to the muscle. The damping was introduced to mimic the high

water content in the muscle [20]. The damping coefficient was set to a value of 0.1, which does not introduce large damping forces but enables the model to attain equilibrium over time. When this muscle model is implemented in the hopping model in a later chapter, it will also assist in the model settling to steady-state.

Chapter 3

Fuzzy Logic Systems

Fuzzy Logic Systems allow the design of controllers by incorporating expert intuition. They utilize vague, imprecise inputs, making them suitable for defining complex real-world problems. Humans can impart nuance to the controller's decision-making process to make it work with systems where traditional methods might struggle.

3.1 How FLS Works?

When describing the quality of something in real life, we often use quantitatively vague terms. For example, when asked to describe temperature at any moment, people use adjectives such as hot, warm, cool, and cold and often add an adverb of degree to it, like very, extremely, mildly, etc. When people are asked to give a range of values for each category, the boundaries set by each individual are not the same across the population. Often the quantitative boundaries set by people for the qualitative values are different. Thus, we can pool in data regarding what people think the boundaries should be and then create a function. This function can determine what percent of the population agrees on categorizing a particular temperature as hot, warm, cool or cold. Such a function is called a membership function.

Membership functions are the building blocks of any Fuzzy Logic System (FLS). An FLS consists of a fuzzifier, an inference system based on IF-THEN rules and a defuzzifier, to get a quantified output. The fuzzifier converts the inputs based on their respective membership functions into fuzzy values. These values are essentially an array with the membership values in every fuzzy set of the membership function for a given input. These fuzzy values are then processed in an inference system with fuzzy rules. These can be designed linguistically in the format "If <antecedants> Then <consequents> ", where antecedents form the conditions and consequents form the result of the statement. In systems with multiple inputs, consequents can

consist of multiple inputs connected using AND or OR. AND considers the minimum of the fuzzified inputs, whereas OR considers the maximum of the fuzzified inputs.

Once the inference is finished, we receive the fuzzy output values. Defuzzification methods are implemented to get meaningful output. These methods could be either a crisp function or another membership function. A flow chart showing the various steps involved in a Fuzzy Logic System is shown in Figure 3.1.

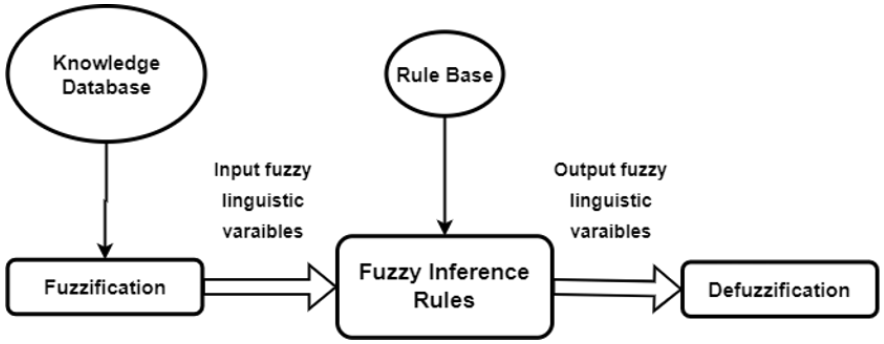

Figure 3.1: Processes involved in a Fuzzy Logic System

Let us have a closer look into Fuzzy Logic Systems with an example of a coffee coaster that has to maintain the coffee's temperature at a specific temperature. To do so, we take the necessary input, the coffee temperature (CoffeeTemp) and the output, the coaster temperature (CoastTemp). The membership functions for the same are shown in Figure 3.2 and 3.3, respectively.

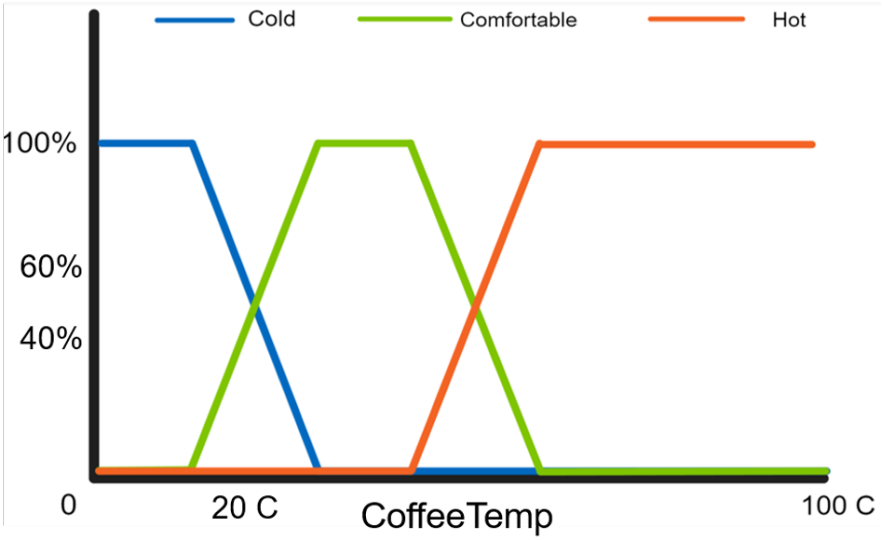

Figure 3.2: Input membership function for Coffee Temperature.

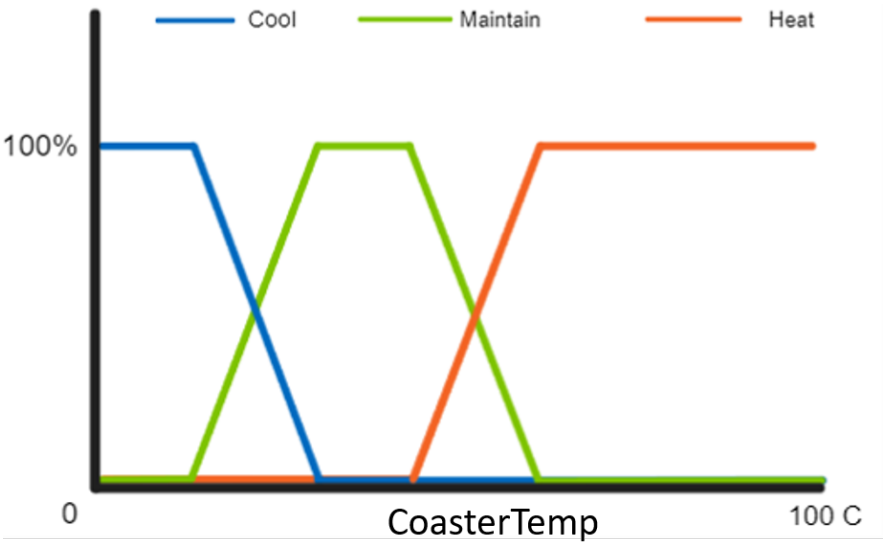

Figure 3.3: Output membership function for Coaster Temperature.

We can fuzzify the input with the help of a membership function, as shown in Figure 3.4. Let us say our coffee is at $20C$. The fuzzified inputs will be [0.6 0.4 0] corresponding to [Cold Comfortable Hot]. This fuzzified input is provided to a rule base consisting of rules:

- If CoffeeTemp is Cold then CoasterTemp is Heat
- If CoffeeTemp is Comfortable then CoasterTemp is Maintain
- If CoffeeTemp is Hot then CoasterTemp is Cool

For the sake of simplicity, we assume that the rules create a fuzzified output on a 1:1 basis. This gives us the fuzzified output as [0 0.4 0.6] for the CoasterTemp [Cold Maintain Heat]. This output then needs to be defuzzified to obtain meaningful output pertaining to our system. To do this, we take the fuzzy output values and use these values as the cut-off height for the area under the fuzzy sets, as shown in Figure 3.5. These areas are merged, and the centroid of this area is determined. The x-coordinate of this centroid is the output of the FLS.

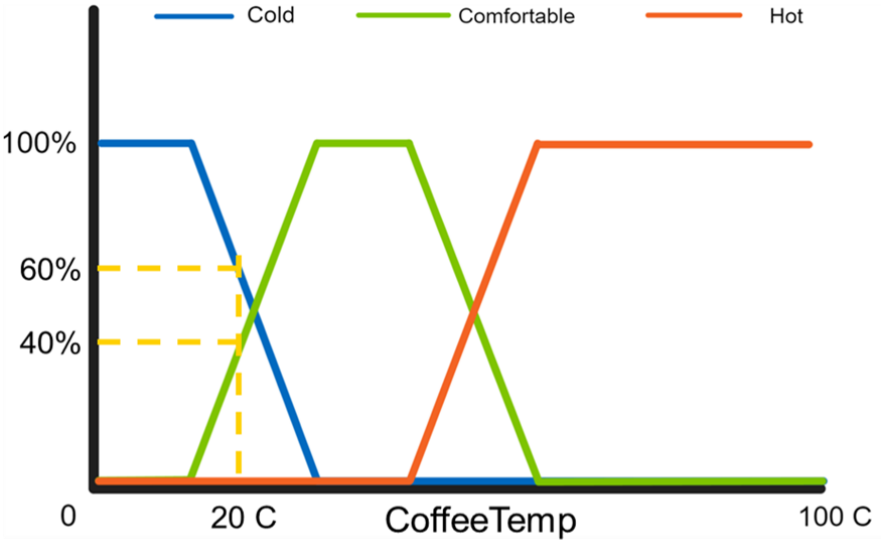

Figure 3.4: Fuzzification of crisp input. Here, 20 C is fuzzified as [0.6 0.4 0].

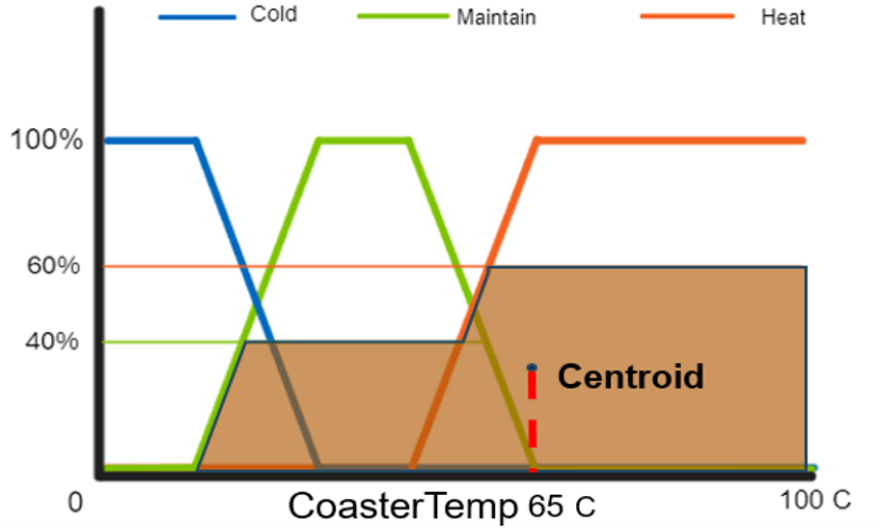

Figure 3.5: Defuzzification of fuzzy output. Here, [0 0.4 0.6] is defuzzified as 65 C.

3.2 Types of Defuzzification technique

Fuzzy Logic Systems can be classified into two major categories depending on their defuzzication method. The first method is the Mamdani method. This method is the same as the one discussed in the example in the previous section. In this method, the fuzzy output values obtained from the inference are used to determine the ceiling on their respective fuzzy sets in the output membership function. The shape enclosed within the membership function under the output ceiling is considered for

calculating the output. Five parameters can be considered as output based on the application. The centroid method is the most common parameter used to defuzzify Fuzzy Logic Controllers (FLC). This method determines the shape's centroid, and its x-coordinate is taken as output. The second method is the bisector method, in which a vertical bisector line is considered, which divides the shape into parts of equal area. The x-intercept of this bisector is considered the output in this scenario. The next three methods are called the Smallest of Maximum (SOM), Middle of Maximum (MOM) and Largest of Maximum (LOM). This technique considers the values with the maximum membership within the shape. Among these values, the one with the smallest x-axis value is considered SOM output, the largest x-axis value is considered LOM output, and the middle x-axis value is MOM output.

The second method is the Takagi-Sugeno-Kang method, commonly known as the Sugeno method. The Sugeno method uses a weighted average method or weighted sum of few data points to defuzzify. This is computationally more efficient compared to the Mamdani method.

Chapter 4

Methodology

This chapter discusses the steps taken in modelling plants and designing controllers related to this thesis topic. It explains why certain decisions were made and what the precursor designs were to the final design presented in this work.

The following sections will take you through the modelling and designing processes for the hopping model first and later for walking model.

4.1 Hopping Model

A modified hill-type muscle model was used in parallel with the actuator for the hopping model. This combination was then connected to a rigid support on one end and a pulley on the other. This pulley is compounded with another pulley at a ratio of 3:1. Finally, a mass analogous to body weight is attached to the secondary pulley [18]. The model discussed in Robertson et al. (Figure 4.1) has been modified for the hopping model in this project. The original model in the literature consists of a contractile element (CE) and a parallel elastic element (PE). The CE is subjected to a non-linear force-length and force-velocity relationship, and first-order activation dynamics has been employed. The PE produces forces at lengths greater than the optimal muscle fibre length (L_o^M). The Tendon dynamics (or the series elastic element, SEE for short) have been modelled linearly except for a non-linear ”toe” region at the beginning.

A slightly more accurate model was created by adding a pennation angle to the MTU in this model. Additionally, a damper was added to the muscle portion of the existing Hill-type MTU model, as shown in Figure 4.2. A low damping allows for faster simulation without excessive damping of the hopping model. Thus, a damping coefficient 0.1 was considered since water constitutes 82.3%

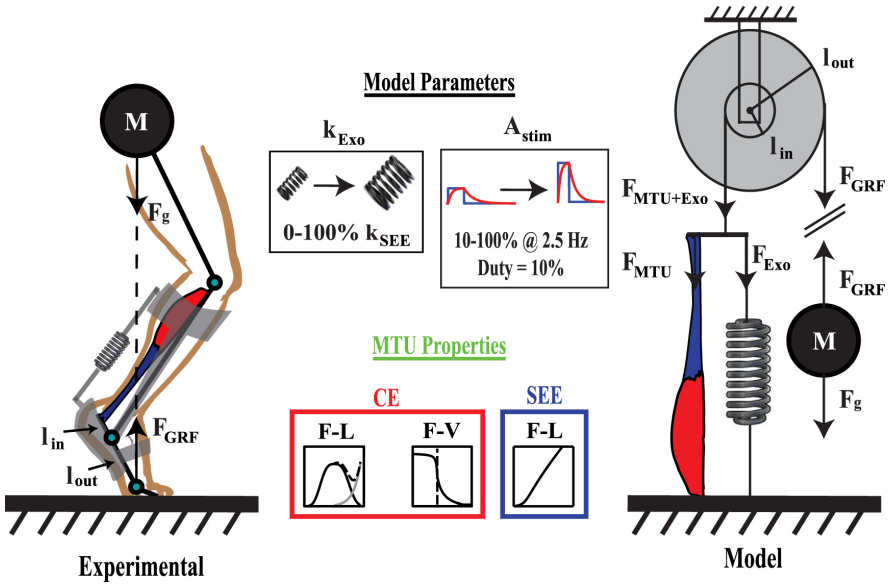

Figure 4.1: Experimental (left) and modelled (right) exoskeleton assisted human hopping [18]. (The model parameters shown do not exactly represent the scenario in this project)

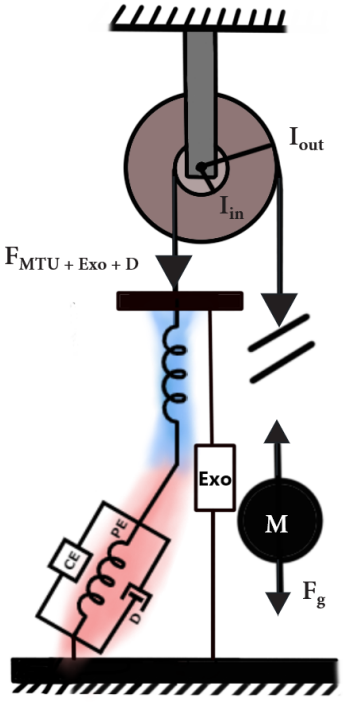

Figure 4.2: The modified damping model has been designed with a similar Hill-type model with pennation angle taken into account. A damper has also been added in parallel to the CE and PE

4.2 Controller Objectives

Any controller design involves validating the controller for a specific task. The controller developed in this project operates in a non-linear time-domain scenario. To evaluate its performance, we set specific objectives. The main objective is to control and maintain the tendon force below a set limit using an assist-as-needed strategy. The exoskeleton can provide a maximum assistive force of 1000 N. Metrics such as the percentage reduction in peak force and the duration of tendon force violations were considered. Ideally, the peak tendon force should be reduced below the set upper limit without exceeding it. The upper limits for hopping ranged from 1200 N to 1900 N in 100 N increments, while for walking, they ranged from 1200 N to 1500 N in 100 N increments.

4.3 Steps in Designing FLC for Hopping

The Fuzzy Logic Controller (FLC) was designed using two inputs from the ankle hopping model: the tendon force and its derivative. These inputs are fuzzified and processed according to predefined rules, resulting in the output of an assistive force. A Mamdani-type Fuzzy Inference System (FIS) was employed for this purpose.

Multiple iterations of the controller were developed:

1. **First Iteration**: The primary goal was to design an FLC that effectively reduces the tendon force in the ankle by providing necessary assistance while hopping.
2. **Second Iteration**: This iteration aimed to control the tendon force across varying frequencies of hopping, enhancing the controller's adaptability.
3. **Third Iteration**:
    a. The focus was on implementing an FLC with normalized inputs tailored for hopping scenarios, ensuring robust performance across different hopping frequencies.
    b. Building upon the FLC for hopping, this version applied the normalized input FLC to walking scenarios, optimizing the controller's functionality for varied walking speeds.

4.3.1 Iteration 1: Baseline Fuzzy Logic Controller (BFLC)

In the first iteration of the Fuzzy Logic Controller (FLC), the primary objective was to assist the ankle in hopping and reduce the tendon force as needed. The block diagram for this iteration is shown in Figure 4.3.

A condition block was implemented to ensure that the controller intervenes only when necessary. This block activates assistance when the tendon force exceeds a predetermined threshold of 900 N. This threshold was chosen arbitrarily within the range of tendon forces observed without assistance, leaning towards the lower end to allow early intervention while still maintaining assistance-as-needed.

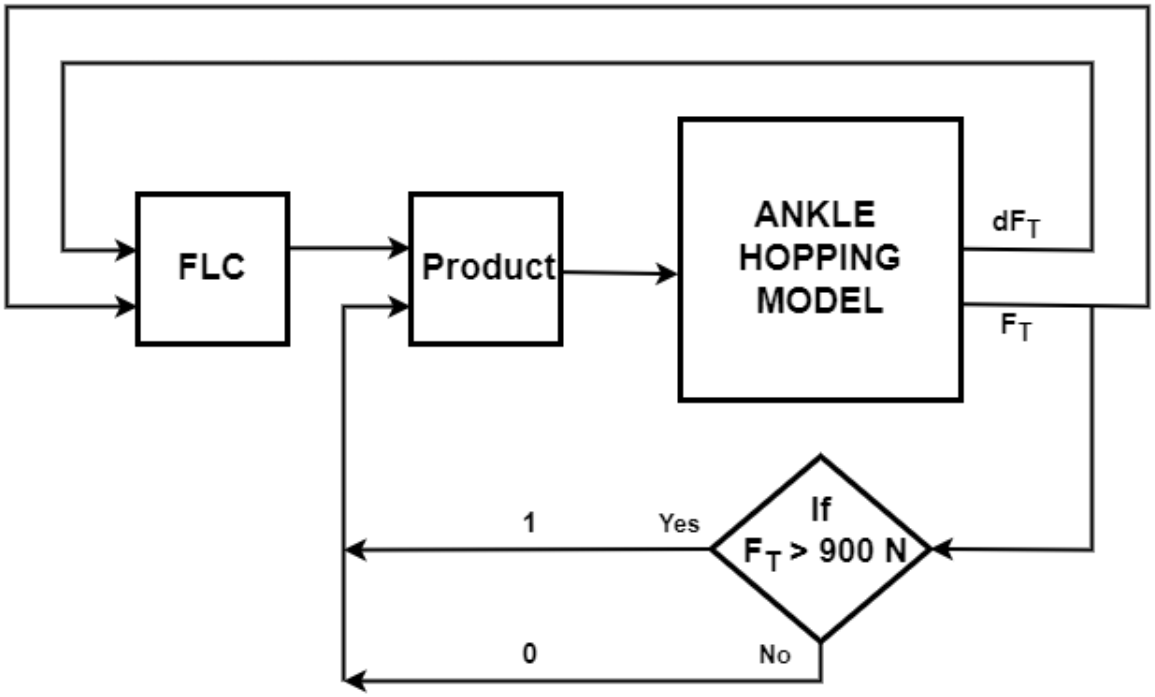

Figure 4.3: The control loop is shown here with the FLC and Ankle Hopping Model

The condition block outputs a multiplier: 1 when the tendon force is above 900 N and 0 when it is under 900 N. This multiplier modulates the FLC's output in the Product block, and the result is fed as input to the Ankle Hopping Model.

Gaussian fuzzy sets were employed for the FLC design for the membership functions. This choice was made to ensure a smooth transition of control output. Figure 4.4 illustrates an example of the membership functions with Gaussian fuzzy sets. The resulting control surface, generated by the fuzzy rules, is depicted in Figure 4.5. The comprehensive design of the FLC for this iteration is detailed in Appendix A.

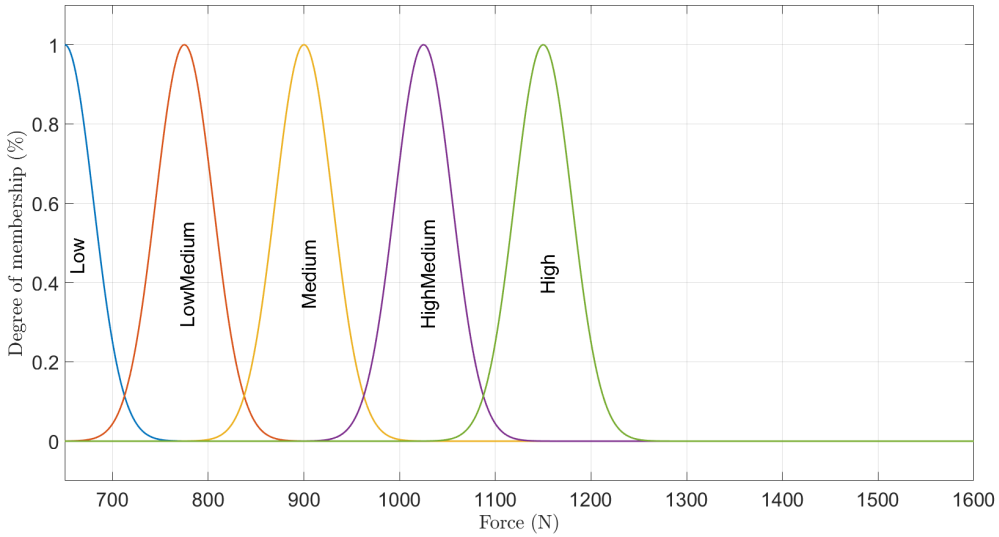

Figure 4.4: The input membership function for the Tendon Force (N) with a Threshold introduced

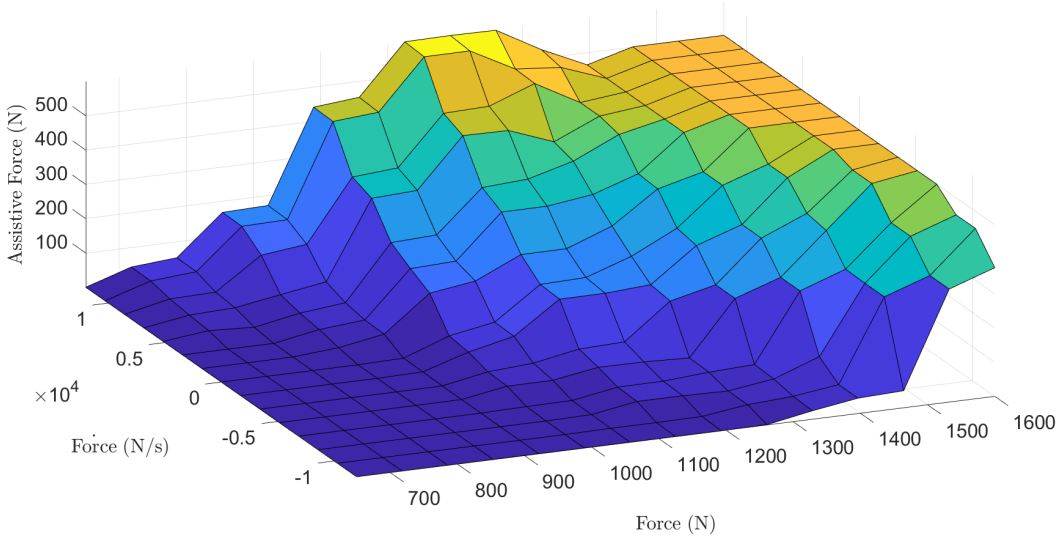

Figure 4.5: The output control surface generated by the rules (Forces in N and Force_dot in N/s)

With this controller the intermittent control concept of assist-as-needed is achieved. However, this is only one objective. Other objectives of controlling the tendon force below a set upper limit are not possible with BFLC, and it cannot limit the tendon force for varying frequencies. This controller was thus designed as a stepping stone

for future controller iterations.

The membership functions and the rules regarding the controller design are shown in Appendix A.

4.3.2 Iteration 2: Frequency-Adaptive Fuzzy logic Controller (FAFLC)

This iteration addressed the challenge of varying frequencies of hopping by introducing a look-up table. This table selects one of three controllers, each tailored for a specific frequency range of hopping. The ranges of the frequencies used in this version of controller were: 1-3 Hz for low frequencies, 1.3-1.8 Hz for medium frequencies and higher than 1.8 Hz for high frequencies. These frequencies were chosen after observing the behaviour of tendon force for excitations at frequencies between 1-4 Hz. All three controllers utilize the same input and output membership functions, differing only in their rule bases. Figure 4.6 shows the block diagram for this iteration. The condition block was eliminated from the control loop and was instead replaced by a fuzzy set 'Thresh' in the input membership function for 'Force' as shown in Figure 4.7. A rule was added to essentially define 0 Assistance force as output for the entirety of this Fuzzy set ('Thresh') as shown in Table A.3. A delay was introduced to mimic the processing delay in the system, which provides time for the controller and plant to process the data. The full controller design is shown in Appendix A.3.

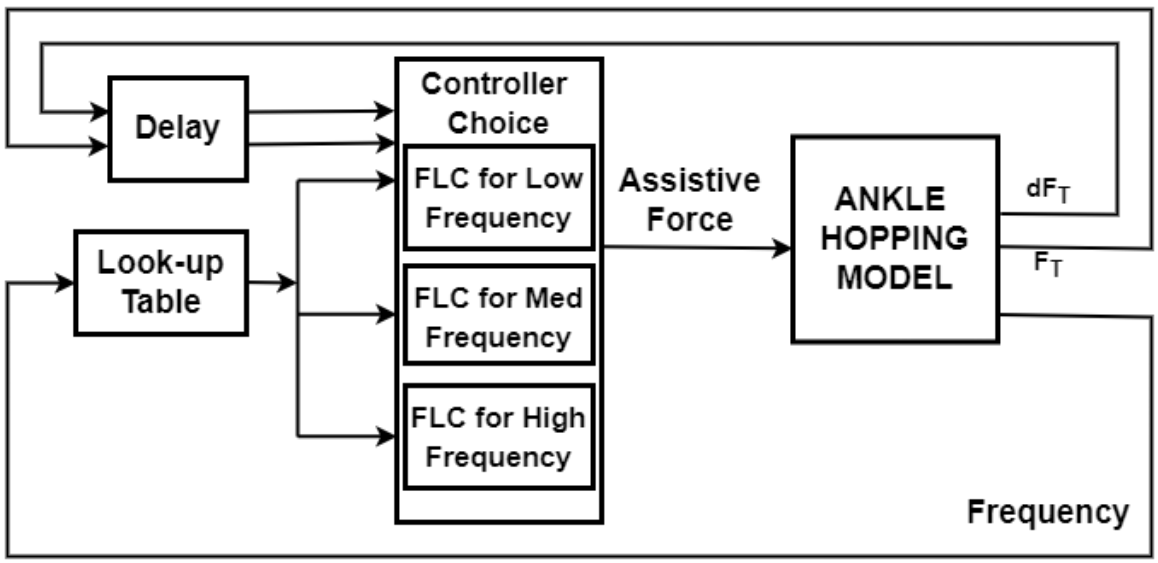

Figure 4.6: Frequency-Adaptive Fuzzy logic Controller (FAFLC): The control loop with Look-up Table, FLC and Ankle Hopping Model

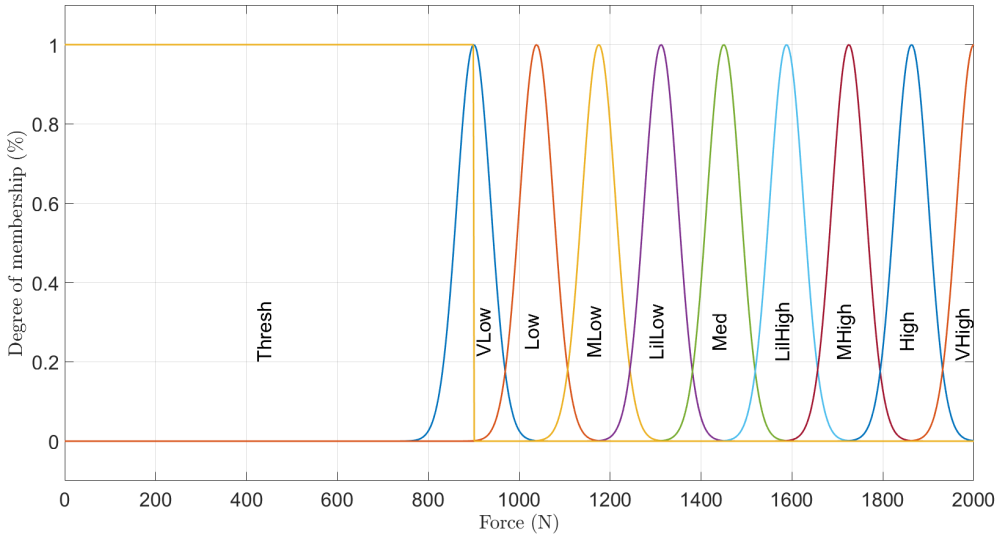

Figure 4.7: The input membership function for the Tendon Force (N) with a Threshold introduced

Although the look-up table provided ways to change the level of assistance for different frequencies, the boundaries of the frequency ranges are sharp/crisp. This may lead to drastic changes in the amount of assistance when the frequency crosses these boundaries. In this iteration also, certain control objectives, such as the Upper limit for tendon force, were ignored. To address these objectives are addressed in the next iteration.

4.3.3 Iteration 3: Fuzzy Logic Controller with Normalized Inputs (NIFLC)

(a) Hopping scenario

In this iteration one FLC was designed which had normalised inputs. The normalisation process has been discussed for two scenarios; hopping and walking. This iteration introduces a more robust method for handling the change in frequencies. A control strategy based on normalised inputs was designed. The inputs from the ankle model to the controller were normalised with respect to the upper limit of tendon force and instantaneous maximal derivative of the tendon force value to obtain the normalised inputs for the controller. Initially, this idea was considered because it was observed that when EMG data is analysed in research, they are usually normalised to remove the human variability factor. Also, all humans have different maximum

force outputs. So, it gave way to normalising the inputs to the FIS. In this manner, we can extend the use of one FLC to control the tendon force at various frequencies. The Normalisation in this version was performed between The Upper Limit of tendon force and 0 tendon force. The Block diagram for this model is shown in Figure 4.8.

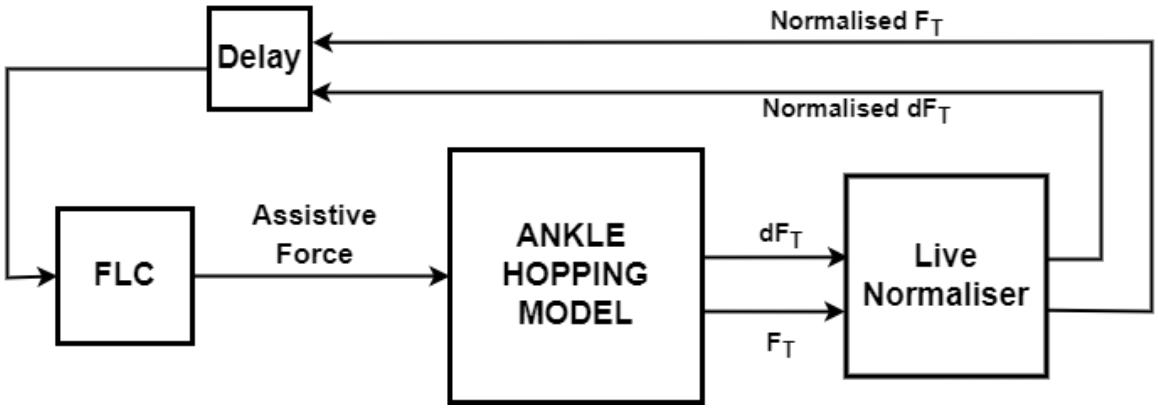

Figure 4.8: The control loop with the Live Normaliser, FLC and Ankle Hopping Model

The fuzzy sets of the input membership functions designed for this controller are shown in Figures 4.9 and 4.10. The output assistive force was not normalised because it need not be subject generic. In fact, it is an actuator-specific parameter.

The Gaussian fuzzy sets were also widened in this iteration to increase the overlap between the Fuzzy sets. Increase in overlap provides a smoother gradient of the control surface. The variation in smoothness is evident when comparing Figure 4.12, and Figure 4.5 from BFLC.

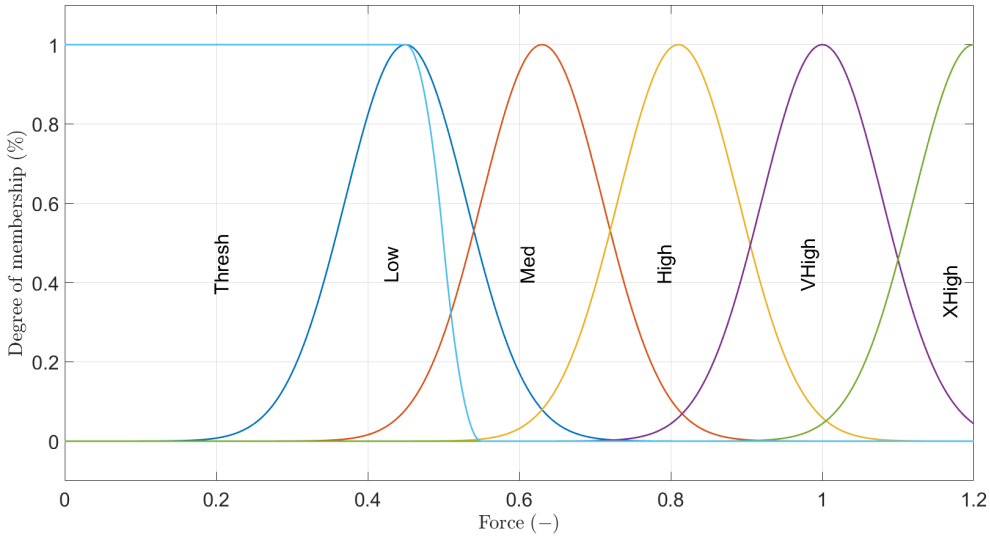

Figure 4.9: The Membership Function for Normalised Tendon Force (-)

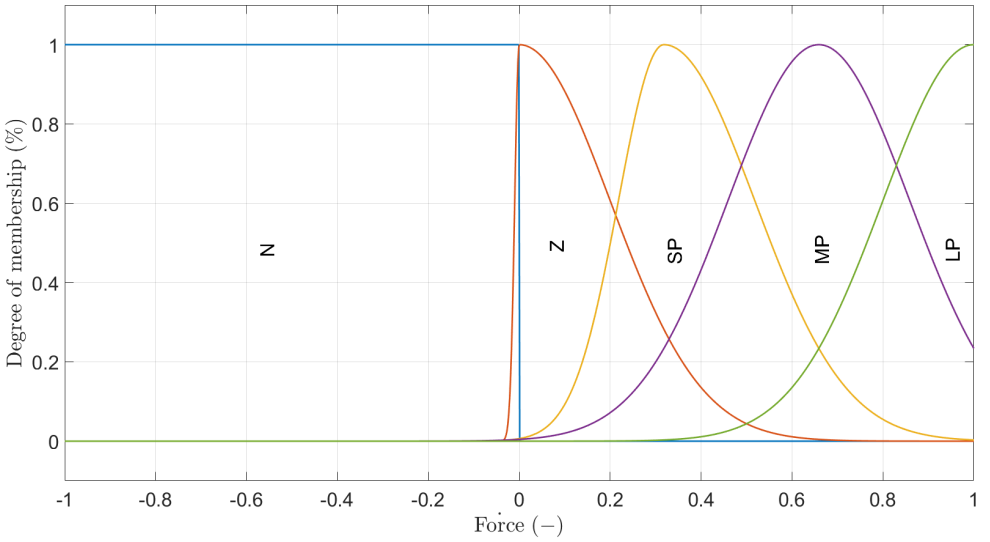

Figure 4.10: The Membership Function for Normalised Derivative of Tendon Force (N/s)

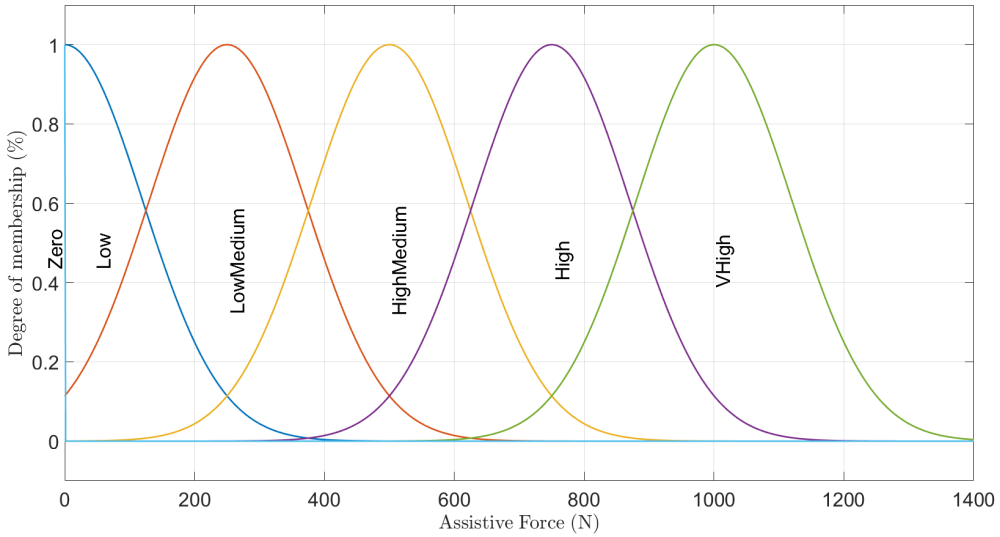

Figure 4.11: The output Assistive Force (N)

The rules for this version are given in Table 4.1. The control surface for the same is given in Figure 4.12.

Table 4.1: Rules for the controller version 5

F / F_dot	Thresh	Low	MediumLow	Medium	LilHigh	MHigh	High	VHigh
N	Zero	Zero						
Z		Zero	Low	LowMedium	LowMedium	HighMedium	HighMedium	High
SP		Low	LowMedium	LowMedium	HighMedium	High	High	High
MP		LowMedium	HighMedium	HighMedium	High	VHigh	VHigh	VHigh
LP		LowMedium	HighMedium	HighMedium	High	VHigh	VHigh	VHigh

(b) Walking scenario

For walking, the hopping model was used with walking excitations. These excitations were obtained based on the muscle synergies involved in the plantar flexion component of a walking gait cycle. It can be argued that this method is an approximation of the walking model since the exoskeleton in focus can, by design, provide assistance only to the plantar flexors. The excitation profiles for the plantar flexors are discussed in detail in a further section. Regarding the walking model for different speeds and elevations, it was noted that the controller became more aggressive for certain conditions than others. To reduce this effect, the normalisation was tweaked while the FLC remained unchanged. This time, the tendon force was normalised

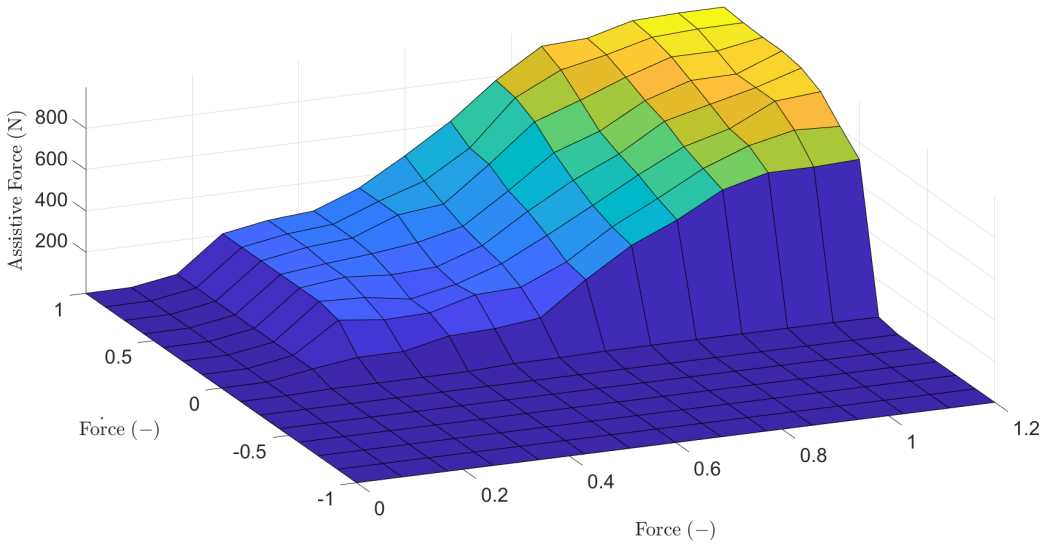

Figure 4.12: Control Surface for normalised inputs based controller for hopping. Force (N); Force_dot (N/s); ForceAC (-)

between the upper limit ($F_{\text{T,limit}}$) and its minimum ($F_{\text{T,min}}$)across the gait cycle.

$$F_{\text{T, Normalised}} = f \times \frac{F_{\text{T}}(i) - F_{\text{T,min}}}{F_{\text{T,limit}} - F_{\text{T,min}}} \tag{4.1}$$

The factor (f) was chosen as 0.8 through trial and error in the Equation 4.1.

4.4 The Excitation and Activation signals

Just like the controller design changed in each iteration, the excitation and activation functions also changed with the iterations. These excitation and activation functions have been discussed below.

4.4.1 Activation Function for BFLC

For this iteration, a sinusoidal activation function was chosen.

$$a = (\sin(t \times \omega))^2, \tag{4.2}$$

where a is the activation, t is the time step and ω is a factor that affects the sinusoid frequency. It is important to note that the angle mentioned in Equation 4.2 (denoted by $t \times \omega$) is in degrees. The sinusoidal activation is shown for $\omega = 200$ (corresponds to a frequency of 1.111Hz) in Figure 4.13.

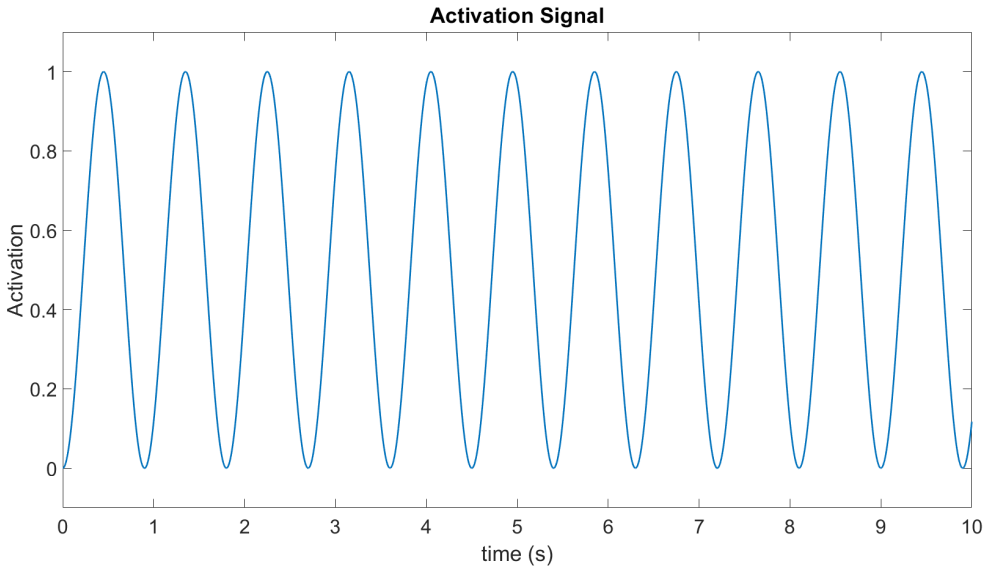

Figure 4.13: Sinusoidal Activation function at 1.111 Hz

4.4.2 Excitation and Activation for FAFLC

For the FAFLC, first-order activation dynamics, a commonly used activation model that simulates muscle models, was used for the simulation. Impulse excitation was adopted to simulate hopping. The excitation duration of one impulse was defined by a 10% duty cycle. Thus, for 10% of the duration of an excitation cycle, there will be muscle activation, and for the remaining duration, there will be muscle deactivation.

$$a(i) = a(i-1) + \frac{dt}{\tau} \times (e(i) - a(i-1)), \tag{4.3}$$

where a is the activation function, e is the excitation and i denotes the time step. The time constant is denoted by τ and is defined as

$$\tau = \begin{cases} 0.033 & e(i) > a(i-1) \\ 0.091 & e(i) \leq a(i-1) \end{cases}. \tag{4.4}$$

For this iteration the frequency was hopping varied from 1 Hz to 2.5 Hz in increments of 0.5Hz. Excitation for each frequency was given 2 repetitions as shown in Figure 4.14.

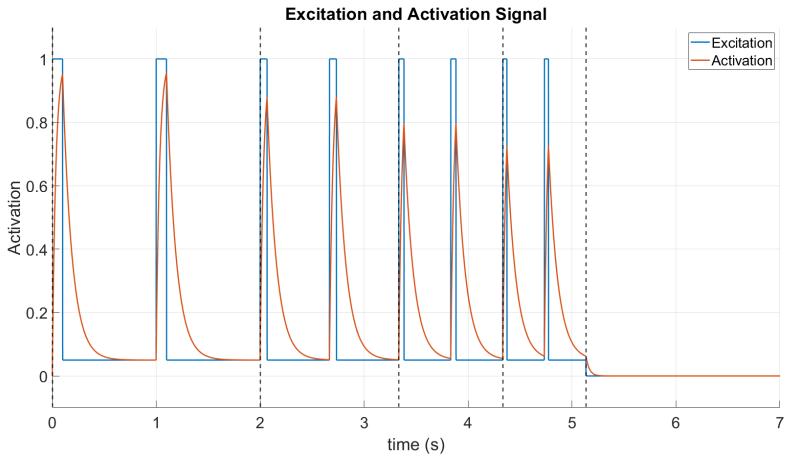

Figure 4.14: First order activation dynamics.The dotted lines shows where the frequency changes. The frequencies are 1 Hz, 1.5 Hz, 2 Hz and 2.5 Hz

4.4.3 Excitation and Activation for NIFLC for Hopping

The NIFLC controller was simulated with the following excitation and activation as shown in Figure 4.15 and 4.16. The excitation signal with frequency focused between 1.9 Hz and 2.5 Hz was used because the comfortable hopping frequency for humans lies in this range. The activation dynamics used in this iteration are also of the first-order type.

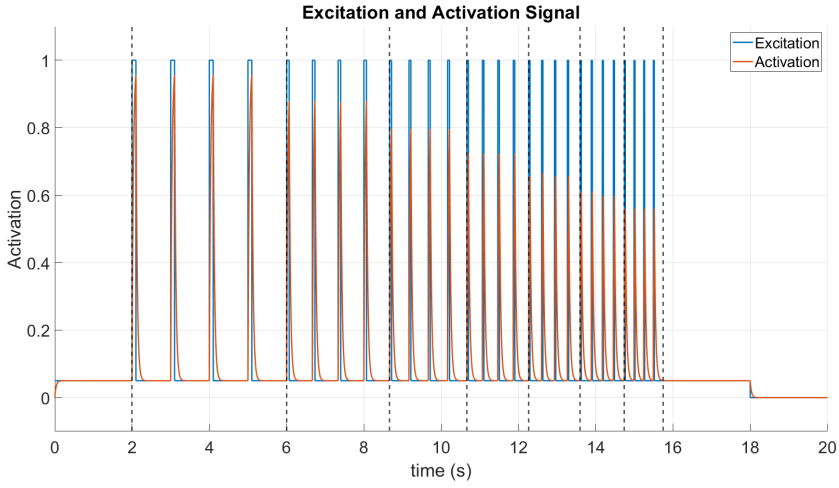

Figure 4.15: First order activation dynamics. The dotted lines show where the frequency changes. The frequencies are 1Hz, 1.5Hz, 2Hz, 2.5Hz, 3Hz, 3.5Hz and 4Hz

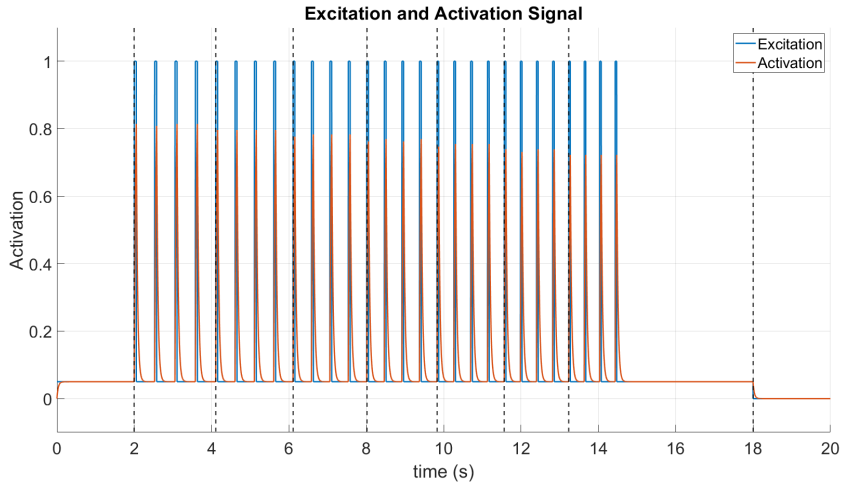

Figure 4.16: First order activation dynamics. The dotted lines show where the frequency changes. The frequencies are 1.9Hz, 2.0Hz, 2.1Hz, 2.2Hz, 2.3Hz, 2.4Hz and 2.5Hz

4.4.4 Excitation and Activation for NIFLC for walking

In this project, a separate walking model was not developed. Rather, only the excitation was changed in the model for simulating walking. The excitation was obtained based on muscle synergies discussed by Sartori et al. [21]. In this research, four different components of a walking gait cycle were extracted. Each component of the gait cycle was determined to be actuated by the synergy of a fixed set of muscles across several subjects and several walking conditions. The hopping model of this project considers only the plantar flexors. Considering this fact, only the plantar flexors component was considered for the simulation. The muscle excitation primitives (XP) for the plantar flexors were computed based on the methods discussed in Sartori et al. for speeds 1, 3, and 5 kmph and elevations of -20, 0, and 20%. The plantar flexors in focus are the Soleous, Peroneous, Gastrocnemius Lateralis and Gastrocnemius Medialis. Further, these excitation primitives were weighted according to the maximum force of each of these muscles against the maximum force generated by soleus.

$$W_{\text{m}} = \frac{F_{\text{max,m}}}{F_{\text{max,Soleus}}} \tag{4.5}$$

$$W_{\text{avg}} = \frac{\sum W_{\text{m}}}{4}, \tag{4.6}$$

where where the subscript m $\in$ {'Soleus', 'Peroneous', 'GastMed', 'GastLat'}. The weights (W_{m}) obtained using Equation 4.5 were used to obtain average of the weights

(W_{avg}) using Equation 4.6.

$$e_{\text{lumped}} = \frac{\sum(XP_{\text{m}} * W_{\text{m}})}{W_{\text{avg}}} \tag{4.7}$$

The weighted excitations were summed and divided by W_{avg} to obtain lumped muscle excitation (e_{lumped}). These excitations were then normalised only if their maximum value exceeded unity. These were named Lumped Muscle Excitation Profiles (LMEP). These LMEPs were in time-normalised form; thus, it was necessary to scale them to realistic time periods of the gait cycle for their respective speeds. These realistic gait cycle periods were obtained from an extensive public data set provided by Fukuchi et al. [22].

Each LMEP cycle was repeated five times, and the five repetitions were fed as excitation signals to the hopping model to mimic the walking activation for our hopping model in each of the 9 conditions. The different stages of this process for the base condition (gait speed 3kmph and elevation 0%) are depicted using a series of figures from Figure 4.17 to Figure 4.19.

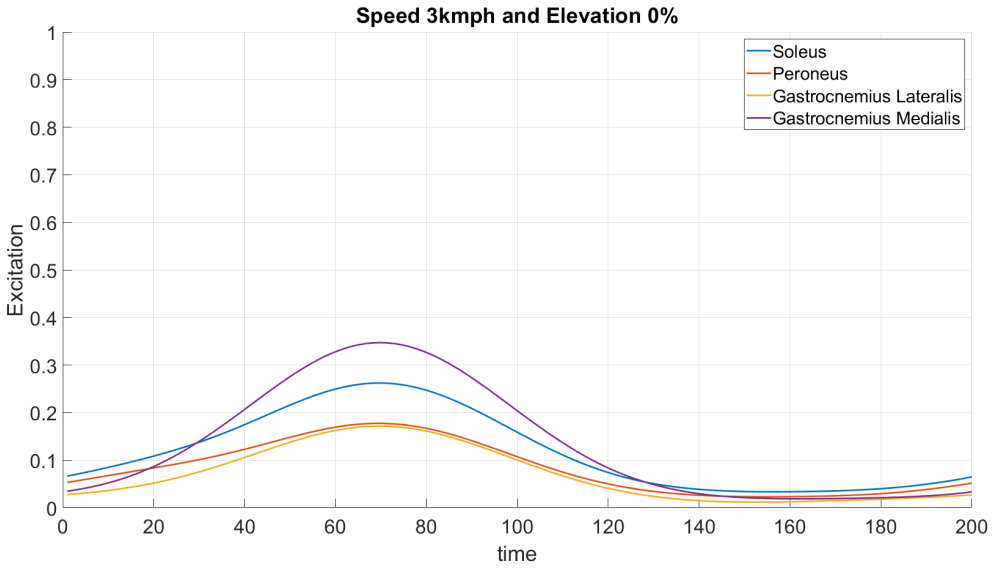

Figure 4.17: The excitation primitives of the four contributors for Plantar Flexion

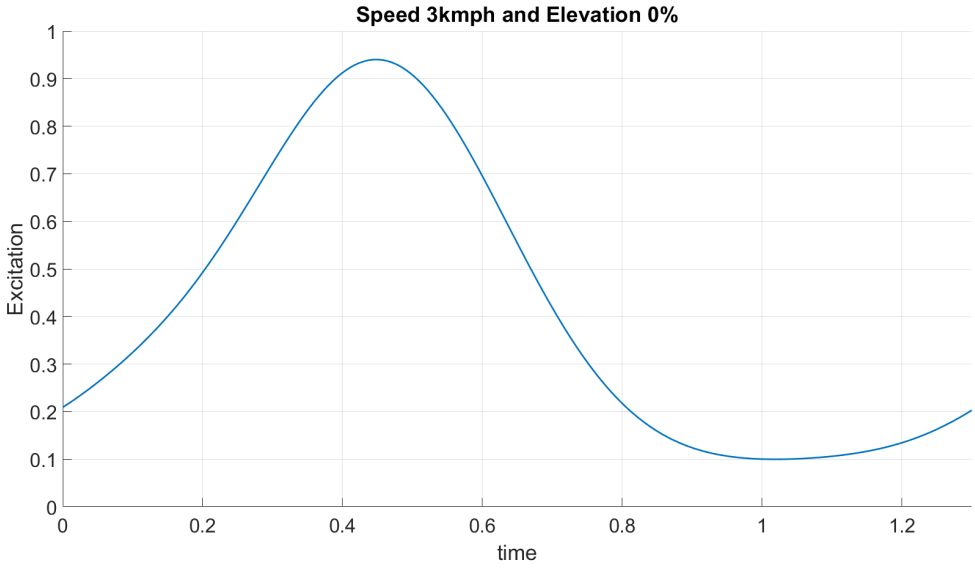

Figure 4.18: The Lumped excitation

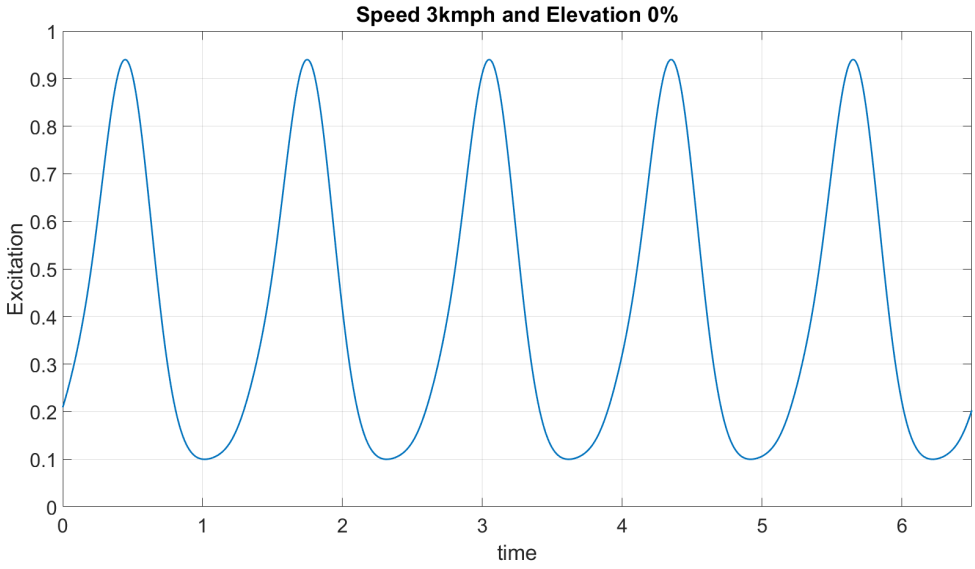

Figure 4.19: The Lumped Excitation repeated 5 times. This was the excitation provided to the Ankle hopping Model

Chapter 5

Results

5.1 Basic Fuzzy Logic Controller (BFLC)

To recall, BFLC had an if-else function block, which allowed the controller to activate only when the Tendon Force was greater than 900 N. Figure 5.1 shows the controller in action and its effect on the tendon force. The top plot compares the unassisted Tendon Force (blue line) and assisted tendon force (red line), with the assisted tendon force having a lower peak value. The bottom plot depicts the assistance provided by the controller

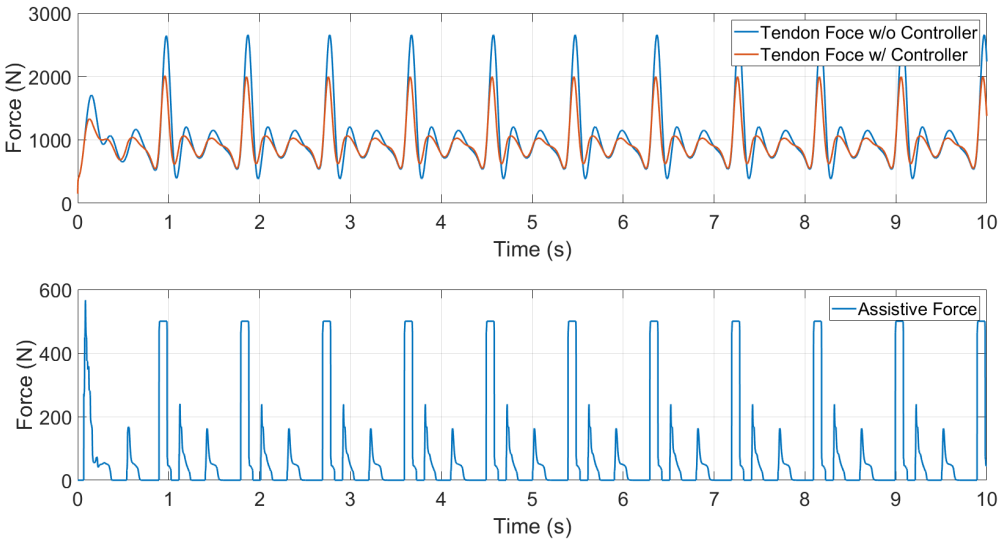

Figure 5.1: For Controller and Model version 2: (Top) Comparison between Tendon Force with and without assistance. (Bottom) Assistive Force

5.2 Frequency-Adaptive Fuzzy logic Controller FAFLC

The response of FAFLC, the controller with a look-up table, is shown in Figure 5.2. The top plot compares the assisted and unassisted tendon force. The bottom plot shows the assistance provided by the controller. Two hopping cycles were done for each frequency of 1 Hz, 1.5 Hz, 2 Hz and 2.5 Hz.

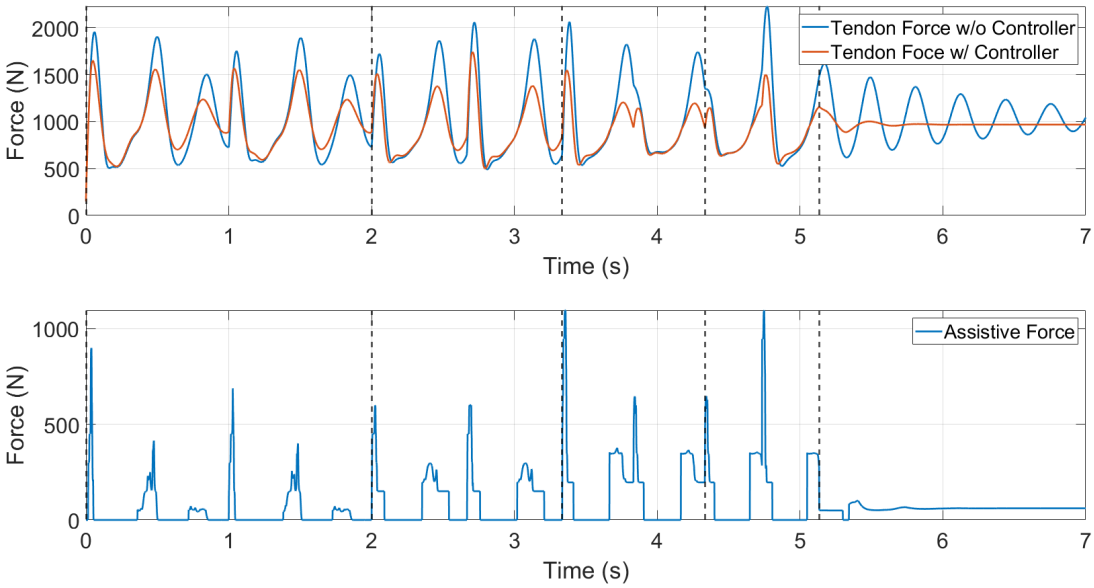

Figure 5.2: For Controller and Model version 3: (Top) Comparison between Tendon Force (N) with and without assistance. (Bottom) Assistive Force (N)

5.3 Fuzzy Logic Controller with Normalized Inputs (NI-FLC)

The results for the hopping scenario are shown in section 5.3.1 and for walking scenario it is discussed in section 5.3.2

5.3.1 Hopping Scenario

In this version of the model, live normalisation was introduced. The controller was tweaked to accommodate the normalised inputs, and the activation signals were

also changed. It was tested with 2 signals shown in Figure 4.15 and 4.16. The response to these activations is shown in Figure 5.3 and 5.4, respectively.

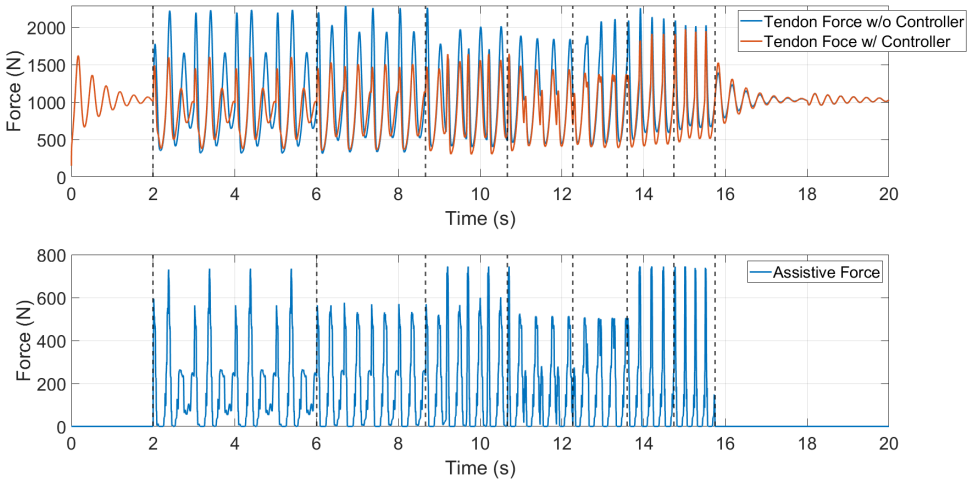

Figure 5.3: Normalised Inputs controller for hopping: (Top) Comparison between Tendon Force with and without assistance. (Bottom) Assistive Force. The frequencies are 1Hz, 1.5 Hz, 2 Hz, 2.5 Hz, 3 Hz, 3.5 Hz and 4 Hz.

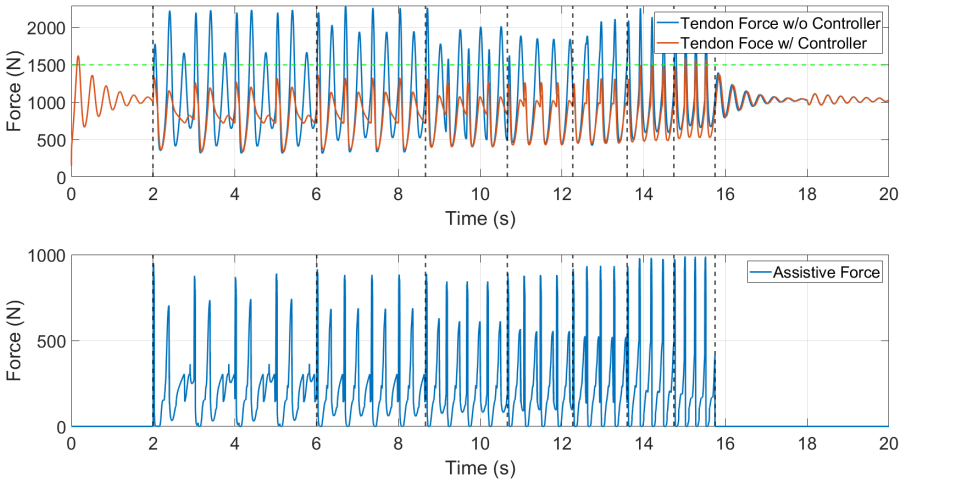

Figure 5.4: For Controller and Model version 5: (Top) Comparison between Tendon Force with and without assistance. (Bottom) Assistive Force

For the above Excitation signals, the upper tendon force limit varied from 1200N to 1900N in 100N increments. Figure 5.5 shows the average peak tendon force value with and without control and a reference expected value in bar graph format. The standard deviation of the averages is depicted by the whiskers, who have a length double the standard deviation. The expected peak values are the same as

the upper limit for the tendon force set during the normalisation. In Figure 5.6, a contour plot is shown that depicts the reduction in peak tendon force across multiple frequencies and the upper limit of tendon force. Figure 5.7 shows the average time spent by tendon force beyond the upper limit. The standard deviation is denoted by the whiskers in the plot.

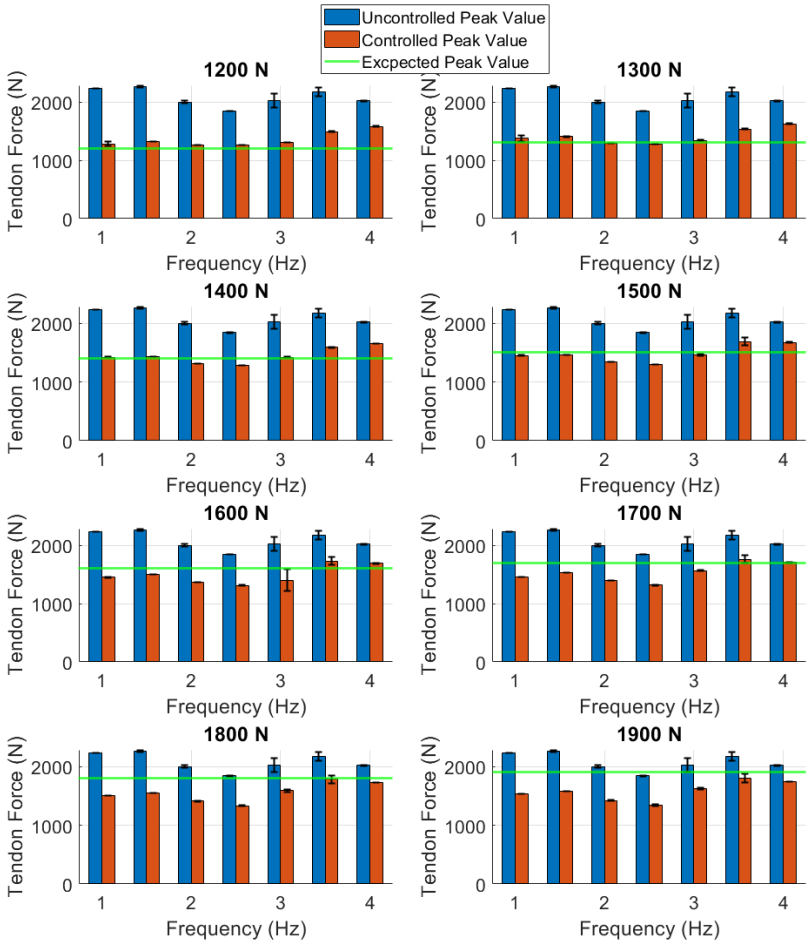

Figure 5.5: Comparison between the mean peak values of tendon force for the controlled (assisted) and uncontrolled (unassisted) scenarios. The whiskers on the bar graph show the standard deviation.

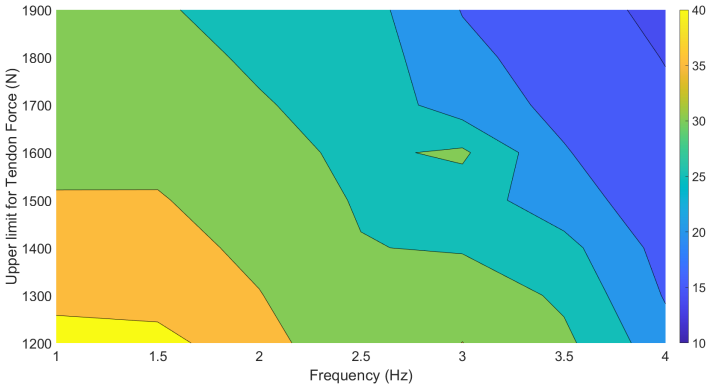

Figure 5.6: Contour plot showing the variation in the percentage reduction of the peak Tendon force.

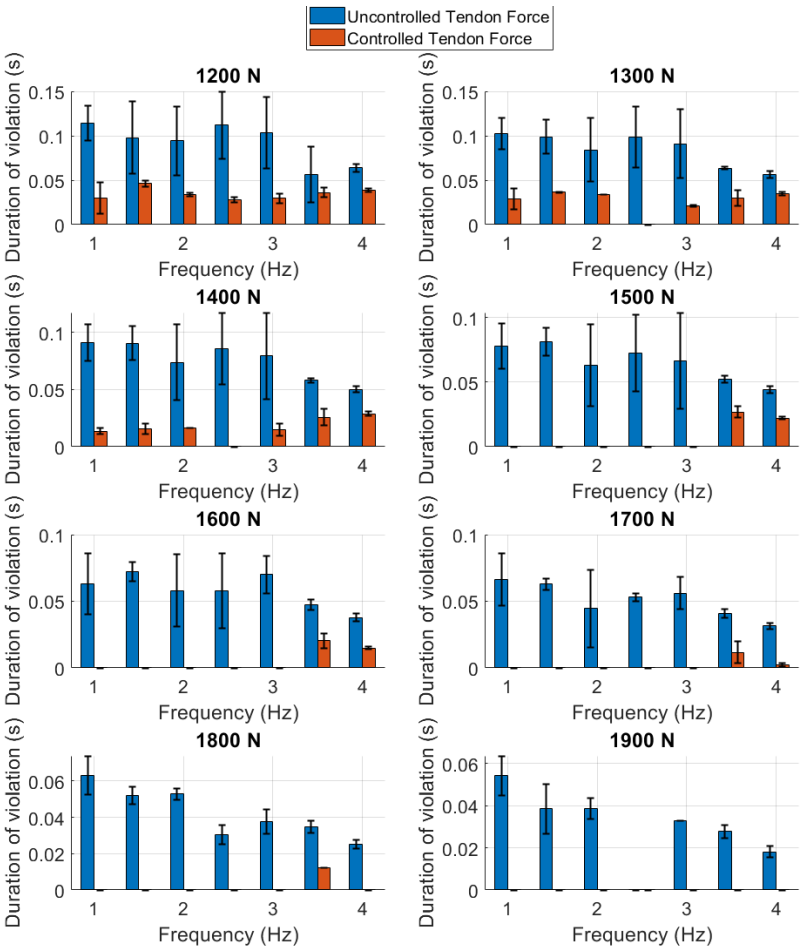

Figure 5.7: (Order: Left to Right, Top to Bottom) 1200N to 1900N Upper limit of Tendon Force. The average time is spent by a set of peaks beyond the upper limit or threshold in a set of hopping cycles.

The following contour plot also shows the reduction percentage of mean time spent beyond the threshold in Figure 5.8.

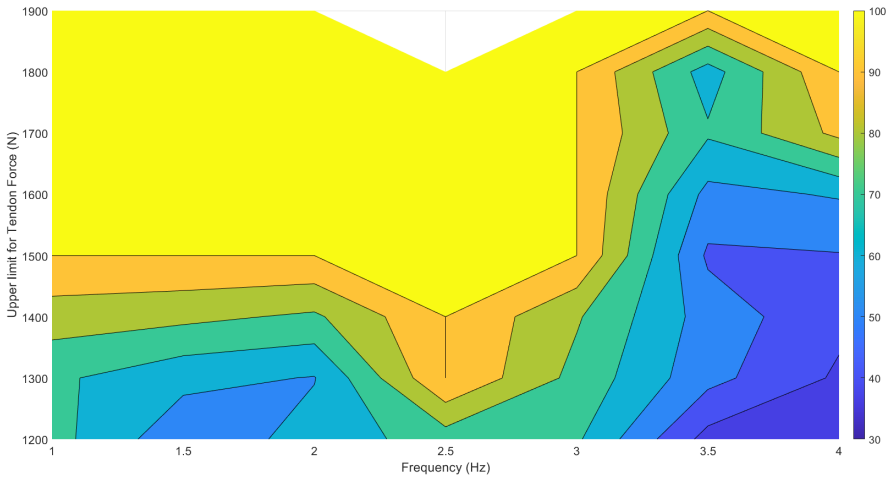

Figure 5.8: Contour plot showing the variation in the percentage reduction of the mean time spent beyond the upper limit/threshold.

A similar analysis has been done for the excitation signal with frequencies ranging from 1.9Hz to 2.5Hz, and the plots on the same are given from Figures 5.9 to 5.11. Figure 5.12 shows the average time spent by tendon force beyond the upper limit. The whiskers on each bar of the bar graphs depict the standard deviation of the duration of violation. Figure 5.12

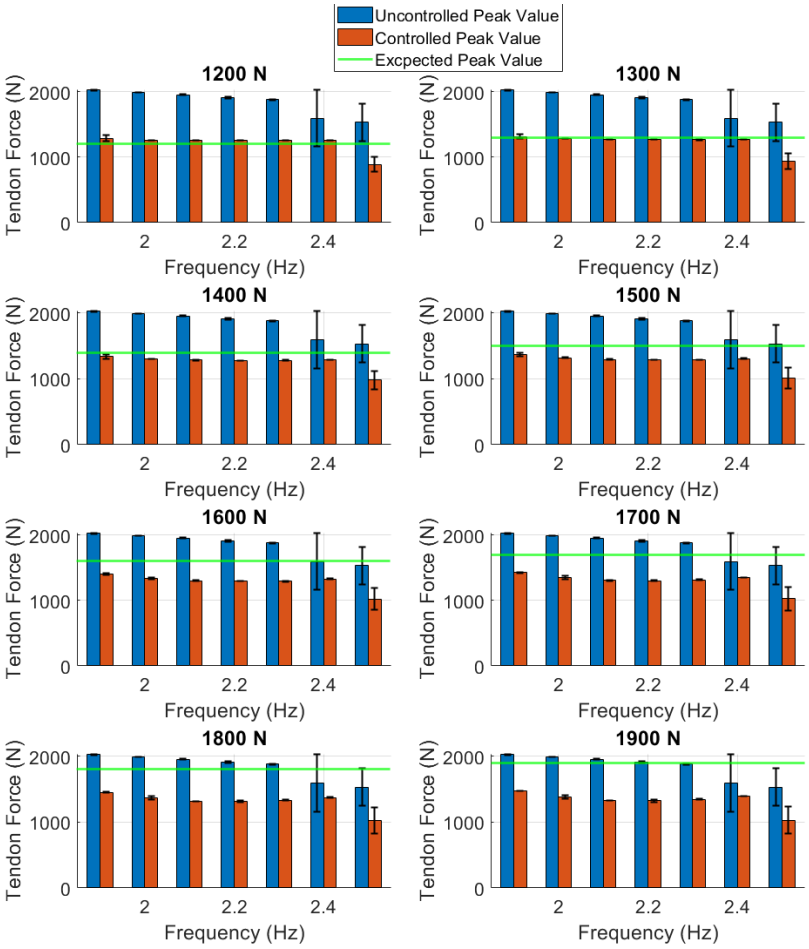

Figure 5.9: (Order: Left to Right, Top to Bottom) 1200N to 1900N Upper limit of Tendon Force.

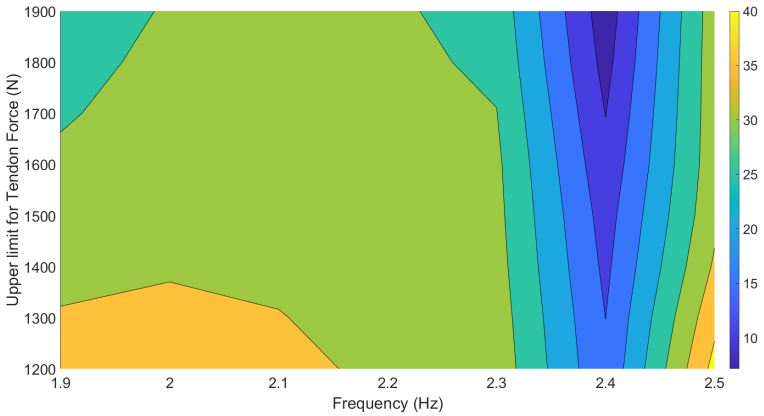

Figure 5.10: Contour plot showing the variation in the percentage reduction of the peak Tendon force.

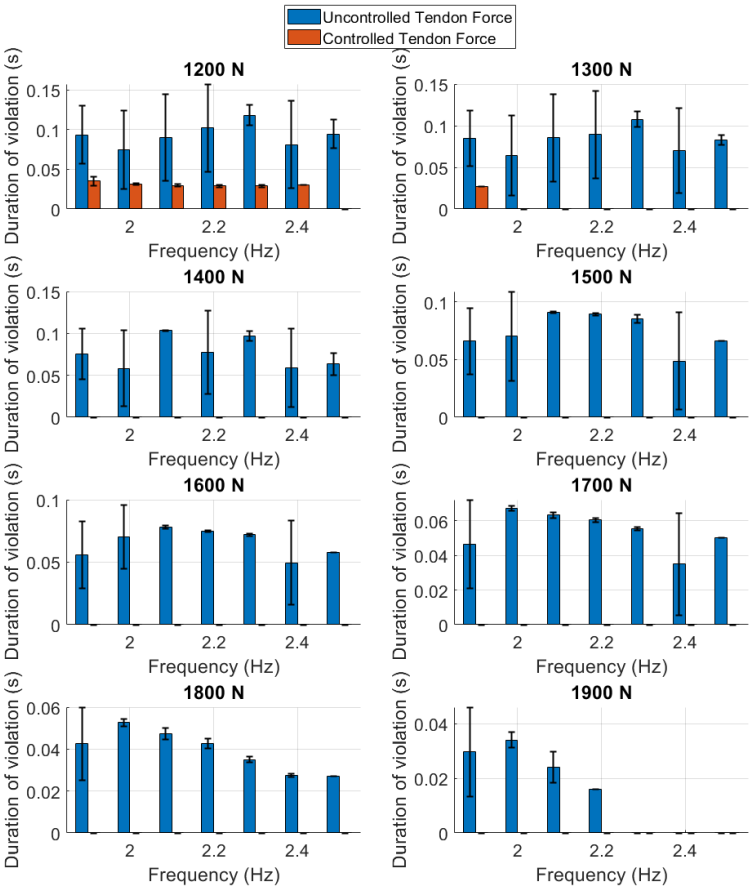

Figure 5.11: (Order: Left to Right, Top to Bottom) 1200N to 1900N Upper limit of Tendon Force. The average time is spent by a set of peaks beyond the upper limit or threshold in a set of hopping cycles.

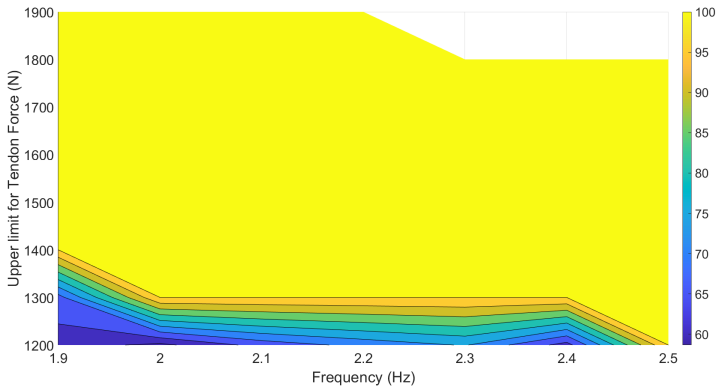

Figure 5.12: Contour plot showing the variation in the percentage reduction of the mean time spent beyond the upper limit/threshold.

5.3.2 Walking scenario

This FLC had the normalised inputs between the upper limit and minimum tendon forces (that occur after the first 100ms) instead of normalising between maximum tendon force and 0 N. This was designed for the model with walking activations. The walking activations obtained from Sartori et al. [23] were used to test the Normalised Inputs controller for walking. One result is shown in Figure 5.13 as an example. The remaining results are shown in Appendix B.

The analysis results are shown in a bar graph (Figure 5.14) and contour plots for different elevations Figures 5.15 and 5.17, respectively. The walking conditions in the x-axis are denoted in the Table 5.1

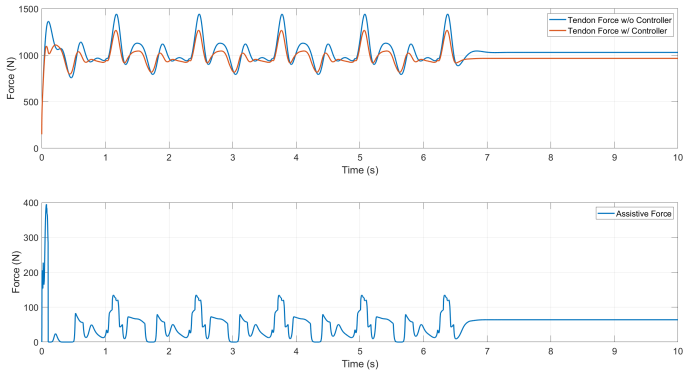

Figure 5.13: Normalised Inputs controller for walking, Speed 3kmph, Elevation 0%: (Top) Comparison between Tendon Force with and without assistance. Upper Limit set to 1500N (Bottom) Assistive Force

Table 5.1: The condition numbers and their corresponding speed and elevation

Condition#	Speed (kmph)	Elevation (%)
1	1	-20
2	1	0
3	1	20
4	3	-20
5	3	0
6	3	20
7	5	-20
8	5	0
9	5	20

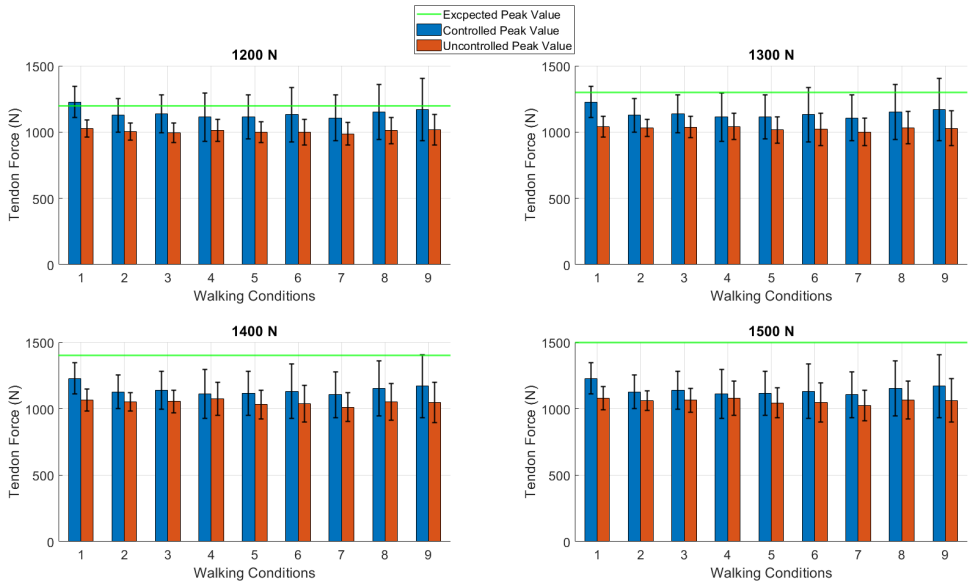

Figure 5.14: These graphs are depicted for the average upper limit for tendon forces set during normalisation and its effect on the behaviour of the peak tendon forces. The standard deviation is denoted by the whiskers on the bars.

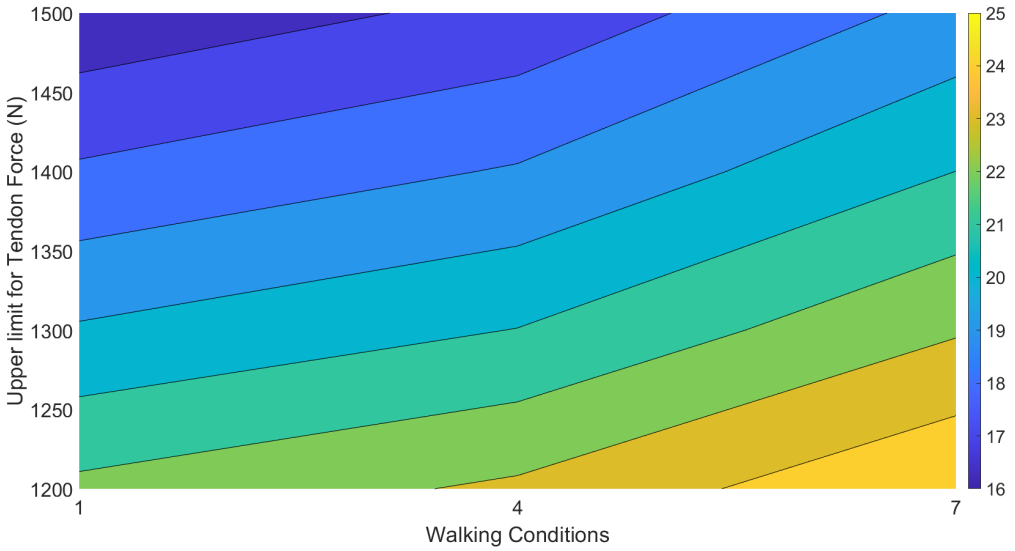

Figure 5.15: This contour plot indicates the reduction percentage in peak tendon force for a variety of walking conditions (Elevation = -20%)

Figure 5.16: This contour plot indicates the reduction percentage in peak tendon force for a variety of walking conditions (Elevation $=$ 0%)

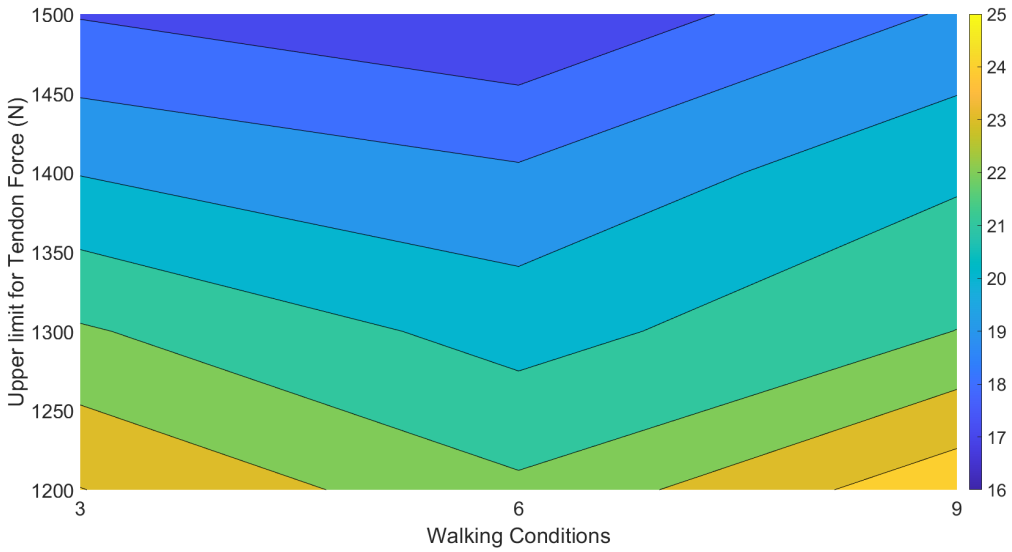

Figure 5.17: This contour plot indicates the reduction percentage in peak tendon force for a variety of walking conditions (Elevation $=$ 20%)

Chapter 6

Discussions

While designing the membership function for the FLCs, certain liberties were taken to explore and determine what might possibly give acceptable results. In this section, the design choices made and their reason will be discussed alongside the discussion of results.

6.1 Basic Fuzzy Logic Controller

Although the Gaussian fuzzy sets were used to design the membership function (Figure 4.4) to obtain a smooth transition of assistive force across varying tendon force, we still notice that there is a visible step-like transition along the 'Force (N)' axis in the control surface (Figure 4.5). At this point, it was hypothesised that to obtain a smoother transition across varying forces, finer control was necessary, and hence, in the next iteration (FAFLC), the number of fuzzy sets was increased for each membership function.

This iteration was designed to fulfil the assist-as-needed criterion. In Figure 5.1, it is observed from the plot from the assistive force that the assistance is intermittent. The BFLC is active only when the tendon force exceeds 900 N and provides 0 N assistance otherwise.

The maximum assistive force provided by the control surface of the BFLC is 600 N. It is evident that BFLC does not utilise the full potential of the exoskeletons maximum assistive force of 1000 N.

Since there were no other constraints defined for the controller to perform with, the performance of this version cannot be evaluated any further.

6.2 Frequency-Adaptive Fuzzy logic Controller FAFLC

Regarding the control surfaces for the FLC (Figure A.14 to A.16), we notice the step-like transition happening across varying 'Force' despite increasing the number of fuzzy sets in the membership functions shown in Figure A.12 to A.13. This suggests that increasing membership functions is does not equate to a smoother control surface. Thus, in the next iteration for NIFLC, the number of Fuzzy sets was reduced, and a different strategy was used to get a smoother output.

From Figure 5.2, it is visible that the Fuzzy Adaptive Frequency-Limited Controller (FAFLC) effectively manages the tendon force, maintaining it between 1500 N and 1700 N across all frequencies. The intermittent activity in the plot for assistive force, which responds to the peaks in tendon force, suggests a successful implementation of the 'Thresh' fuzzy set in the input membership function. However, while the tendon force is reduced, it is important to note that this behaviour might not be consistent with different excitation signals. Additionally, this controller does not account for the upper limit of tendon force that the user may wish to set. Essentially, this led to the design of the next iteration.

6.3 Fuzzy Logic Controller with Normalized Inputs (NIFLC)

While designing the FLC for NIFLC, it was decided to increase the overlap between the fuzzy sets of the membership function in an attempt to obtain a smooth control surface. The increased overlap can be observed by observing Figures 4.4 and Figure 4.9. This was the correct factor necessary for obtaining a smooth control surface, as observed in Figure 4.12.

6.3.1 Hopping Scenario

This controller has been tested with varying upper limits/thresholds of tendon force. It is intuitive to think that increasing the upper limit for the tendon force should result in a decrease in controller assistance, and thus, the controlled peak value of the tendon force will increase. Figure 5.5 shows that the reduction in tendon force varies with varying thresholds. The whiskers in Figure 5.5 indicate very little to no variation in the peak tendon force across multiple hopping cycles. To better understand how the reduction varies with both frequency and threshold, we can look at Figure 5.7.

Here, we see the expected trend of peak tendon force reduction percentage. It is also noticeable that the reduction percentage decreases as the frequency increases. The decrease in reduction percentage is justified for frequencies between 2 HZ and 3 Hz since the uncontrolled peak tendon force decreases, and the controller is able to sustain a similar peak tendon force to that between 1 Hz and 2 Hz. The lower values of peak reduction percentage at high frequencies ($>$ 3 Hz) indicate that the controller is struggling to reduce the peak tendon force sufficiently as we compare the Figures 5.5 and 5.7.

From Figure 5.7, we can see that the maximum time spent beyond the threshold is 50ms. Comparing this data with the tendon force peaks from Figure 5.5, we can see that the worst threshold violation happens at 3.5Hz to 4Hz, with about 200N to 300N excess thresholds at thresholds 1300N to 1500N. However, this violation can be ignored since most humans cannot hop with full strength at frequencies higher than 3Hz to 3.5Hz. From Figure 5.8, we can infer that the controller successfully provides assistance for upper limits greater than 1500N and frequencies less than 3Hz since this is the range where we see 100% reduction in the duration of violation of the upper limit

The reduction in the whisker length across all the plots Figure 5.12, 5.7, 5.9 and 5.11

Considering that the comfortable range for human hopping frequency is around 2.2Hz, it the controller was also tested between 1.9Hz and 2.5Hz with increments of 0.1Hz [24]. Figure 5.9 shows the mean peak tendon force value change with varying thresholds. Only for an upper limit of 1200N do we notice that the controller fails to maintain the tendon force below the threshold across most of the frequencies in the range. Figure 5.10 shows the reduction percentage of the peak tendon force. We observe a decrease in the reduction percentage contour plot between the frequencies of 2.3 Hz and 2.5 Hz. To understand why that is happening we can look at Figure 5.9, especially the bars related to this frequency range. Here, we notice that the uncontrolled average peak tendon forces are already lower due to the dynamics of the Ankle hopping model. Meanwhile, the controller is able to maintain the peak tendon force at the same level across the frequencies 1.9 Hz to 2.4 Hz. Figure 5.11 compares the duration of violation for the uncontrolled and controlled tendon force. We can see that there is no violation of the upper limit of tendon forces for limits greater than 1300 N. Considering the results for the reduction in violation duration from both cases (Figure 5.8 and Figure 5.12), we can conclude that the controller works best for upper limits of tendon force greater than 1500 N, between the frequencies of 1 Hz to 3 Hz.

When comparing this result against the result shown in Figure 5.8 and Fig-

ure 5.12 between 2 Hz and 2.5 Hz, we see that we have better controller performance in the scenario where frequency ranges from 1.9 Hz to 2.5 Hz. This suggests that there is some level of history dependency on the duration of the violation. This can be attributed to the dynamics of the system. The inertia of the mass in the model makes it move in different directions with different accelerations, hence, different initial conditions when a new hopping cycle begins. This history dependency might also be the reason why, at high frequencies ($>$ 3 Hz), we see an increase in the peak tendon force.

6.3.2 Walking Scenario

The hopping model was used for walking activations. The walking activations chosen comprised the plantar flexor synergy only since the exoskeleton model only assists the plantar flexors. The model has been simulated for nine conditions, as discussed in Table reftab:Conditiontable, and 4 upper limits for tendon force (1200 N, 1300 N, 1400 N, and 1500 N). Looking at Figure 5.14, we immediately notice that the controller successfully maintains the average peaks within the upper limits. As expected, when increasing the threshold for the same condition, we require a decrease in the percentage reduction of the peak tendon force. We know that as speed increases, peak tendon force increases. Thus, we would expect to notice an increase in the percentage reduction of the tendon force reduction to maintain the tendon force under the same threshold.

6.4 Limitations

Although we have seen some favourable results, certain limitations arise in various areas of this project. In this section, the limitations under each area of control will be discussed.

6.4.1 Fuzzy Logic Controllers

In this project, the Fuzzy Logic Controllers are designed with only two inputs: Tendon Force and its derivative. Although this simplifies the design of the FLCs, it also ignores potential inputs that could improve the controller output, such as frequency (in the case of hopping), speed, and elevation (in the case of walking). This improvement comes at the cost of increasing the complexity of the Fuzzy Inference System (FIS).

The controller's membership functions were designed through trial and error, making it challenging to achieve an optimal strategy. Consequently, the controller presented in this project is far from optimal and can be improved significantly. For example, the number of fuzzy sets for the tendon force membership function could be reduced from six to four. Fewer fuzzy sets would allow for wider Gaussian bases, increasing overlap between adjacent sets and providing smoother control surfaces. Initially, it was believed that overlapping alternate fuzzy sets could cause issues, but it was later discovered while with NIFLC that such overlaps can be advantageous. The FIS considers the area of more than two output fuzzy sets during defuzzification, making this overlap beneficial in our case. A better, more optimal rule base can also be designed based on these newer membership functions.

6.4.2 Online Normalising Block

The current normalisation method does not account for upper limits on tendon force, which would be greater than the maximum unassisted tendon force. The controller should not assist in such scenarios. However, since the normalised input still falls within the range of the controller inputs for assistance, the controller inadvertently assists in this scenario. This can be tackled by considering the maximum tendon force achieved in the history of the simulation and using that knowledge to either lower or increase the current assistance.

6.4.3 Excess Assistive Force

In certain scenarios, it was observed that when the controller successfully keeps the tendon force within limits, the peak tendon force is reduced more than necessary. This could lead to discomfort during the pilot's hopping and walking tasks and be detrimental to the pilot and the study being done. The assistive force also seems to be providing inputs with very quickly increasing forces. This could be detrimental to both the pilot and the exoskeleton.

Chapter 7

Conclusions and recommendations

7.1 Conclusions

This project has successfully demonstrated the feasibility of employing FLC in an assist-as-needed scenario. However, the FLC performs and fulfils objectives only in particular ranges the necessary amount of assistance only in particular conditions. A suitable control strategy has been designed and employed to improve the controller's effectiveness in specific motor tasks (hopping and walking).

A Normalised Input Fuzzy Logic Design has been proposed for the hopping and walking scenarios, with different normalisation techniques suitable for each. In the case of hopping, the controller effectively controlled the tendon force for hopping frequencies up to 3 HZ with a minimum upper limit of tendon force of 1500 N. However, it is not suitable for use outside this range due to its inability to maintain the tendon force under the limit.

The controller has been tested for 9 walking conditions, for a combination of speeds of 1 kmph, 3 kmph, 5 kmph and elevation of -20%, 0% and 20%. It successfully provided assistance, keeping the tendon force within limits between 1300 N and 1500 N across all conditions.

Despite the promising results, the FLC design had limitations. These include the inability to effectively reduce the tendon force at high frequencies within limits, excessive assistance when able to control within limits and the requirement of different normalisation techniques for different motor tasks.

7.2 Recommendations

1. The FLC can be improved by modifying the membership functions.
2. Realistic activation dynamics and tendon force dynamics can be obtained from experiments. The insights from this will contribute to the expert knowledge required for better tuning the FLC parameters.
3. More inputs can be considered while designing the FLC, such as hopping frequency, speed and elevation of walking.
4. The control loop can be modified to include the actuator dynamics. This way, the assistance provided can be simulated more realistically. Designing the controller around this ensures the assistive force provided is more realistic and will not cause damage to the pilot or the exoskeleton.
5. Machine learning techniques can be employed to improve the FLC.
   (a) ML can automate parts of the process of designing by learning the fuzzy rules and tuning the membership functions, reducing the manual effort in designing the FLC and enhancing its overall performance.
   (b) ML can enable FLC to adapt to changing conditions over time by learning from new datasets.
   (c) With ML's predictive capabilities, the FLC can be enhanced and improved to provide more optimal assistance.
6. To make the FIC adaptive the transition dynamics between hopping and walking can be explored. Further more realistic activations for hopping can be considered to test the performance of the controller.

Bibliography

[1] M. Grimmer, B. T. Quinlivan, S. Lee, P. Malcolm, D. M. Rossi, C. Siviy, and C. J. Walsh, "Comparison of the human-exosuit interaction using ankle moment and ankle positive power inspired walking assistance," *Journal of Biomechanics*, vol. 83, pp. 76–84, 1 2019.

[2] J. Zhang, P. Fiers, K. A. Witte, R. W. Jackson, K. L. Poggensee, C. G. Atkeson, and S. H. Collins, "Human-in-the-loop optimization of exoskeleton assistance during walking," *Science*, vol. 356, no. 6344, pp. 1280–1283, 6 2017. [Online]. Available: https://www.science.org/doi/10.1126/science.aal5054

[3] P. S. Pridham and L. Stirling, "Ankle exoskeleton torque controllers based on soleus muscle models," *PLOS ONE*, vol. 18, no. 2, p. e0281944, 2 2023. [Online]. Available: https://journals.plos.org/plosone/article?id=10.1371/journal.pone.0281944

[4] S. Song and S. H. Collins, "Optimizing Exoskeleton Assistance for Faster Self-Selected Walking," *IEEE Transactions on Neural Systems and Rehabilitation Engineering*, vol. 29, pp. 786–795, 2021.

[5] K. A. Ingraham, C. D. Remy, and E. J. Rouse, "User preference of applied torque characteristics for bilateral powered ankle exoskeletons," *Proceedings of the IEEE RAS and EMBS International Conference on Biomedical Robotics and Biomechatronics*, vol. 2020-November, pp. 839–845, 11 2020.

[6] G. S. Sawicki and D. P. Ferris, "Mechanics and energetics of level walking with powered ankle exoskeletons," *Journal of Experimental Biology*, vol. 211, no. 9, pp. 1402–1413, 5 2008. [Online]. Available: https://dx.doi.org/10.1242/jeb.009241

[7] G. Durandau, W. F. Rampeltshammer, H. V. D. Kooij, and M. Sartori, "Neuromechanical Model-Based Adaptive Control of Bilateral Ankle Exoskeletons: Biological Joint Torque and Electromyogram Reduction Across Walking Conditions," *IEEE Transactions on Robotics*, vol. 38, no. 3, pp. 1380–1394, 6 2022.

[8] L. M. Mooney, E. J. Rouse, and H. M. Herr, "Autonomous exoskeleton reduces metabolic cost of human walking during load carriage," *Journal of NeuroEngineering and Rehabilitation*, vol. 11, no. 1, pp. 1–11, 5 2014. [Online]. Available: https://jneuroengrehab.biomedcentral.com/articles/10.1186/1743-0003-11-80

[9] D. G. Schmitz, R. W. Nuckols, S. Lee, T. Akbas, K. Swaminathan, C. J. Walsh, and D. G. Thelen, "Modulation of Achilles tendon force with load carriage and exosuit assistance," *Science Robotics*, vol. 7, no. 71, 10 2022. [Online]. Available: https://www.science.org/doi/10.1126/scirobotics.abq1514

[10] P. Slade, M. J. Kochenderfer, S. L. Delp, and S. H. Collins, "Personalizing exoskeleton assistance while walking in the real world," *Nature 2022 610:7931*, vol. 610, no. 7931, pp. 277–282, 10 2022. [Online]. Available: https://www.nature.com/articles/s41586-022-05191-1

[11] M. Nabipour, M. Sartori, and N. Nl, "Closed-form Modeling of the Soleus Musculotendon Unit," 2023. [Online]. Available: https://research.utwente.nl/en/publications/closed-form-modeling-of-the-soleus-musculotendon-unit

[12] M. Nabipour, G. S. Sawicki, and M. Sartori, "Predictive Control of Peak Achilles Tendon Force in a Simulated System of the Human Ankle Joint with a Parallel Artificial Actuator During Hopping," *IEEE International Conference on Rehabilitation Robotics*, 2023.

[13] M. Nabipour, G. S. Sawicki, M. Sartori, and N. Nl, "Predictive Control of Plantarflexor Muscle-Tendon Force During Simulated Human Hopping," 2023. [Online]. Available: https://research.utwente.nl/en/publications/predictive-control-of-plantarflexor-muscle-tendon-force-during-si

[14] M. Nabipour, G. S. Sawicki, and M. Sartori, "Predictive Control of Musculotendon Loads Across Fast and Slow-twitch Muscles in a Simulated System with Parallel Actuation," *bioRxiv*, p. 2024.05.14.594110, 5 2024. [Online]. Available: https://www.biorxiv.org/content/10.1101/2024.05.14.594110v1https://www.biorxiv.org/content/10.1101/2024.05.14.594110v1.abstract

[15] S. A. Zalapa and R. T. Sánchez, "Exoskeleton robot modeling and Fuzzy Logic Control," *2016 IEEE International Autumn Meeting on Power, Electronics and Computing, ROPEC 2016*, 1 2017.

[16] X. Wang and M. Meng, "The fuzzy control of tendon-driven fingers based on position and tendon tension," *Proceedings of the 30th Chinese Control and Decision Conference, CCDC 2018*, pp. 6188–6193, 7 2018.

[17] G. A. Rezage and M. O. Tokhi, “Fuzzy PID control of lower limb exoskeleton for elderly mobility,” *2016 20th IEEE International Conference on Automation, Quality and Testing, Robotics, AQTR 2016 - Proceedings*, 6 2016.

[18] B. D. Robertson, D. J. Farris, and G. S. Sawicki, “More is not always better: modeling the effects of elastic exoskeleton compliance on underlying ankle muscle–tendon dynamics,” *Bioinspiration & Biomimetics*, vol. 9, no. 4, p. 046018, 11 2014. [Online]. Available: https://iopscience.iop.org/article/10.1088/1748-3182/9/4/046018https://iopscience.iop.org/article/10.1088/1748-3182/9/4/046018/meta

[19] “Equations for Modeling the Forces Generated by Muscles... - Google Scholar.” [Online]. Available: https://scholar.google.com/scholar?hl=en&as_sdt=0%2C5&q=Equations+for+Modeling+the+Forces+Generated+by+Muscles+and+Tendons&btnG=

[20] M. Millard, T. Uchida, A. Seth, and S. L. Delp, “Flexing computational muscle: modeling and simulation of musculotendon dynamics,” *Journal of biomechanical engineering*, vol. 135, no. 2, 2013. [Online]. Available: https://pubmed.ncbi.nlm.nih.gov/23445050/

[21] J. Gonzalez-Vargas, M. Sartori, S. Dosen, D. Torricelli, J. L. Pons, and D. Farina, “A predictive model of muscle excitations based on muscle modularity for a large repertoire of human locomotion conditions,” *Frontiers in Computational Neuroscience*, vol. 9, no. SEP, p. 155771, 9 2015.

[22] C. A. Fukuchi, R. K. Fukuchi, and M. Duarte, “A public dataset of overground and treadmill walking kinematics and kinetics in healthy individuals,” *PeerJ*, vol. 2018, no. 4, p. e4640, 4 2018. [Online]. Available: https://peerj.com/articles/4640

[23] J. Gonzalez-Vargas, M. Sartori, S. Dosen, D. Torricelli, J. L. Pons, and D. Farina, “A predictive model of muscle excitations based on muscle modularity for a large repertoire of human locomotion conditions,” *Frontiers in Computational Neuroscience*, vol. 9, no. SEP, p. 155771, 9 2015.

[24] C. T. Farley, R. Blickhan, J. Saito, and C. R. Taylor, “Hopping frequency in humans: a test of how springs set stride frequency in bouncing gaits,” *Journal of applied physiology (Bethesda, Md. : 1985)*, vol. 71, no. 6, pp. 2127–2132, 1991. [Online]. Available: https://pubmed.ncbi.nlm.nih.gov/1778902/

Appendix A: Various Iterations of the Controller

A.1 Initial Design of FLC

This Controller was designed with only piece-wise fuzzy sets, as shown in Figures A.1 to A.3. Only 3 fuzzy sets were used to describe the membership function for the tendon force input and the assistive force output. the rules to build the control surface shown in Figure A.4 have been given in Table A.1. The controller is always active.

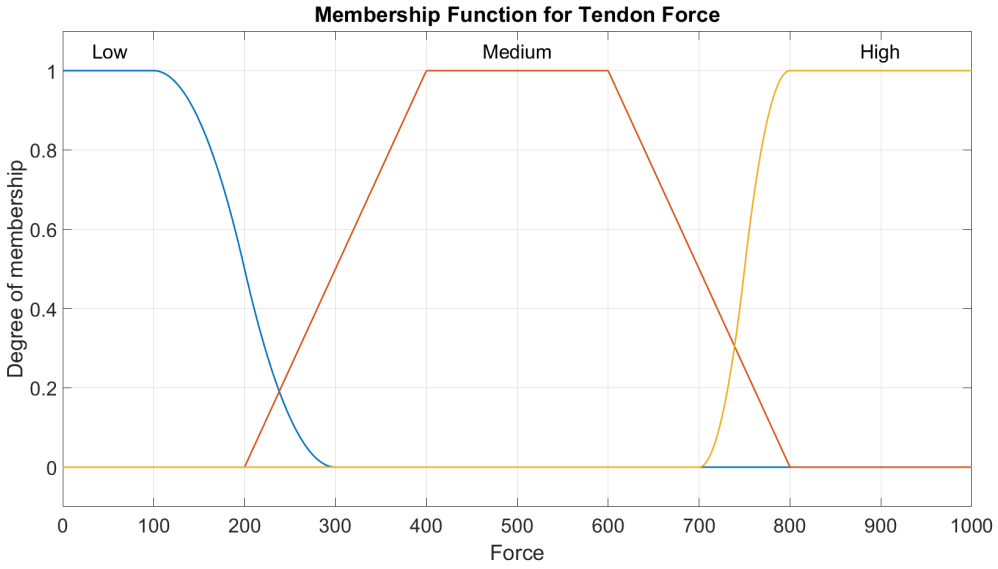

Figure A.1: The input membership function for the Tendon Force (N)

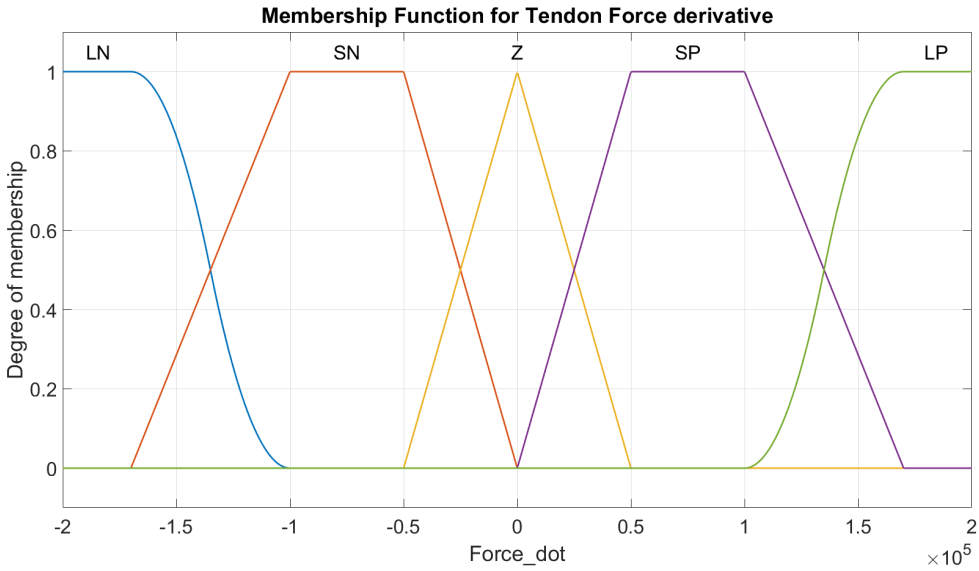

Figure A.2: The input membership function for the Tendon Force Derivative (N/s)

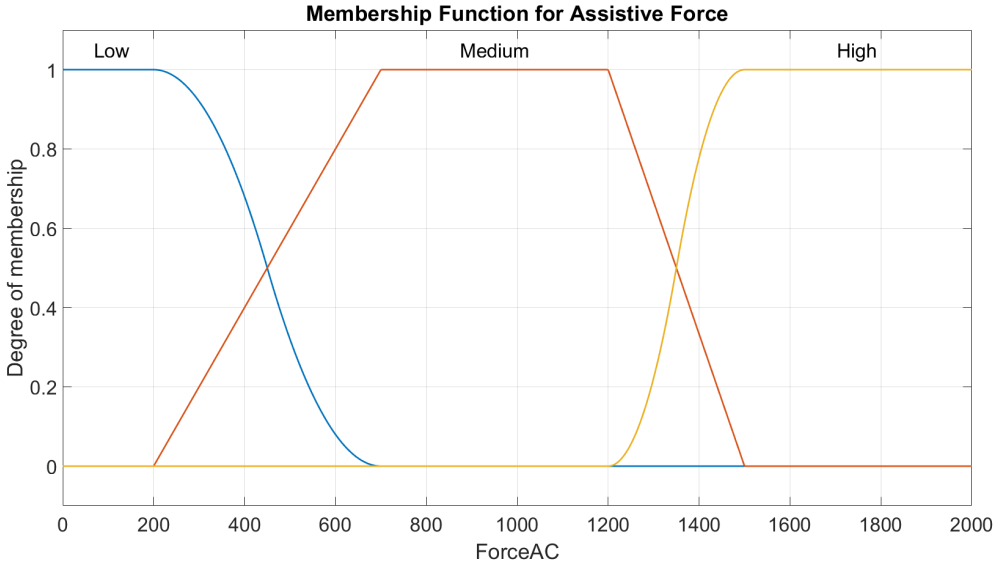

Figure A.3: The output membership function for the Assistive Force (N)

Table A.1: Rules for FLC Version 1

F / F_dot	Low	Medium	High
LN	Low	Low	Low
SN	Low	Medium	Medium
Z	Low	Medium	High
SP	Medium	High	High
LP	High	High	High

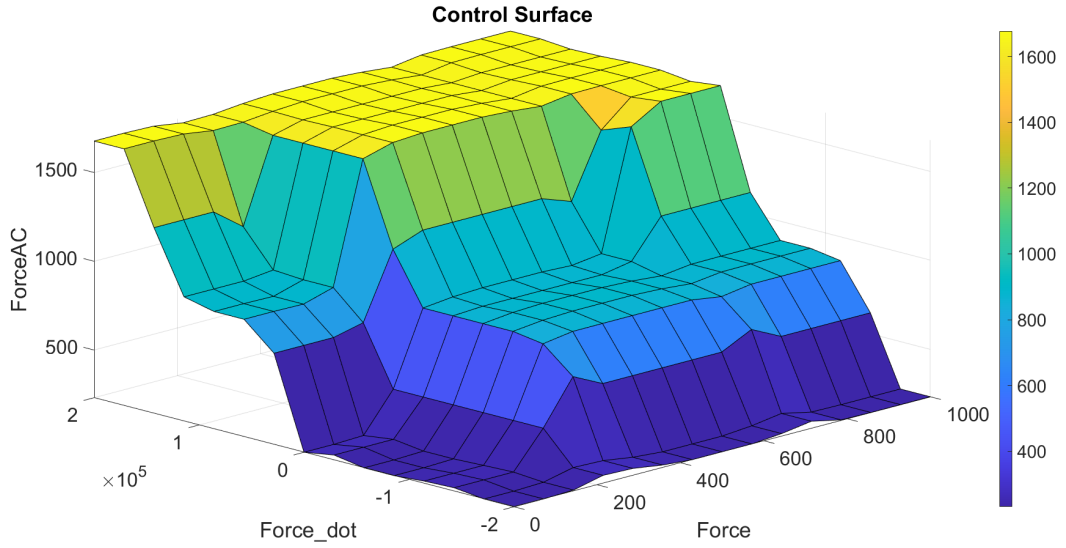

Figure A.4: The output control surface generated by the rules (Forces in N and Force_dot in N/s)

The Ankle model was given a sinusoidal activation with 1.111 Hz as shown in Figure 4.13. The function used to determine the sinusoid is given in the Equation 4.2.

The control loop block diagram is shown in Figure A.5 and A.6

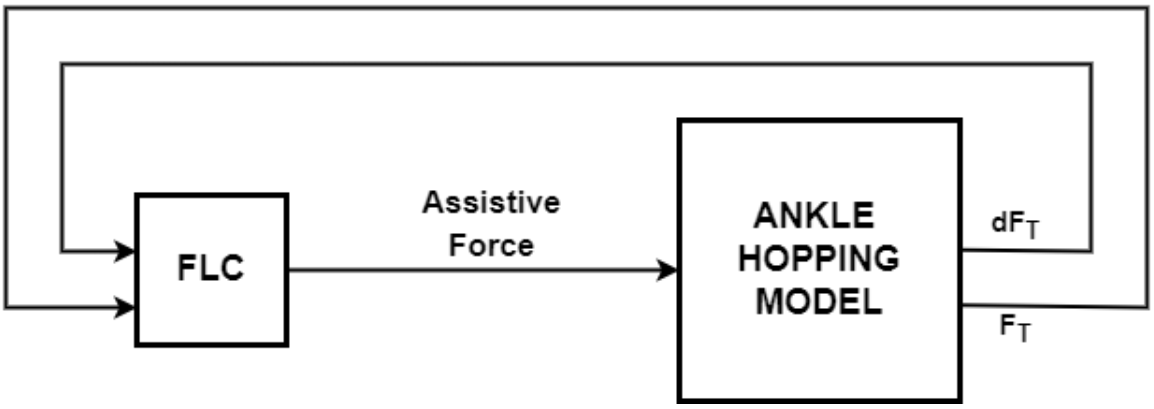

Figure A.5: The control loop is shown here with the FLC and Ankle Hopping Model

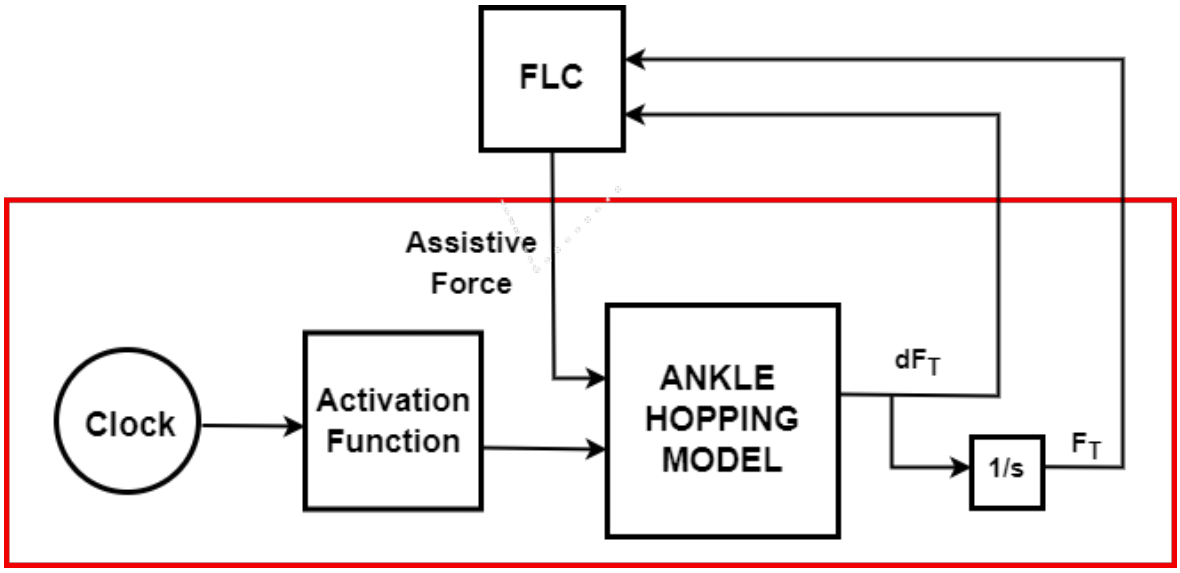

Figure A.6: Ankle Hopping Model Design is shown here

A.2 Basic Fuzzy logic Control

The input membership functions were modified to use Gaussian fuzzy sets, as shown in Figures A.7 toA.9. Gaussian curves were used for fuzzy sets to enable smoother contours for the control surface. The number of fuzzy sets was also increased to provide finer control over the system. The rules for this version of FLC are shown in Table A.2.The resultant control surface is also shown in Figure A.10. Since the controller in the previous section was always active, a minimum threshold of around 900N (an arbitrary force value below 1000N) was chosen for the tendon

force input. A condition block in Simulink was added to execute this, thus activating the FLC only when the tendon force was above 900N. The updated block diagram is shown in Figure 4.3.

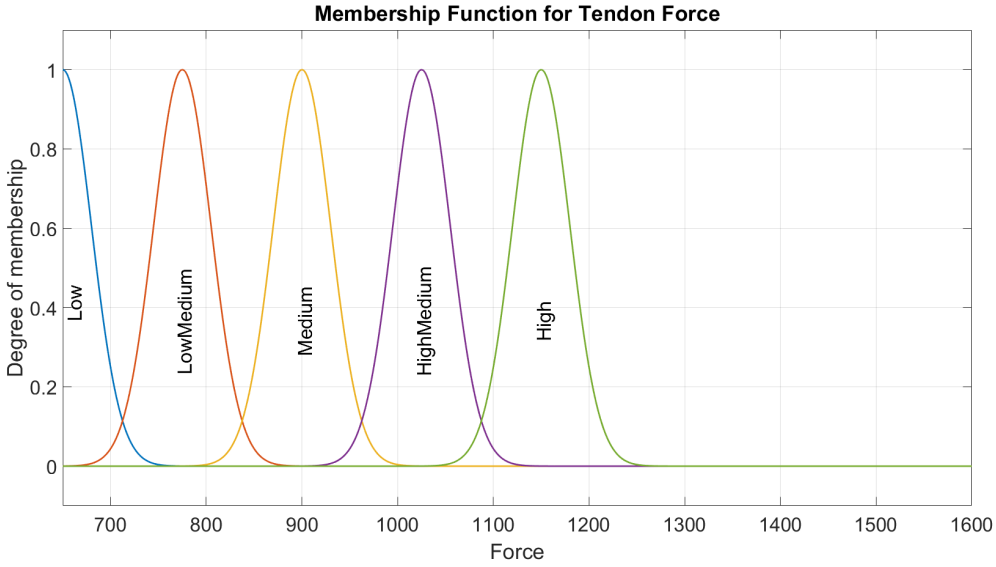

Figure A.7: The input membership function for the Tendon Force (N) with a Threshold introduced

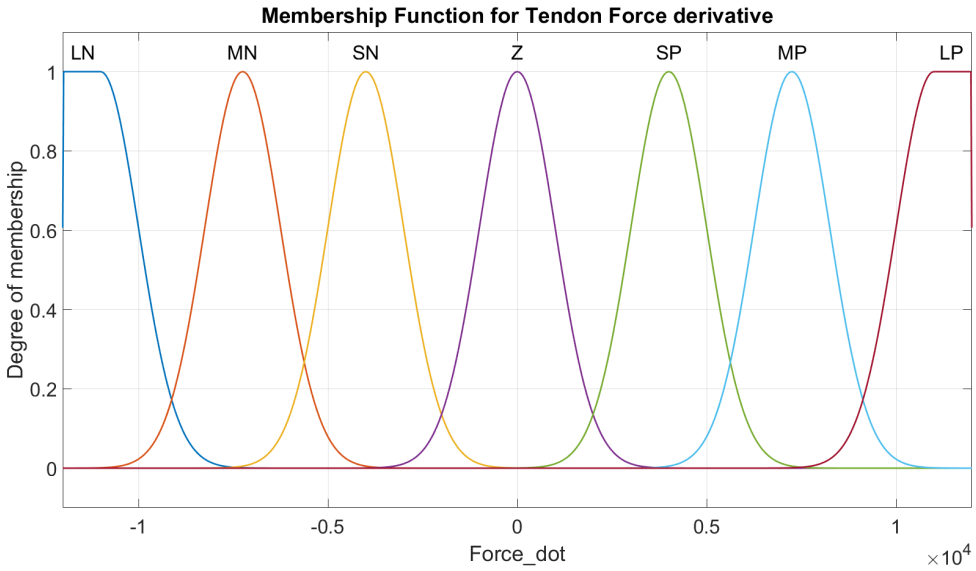

Figure A.8: The input membership function for the Tendon Force Derivative (N/s)

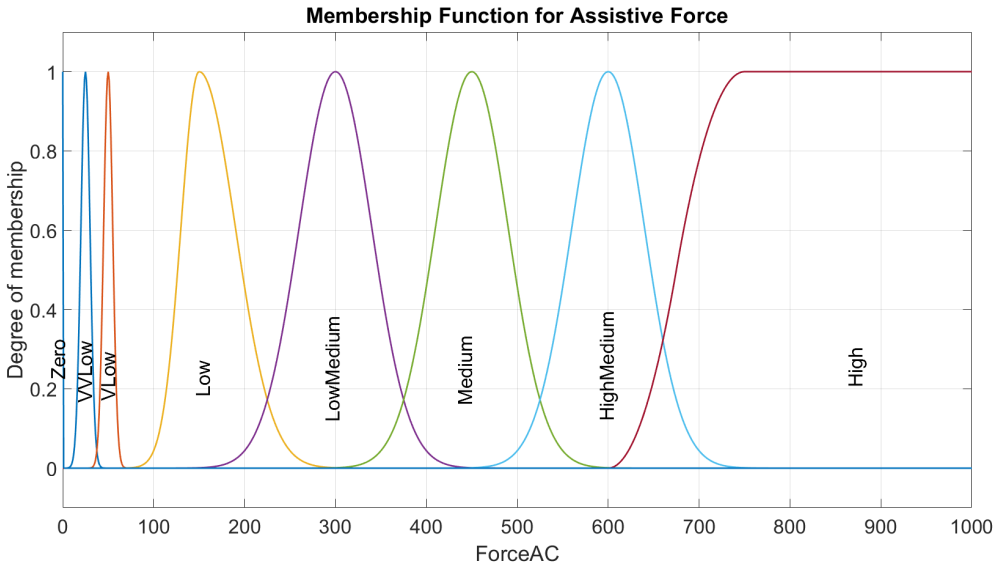

Figure A.9: The output membership function for the Assistive Force (N)

Table A.2: Rules for FLC Version 2

F / F_dot	Low	LowMedium	Medium	HighMedium	High
LN	Zero	Zero	Zero	Zero	Zero
MN	Zero	Zero	Zero	Zero	VVLow
SN	Zero	Zero	Zero	VVLow	VLow
Z	Zero	Zero	Zero	VLow	Low
SP	Zero	Zero	VVLow	Low	LowMedium
MP	Zero	VVLow	VLow	LowMedium	Medium
LP	Zero	VLow	Low	Medium	HighMedium

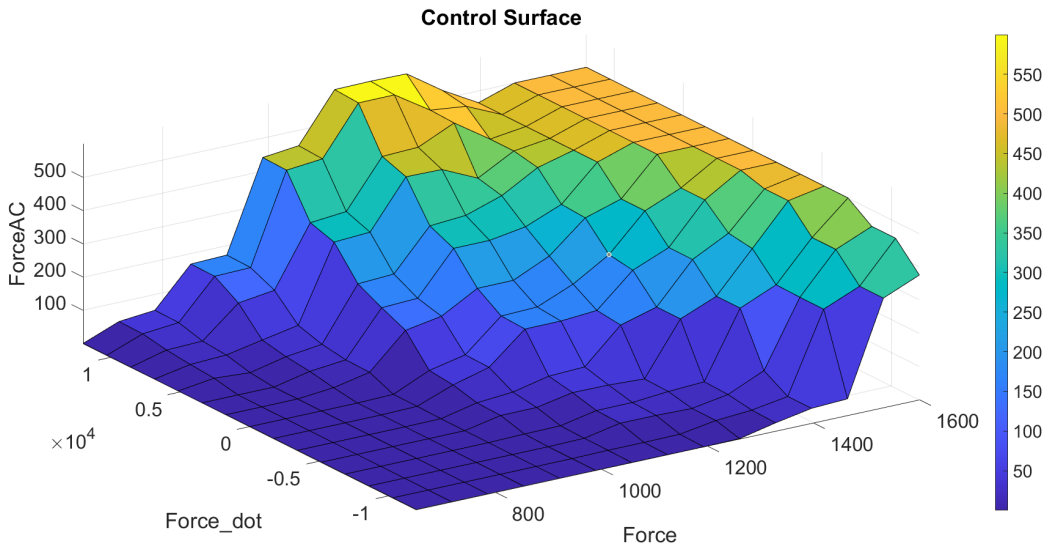

Figure A.10: The output control surface generated by the rules (Forces in N and Force_dot in N/s)

This controller was then used to check if it works for different frequencies by substituting 100, 150 and 200 as values for ω in 4.2. These ω values create sinusoids of frequencies 1.111Hz, 1.388Hz and 1.667Hz, respectively. The response have been discussed in the next chapter.

A.3 Frequency-Adaptive Fuzzy Logic Systems (FAFLC)

This version has been discussed in Chapter 4. Here the design choices for this controller regarding the membership functions and the different control surfaces are discussed.

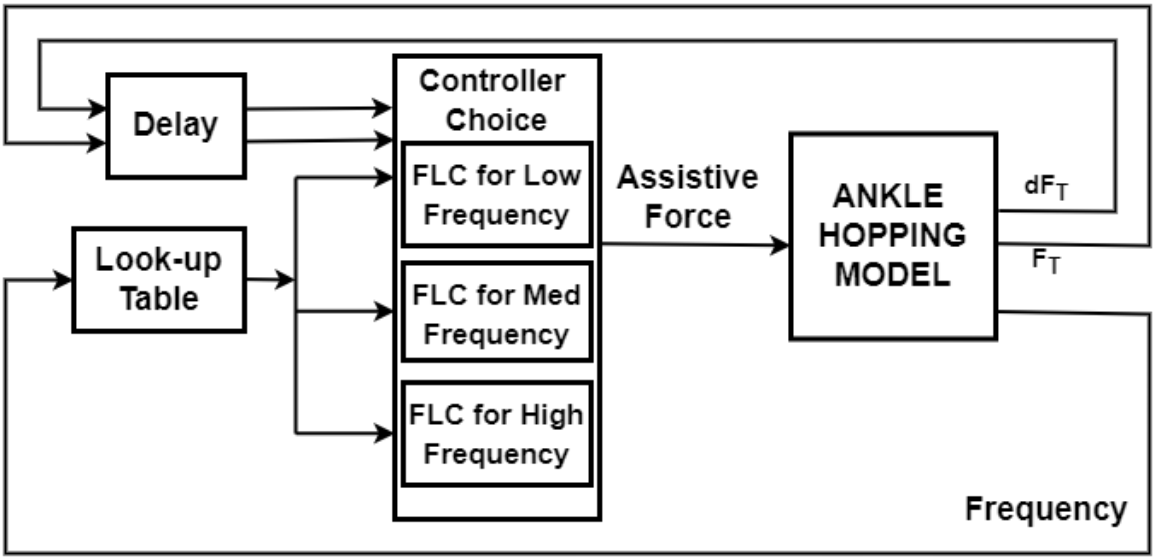

Figure A.11: The control loop with Look-up Table, FLC and Ankle Hopping Model

Along with these changes, the membership functions were again updated. This time, the range of Tendon Force was increased, now ranging in [0 2000]N. The number of fuzzy sets was also increased from 5 to 10. Also, the Simulink function block used for gating the tendon force below 900N was removed and instead incorporated as a fuzzy set in the tendon force membership function. The range of the membership function for Assisstive force (ForceAC) was set as [0, 1000]N. The number of fuzzy sets for the same was increased to 9. These changes can be seen in Figures A.12 and A.13, respectively. The number of fuzzy sets was increased in both membership functions. The 'VVLow' fuzzy set was eliminated. The 'High' fuzzy set was changed from an s-shaped function to a Gaussian function, and the 'VLow' and 'XHigh' fuzzy sets were designed as z-shaped and s-shaped functions in Figure A.13.

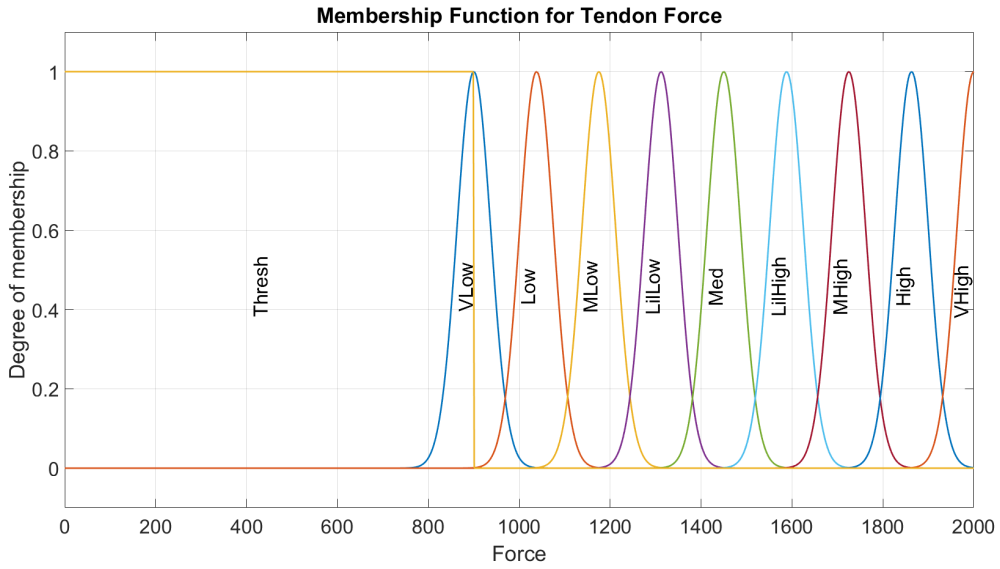

Figure A.12: The input membership function for the Tendon Force (N) with a Threshold introduced

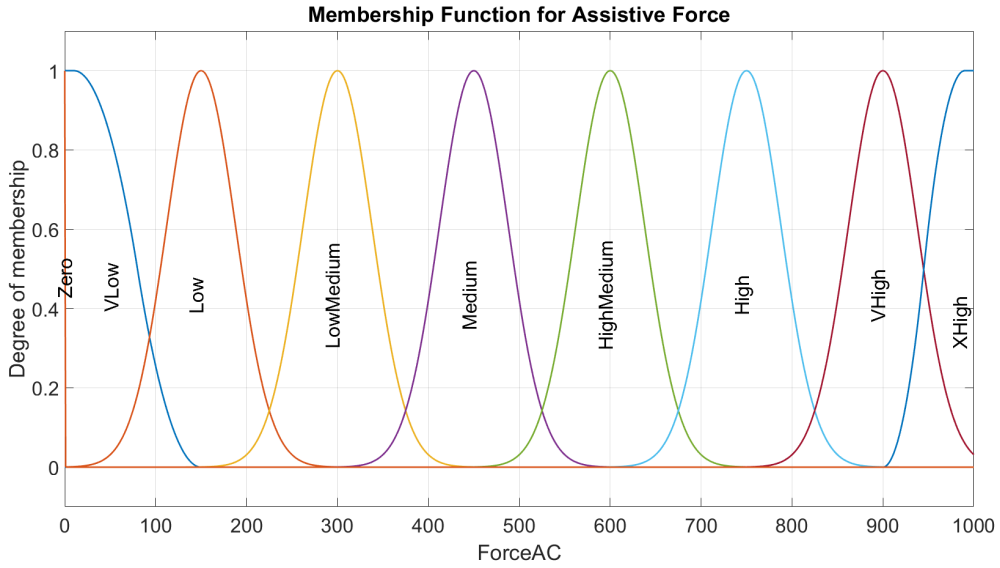

Figure A.13: The output membership function for the Assistive Force (N)

The rules for the three controllers, Low frequency, Medium frequency and High frequency, are given in Tables A.3 to A.5. These have been designed by trial and error based on the trends noticed in the uncontrolled tendon force.

Table A.3: Rule Table for Low Frequencies

F / F_dot	Thresh	Vlow	Low	MediumLow	LilLow	Medium	LilHigh	MHigh	High	VHigh
LN		Zero	Zero	Zero	Zero	Zero	Zero	Zero	Zero	Zero
MN		Zero	Zero	Zero	Zero	Zero	Zero	Zero	Zero	Zero
SN		Zero	Zero	Zero	Zero	Zero	Zero	Zero	Zero	Zero
Z	Zero	Zero	Zero	Zero	VLow	Low	Low	Low	LowMedium	VHigh
SP		VLow	VLow	VLow	VLow	Low	Medium	Medium	HighMedium	VHigh
MP		Low	Low	Low	Low	Low	HighMedium	High	High	XHigh
LP		Low	LowMedium	LowMedium	Medium	Medium	VHigh	XHigh	XHigh	XHigh

Table A.4: Rule Table for Medium Frequencies

F / F_dot	Thresh	Vlow	Low	MediumLow	LilLow	Medium	LilHigh	MHigh	High
LN		Zero	Zero	Zero	Zero	Zero	Zero	Zero	Zero
MN		Zero	Zero	Zero	Zero	Zero	Zero	Zero	Zero
SN		Zero	Zero	Zero	Zero	Zero	Zero	Zero	Zero
Z	Zero	Zero	Zero	Zero	Zero	Zero	Zero	Low	Low
SP		VLow	VLow	VLow	VLow	Low	Low	Low	LowMedium
MP		VLow	Low	Low	Low	LowMedium	Medium	LowMedium	Medium
LP		VLow	LowMedium	LowMedium	LowMedium	Medium	Medium	Medium	HighMedium

Table A.5: Rule Table for High Frequencies

F / F_dot	Thresh	Vlow	Low	MediumLow	LilLow	Medium	LilHigh	MHigh	High	VHigh
LN		Zero	Zero	Zero	Zero	Zero	Zero	Zero	Zero	Zero
MN		Zero	Zero	Zero	Zero	Zero	Zero	Zero	Zero	Zero
SN		Zero	Zero	Zero	Zero	Zero	Zero	Zero	Zero	Zero
Z	Zero	VLow	Zero	Zero	VLow	VLow	Low	Medium	High	VHigh
SP		Low	Low	Low	Medium	HighMedium	HighMedium	VHigh	Vhigh	XHigh
MP		LowMedium	LowMedium	HighMedium	HighMedium	High	High	VHigh	Xhigh	XHigh
LP		LowMedium	Medium	High	High	VHigh	VHigh	XHigh	XHigh	XHigh

The control surfaces for the same have been shown from Figure A.14 to A.16

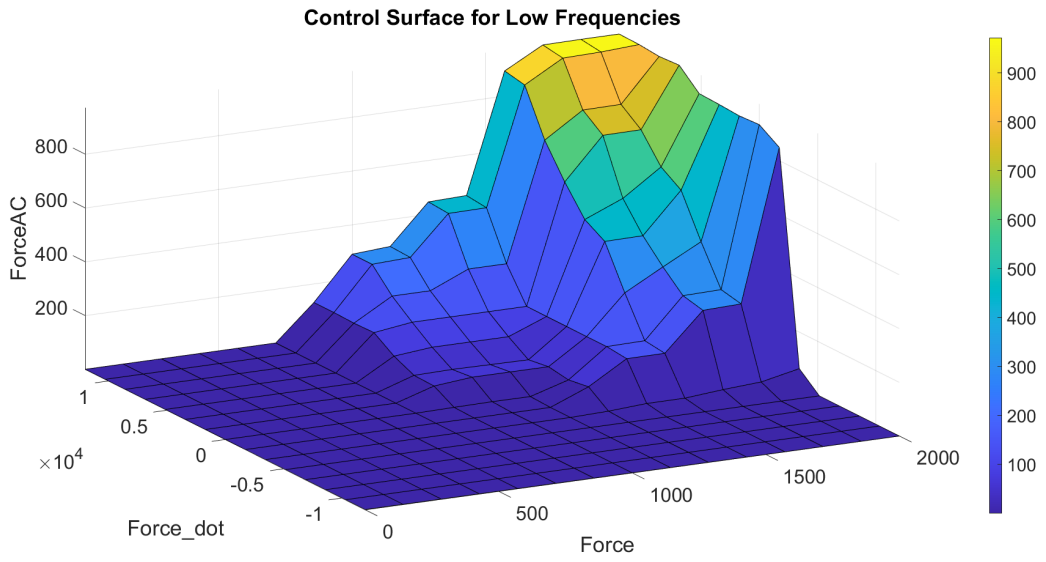

Figure A.14: The output control surface generated for Low Frequencies (Forces in N and Force_dot in N/s)

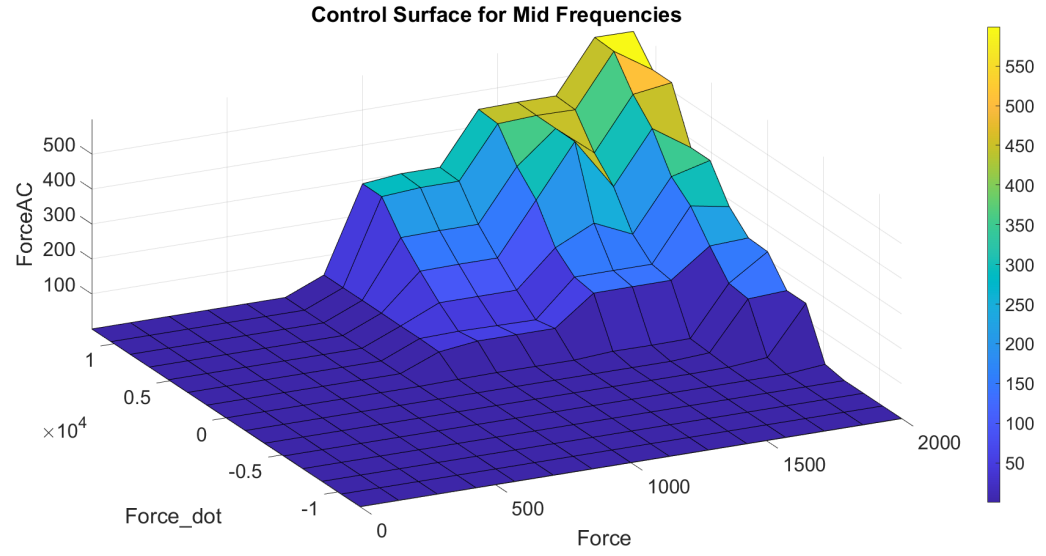

Figure A.15: The output control surface generated for Medium Frequencies (Forces in N and Force_dot in N/s)

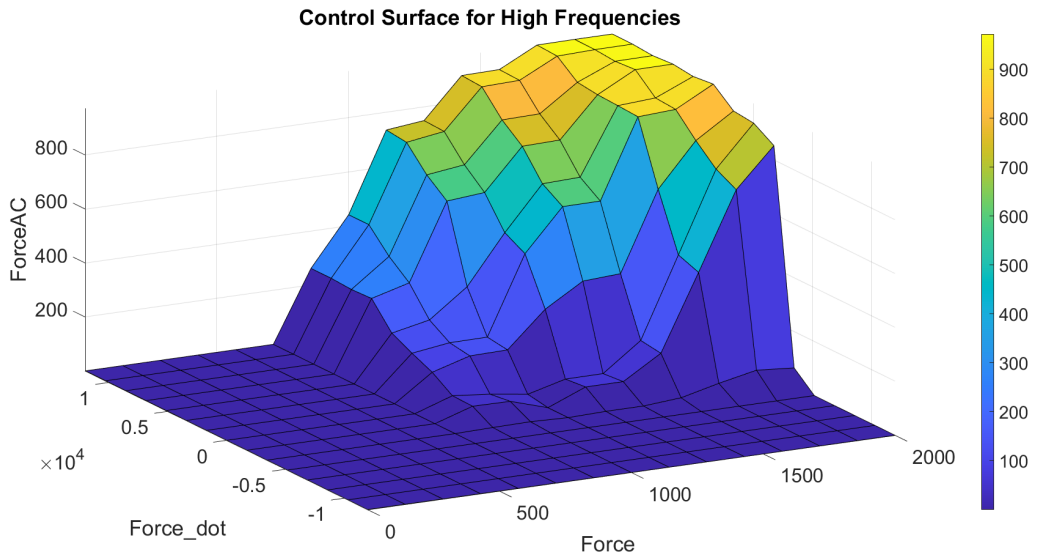

Figure A.16: The output control surface generated for Low Frequencies (Forces in N and Force_dot in N/s)

A.3.1 Margin based FLC

An additional FIS was designed and added parallel to the existing controller as a side quest. The objective of this controller was to aggravate the controller output if it detected that the tendon force was approaching a set upper limit. This method was conceptualised in an attempt to limit the maximum tendon force exerted by the subject. The input to this FIS was the difference between the maximum required limit of the tendon force and the current tendon force, which was deemed the ”Margin”. The FIS then outputs an additional assistive force based on the margin remaining. This is shown as a block diagram in Figure A.17. The membership function for the Margin and the additional assistive force are shown in Figure A.18 and Figure A.20, respectively. The rules for the output control surface is given in Table A.6 and the control Surface is show in Figure A.20.

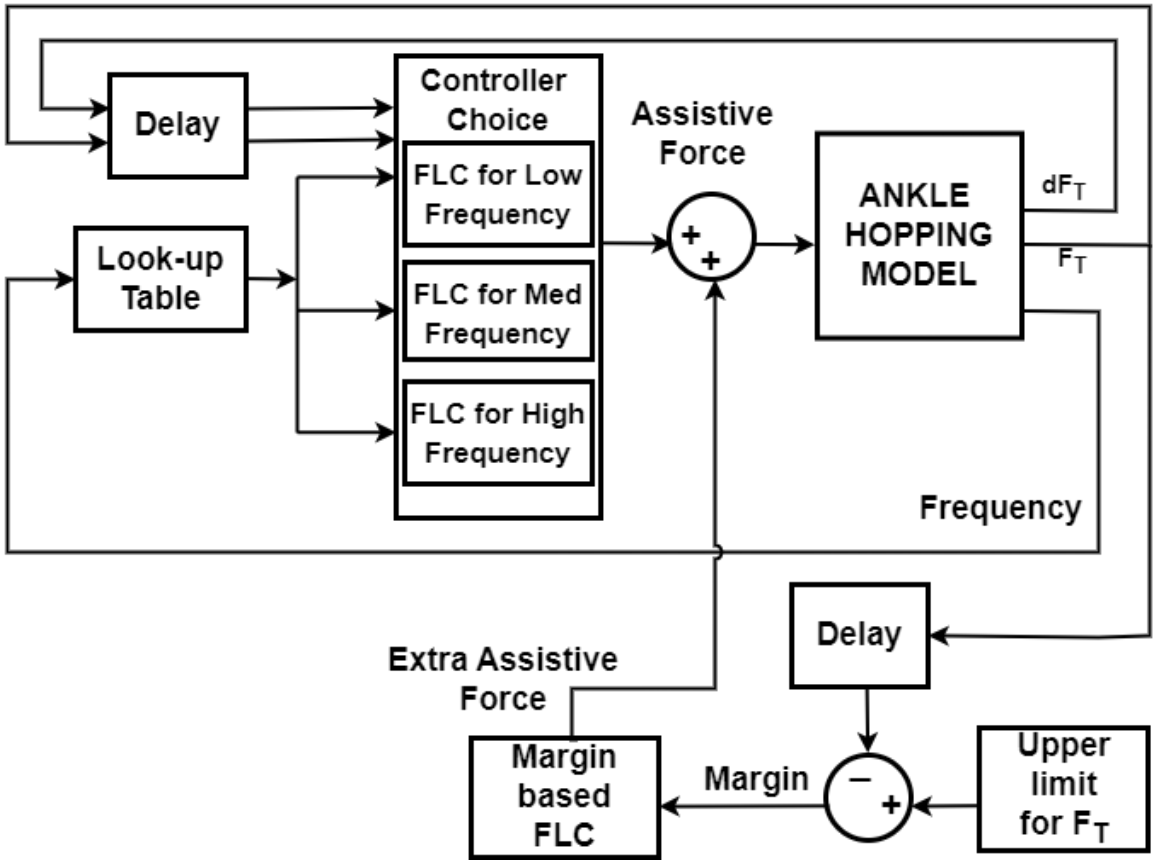

Figure A.17: The control loop with the Margin based FLC and Ankle Hopping Model

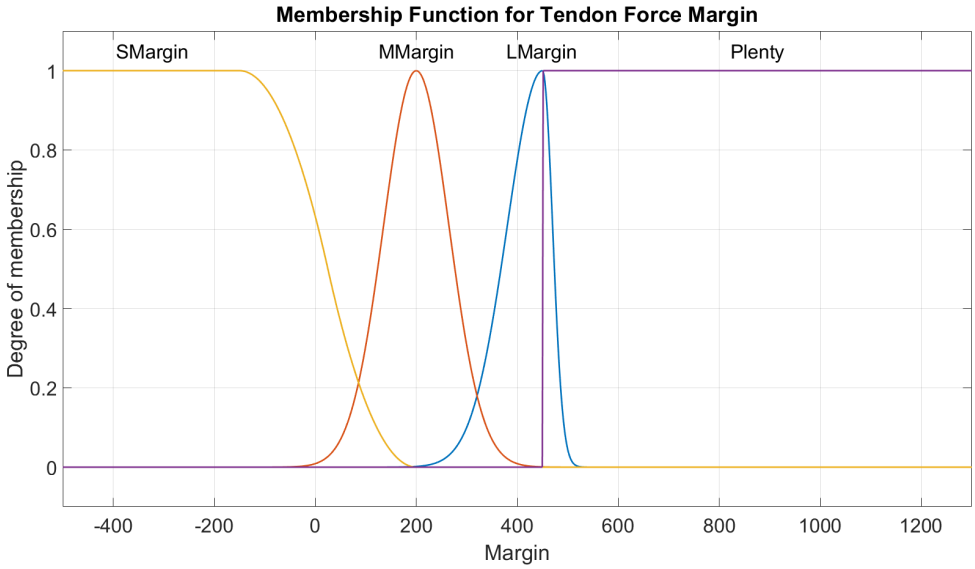

Figure A.18: The Margin Membership Function

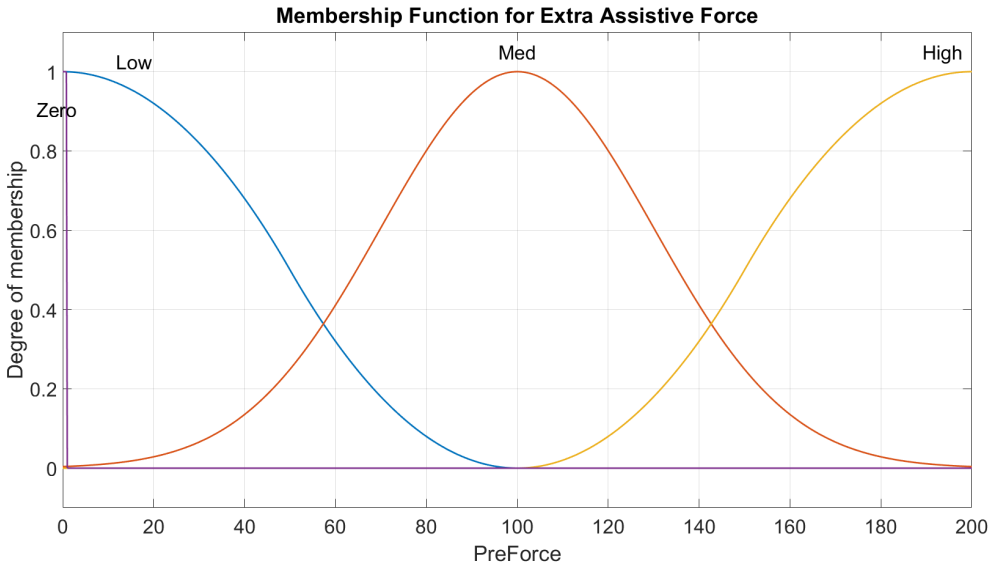

Figure A.19: The Extra Assistive Force Membership Function

Table A.6: Margin

INPUT	OUTPUT
Margin	**Preforce**
Plenty	Zero
Lmargin	Low
Mmargin	Med
Smargin	High

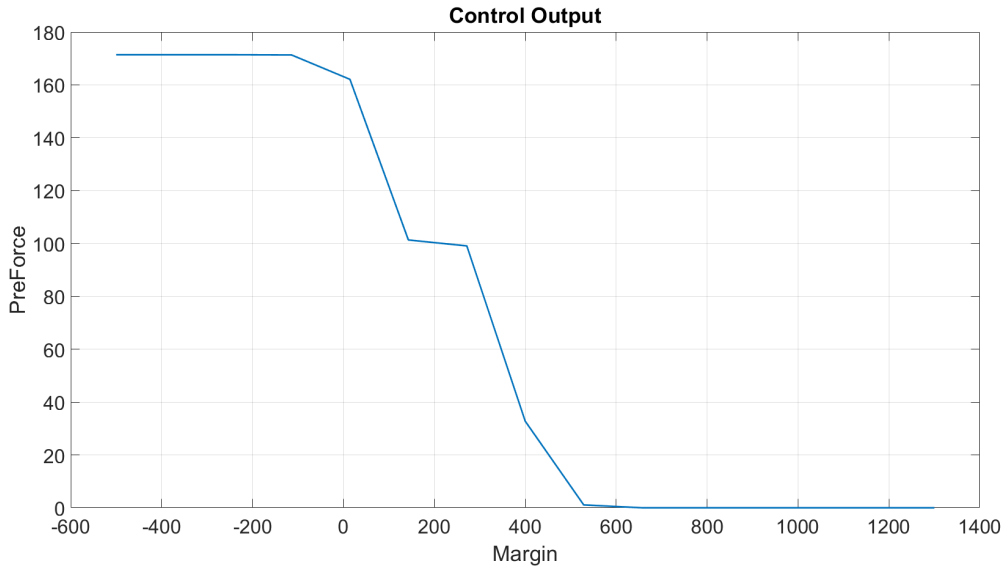

Figure A.20: The Control Output of the Margin FLC

Appendix B

Appendix B: Results for the Controllers in Appendix A

B.1 Initial Design of FLC

The initial design of FLC was simulated with a sinusoidal activation as shown in Figure B.1

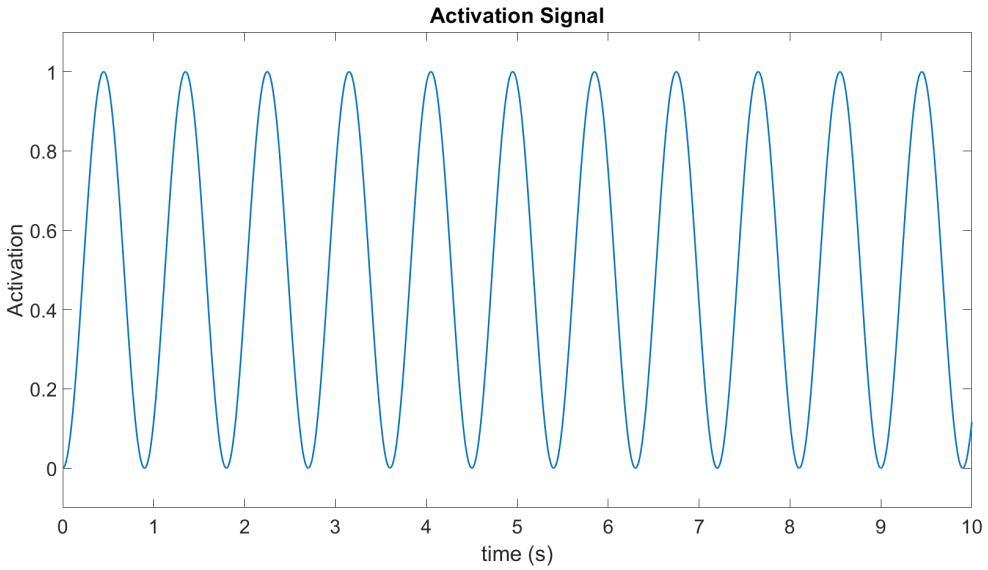

Figure B.1: A sinusoidal activation function of frequency 1.111Hz

This controller was designed to output assistive force upwards of 1500 N. However, the design objective for this controller was to reduce the tendon force which it achieved as observed in Figure B.2

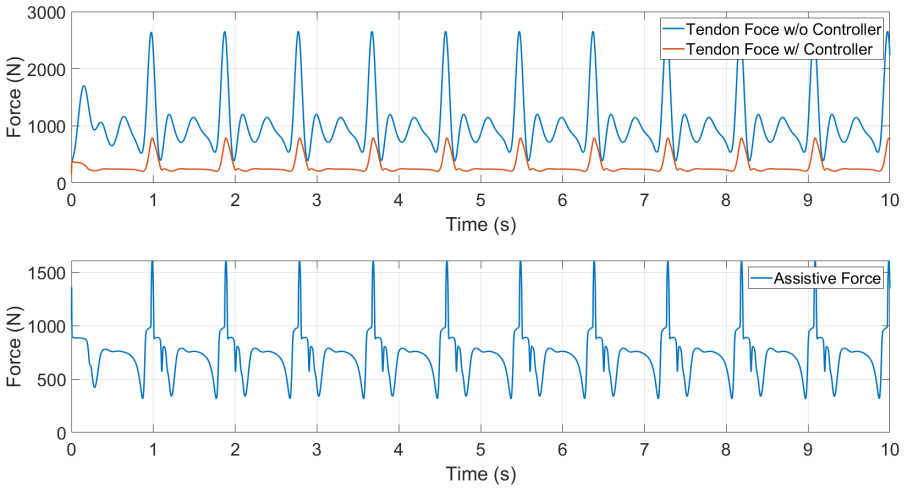

Figure B.2: For the initial controller design: (Top) Comparison between Tendon Force with and without assistance. (Bottom) Assistive Force

B.2 Basic Fuzzy Logic Control

To recall, model version 2 had an if-else function block, which allowed the controller to activate only when the Tendon Force was greater than 900N. For model version 2, the activation function input is the same as that for model version 1 shown in Figure B.1.

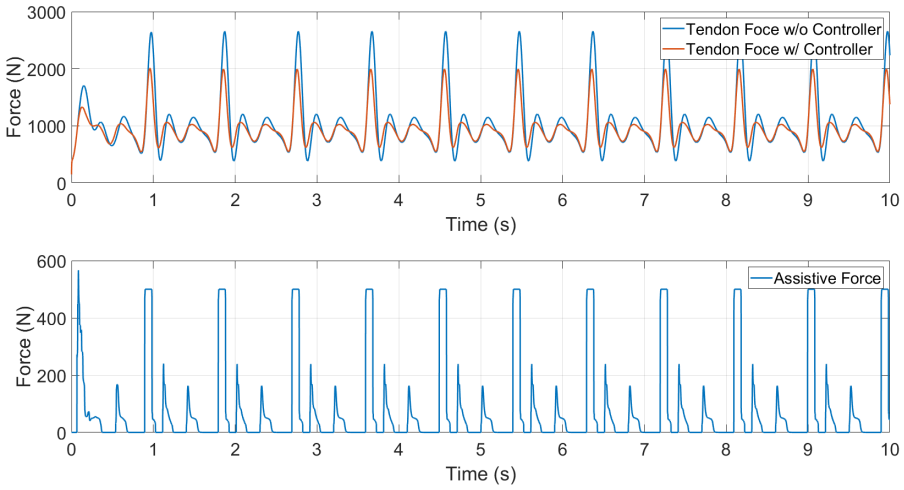

Figure B.3: For Controller and Model version 2: (Top) Comparison between Tendon Force with and without assistance. (Bottom) Assistive Force

This controller was then also run with sinusoidal activation of multiple frequencies

(1.111Hz, 1.388Hz, and 1.667Hz). The response is shown below in Figure B.4. From the figure, it is evident that the controller cannot maintain the tendon force for varying frequency under a particular limit.

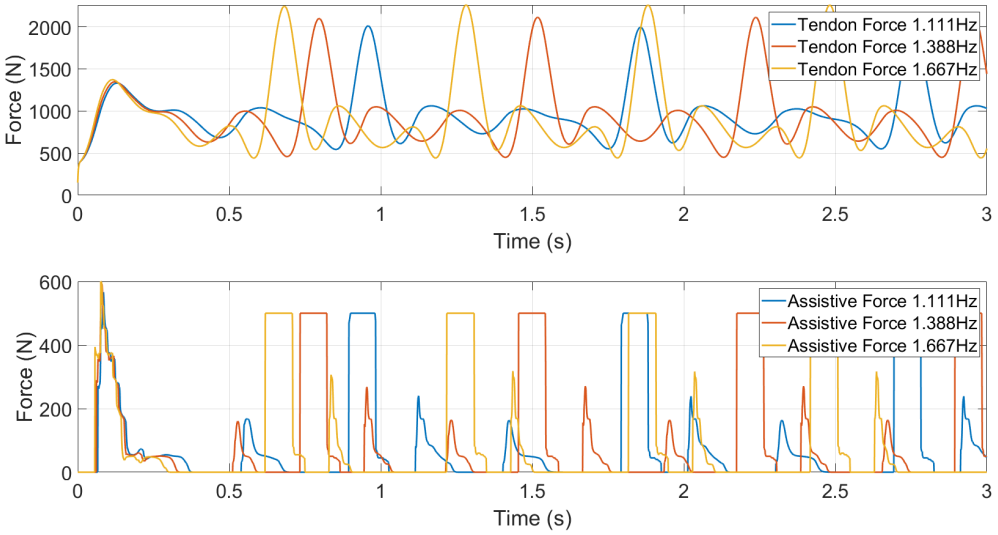

Figure B.4: (Top) Tendon Force at multiple frequencies (Note the max tendon forces at each frequency). (Bottom) The assistive forces for the same frequencies.

B.3 Fuzzy Logic Controller with Normalized Inputs (NIFLC) for Walking

The walking activations obtained from Sartori et al. [23] were used to test the Normalised Inputs controller for walking. The results are shown in Figures **??** to **??**. The upper limit was set ranging from 1200 N to 1500 N. The Speeds vary in 1kmph, 3kmph and 5kmph. Elevation varies in -20%, 0% and 20%. The top plot shows comparison between the controlled and uncontrolled tendon force. The bottom plot depicts the assistive force. For all the cases the controller is able to maintain the tenon force below the upper limit.

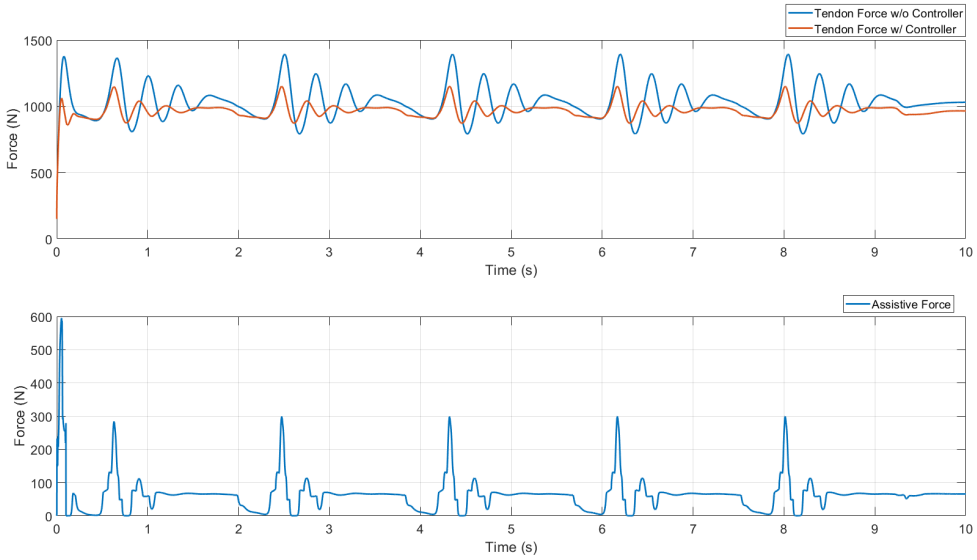

Figure B.5: NIFLC, Speed 1kmph, Elevation -20%, Upper limit on Tendon Force 1200N: (Top) Comparison between Tendon Force with and without assistance. (Bottom) Assistive Force

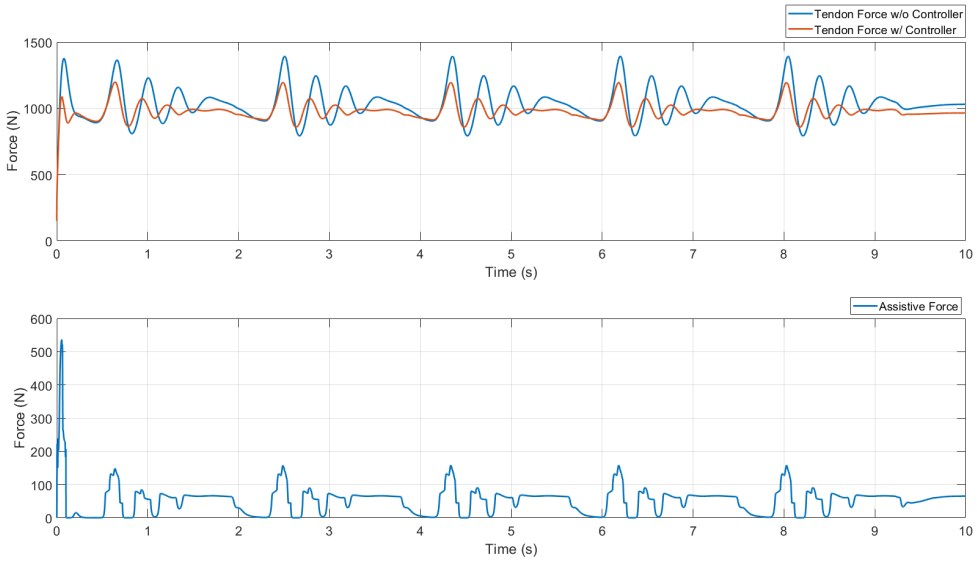

Figure B.6: NIFLC, Speed 1kmph, Elevation -20%, Upper limit on Tendon Force 1300N: (Top) Comparison between Tendon Force with and without assistance. (Bottom) Assistive Force

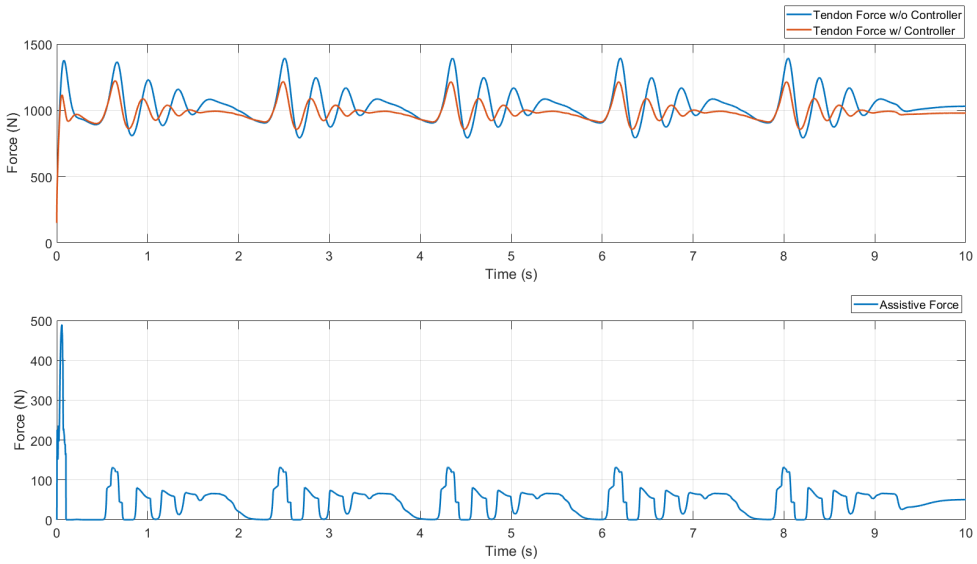

Figure B.7: NIFLC, Speed 1kmph, Elevation -20%, Upper limit on Tendon Force 1400N: (Top) Comparison between Tendon Force with and without assistance. (Bottom) Assistive Force

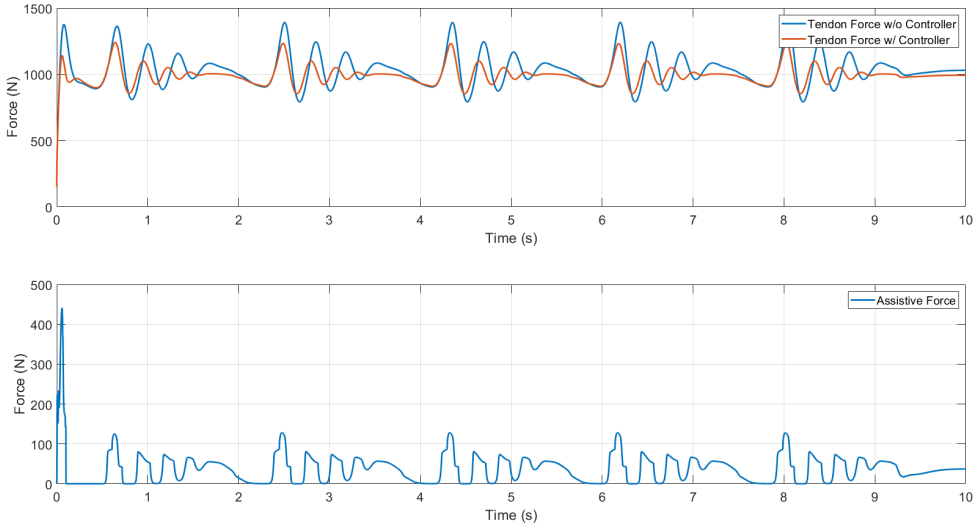

Figure B.8: NIFLC, Speed 1kmph, Elevation -20%, Upper limit on Tendon Force 1500N: (Top) Comparison between Tendon Force with and without assistance. (Bottom) Assistive Force

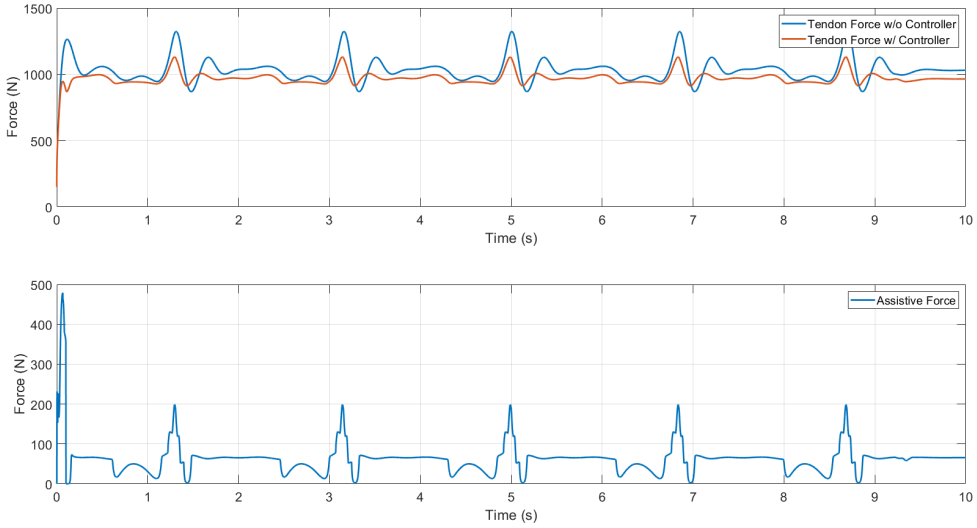

Figure B.9: NIFLC, Speed 1kmph, Elevation 0%, Upper limit on Tendon Force 1200N: (Top) Comparison between Tendon Force with and without assistance. (Bottom) Assistive Force

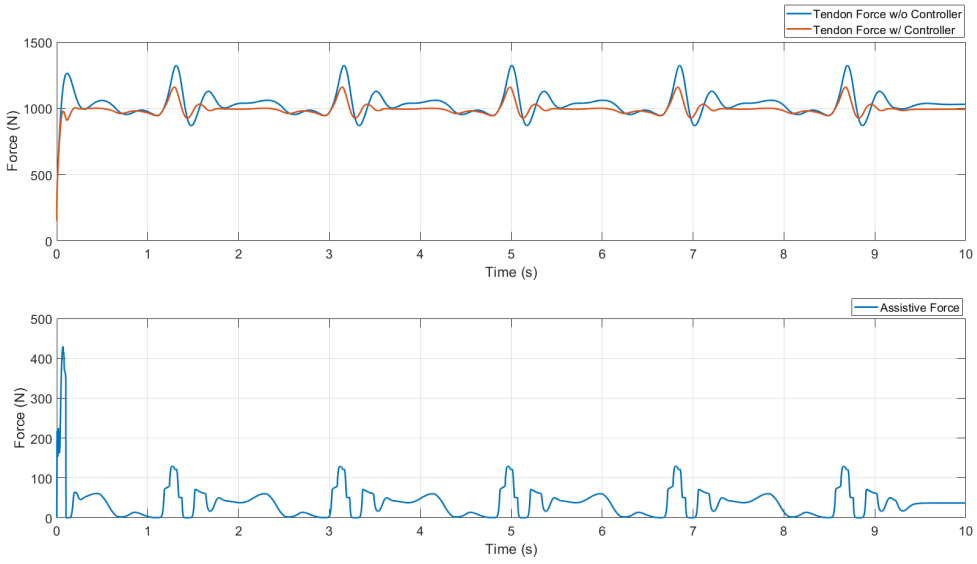

Figure B.10: NIFLC, Speed 1kmph, Elevation 0%, Upper limit on Tendon Force 1300N: (Top) Comparison between Tendon Force with and without assistance. (Bottom) Assistive Force

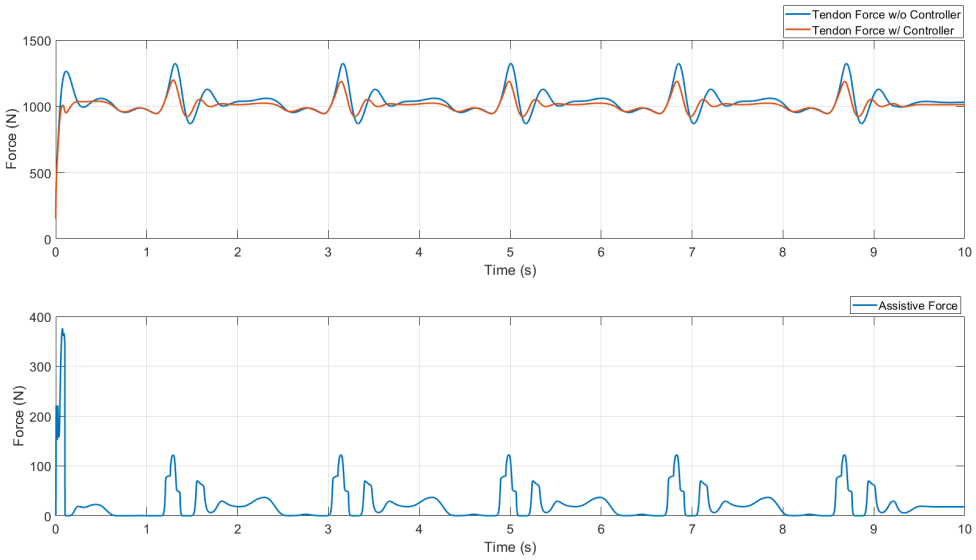

Figure B.11: NIFLC, Speed 1kmph, Elevation 0%, Upper limit on Tendon Force 1400N: (Top) Comparison between Tendon Force with and without assistance. (Bottom) Assistive Force

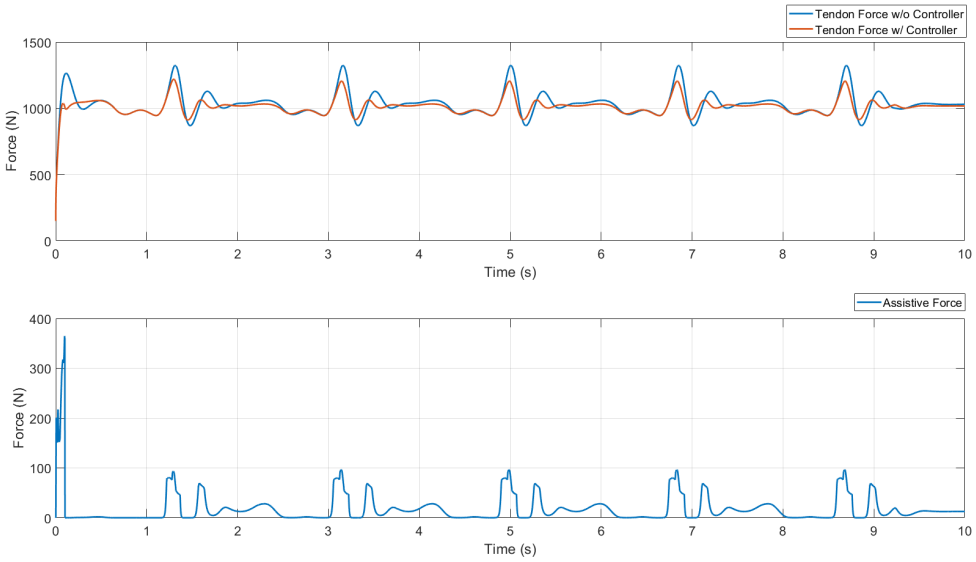

Figure B.12: NIFLC, Speed 1kmph, Elevation 0%, Upper limit on Tendon Force 1500N: (Top) Comparison between Tendon Force with and without assistance. (Bottom) Assistive Force

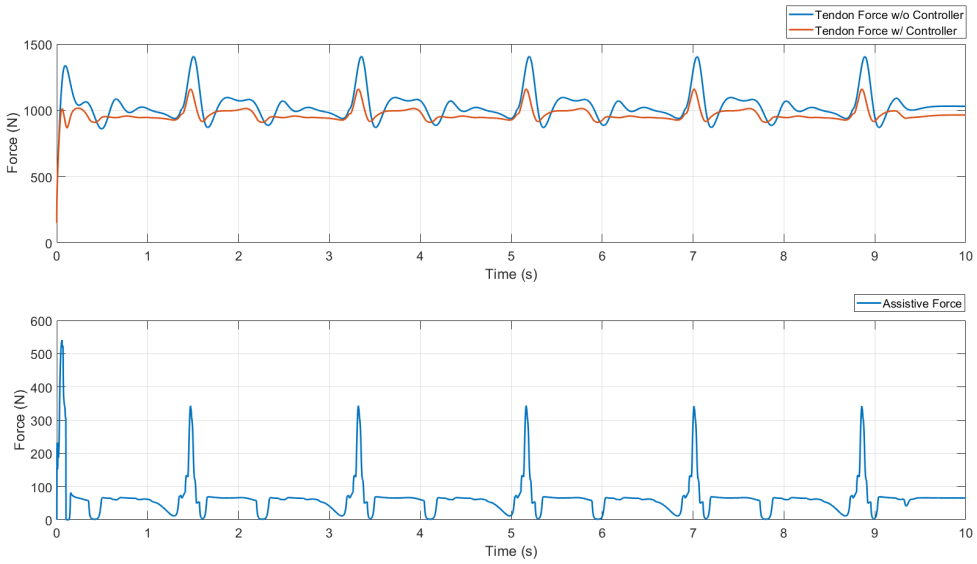

Figure B.13: NIFLC, Speed 1kmph, Elevation 20%, Upper limit on Tendon Force 1200N: (Top) Comparison between Tendon Force with and without assistance. (Bottom) Assistive Force

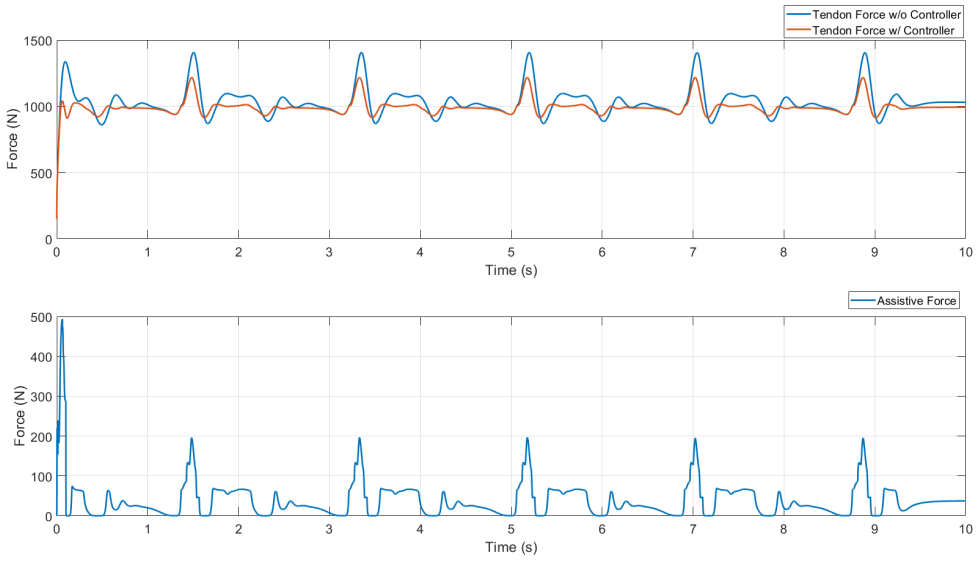

Figure B.14: NIFLC, Speed 1kmph, Elevation 20%, Upper limit on Tendon Force 1300N: (Top) Comparison between Tendon Force with and without assistance. (Bottom) Assistive Force

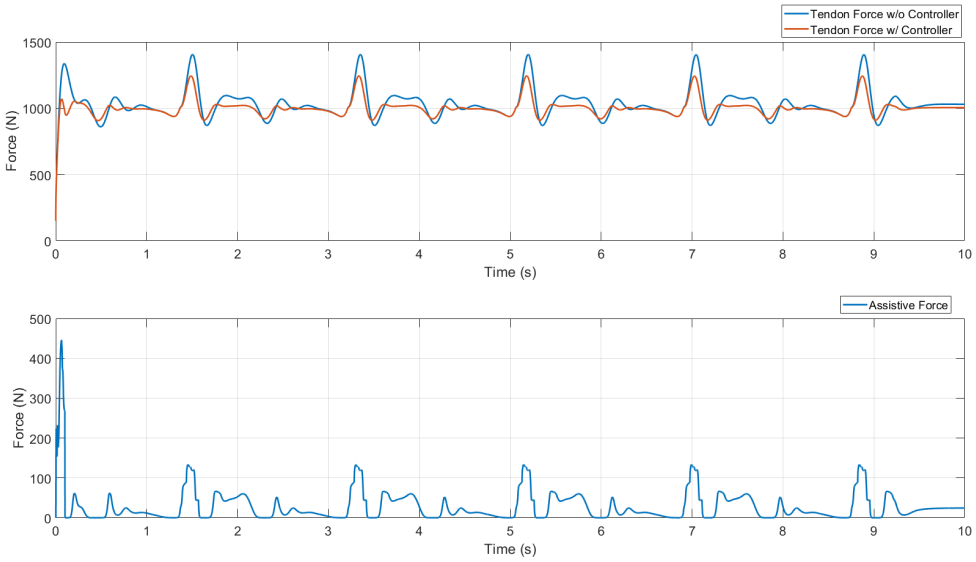

Figure B.15: NIFLC, Speed 1kmph, Elevation 20%, Upper limit on Tendon Force 1400N: (Top) Comparison between Tendon Force with and without assistance. (Bottom) Assistive Force

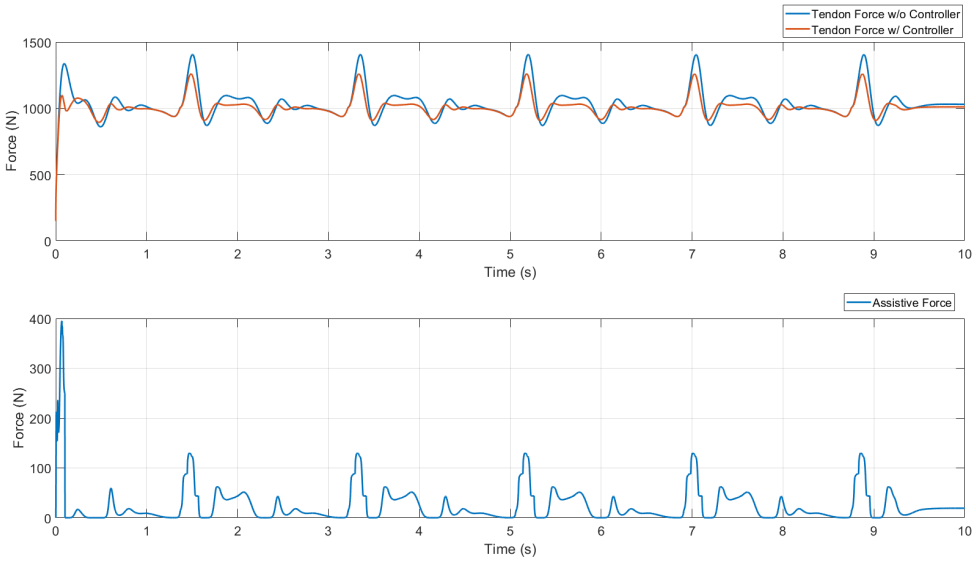

Figure B.16: NIFLC, Speed 1kmph, Elevation 20%, Upper limit on Tendon Force 1500N: (Top) Comparison between Tendon Force with and without assistance. (Bottom) Assistive Force

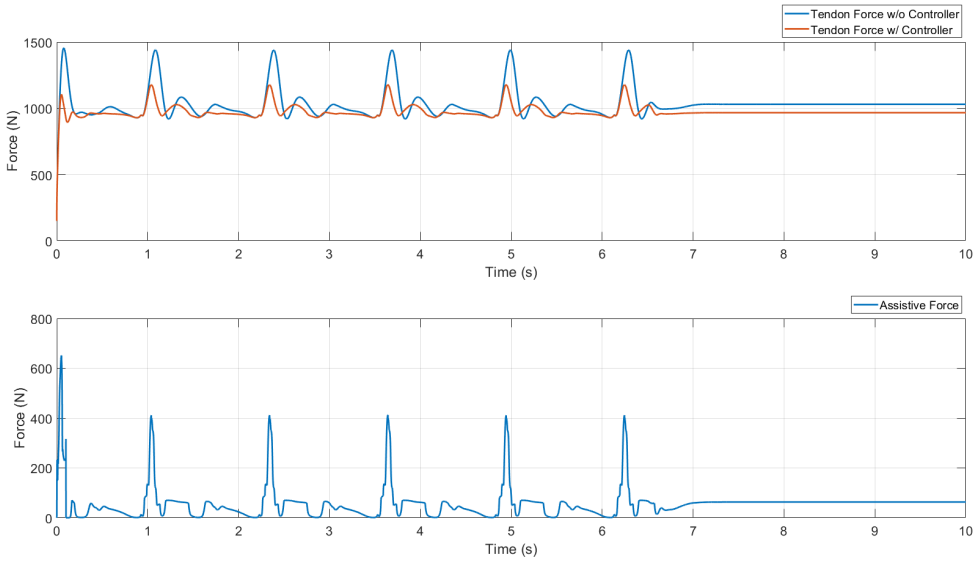

Figure B.17: NIFLC, Speed 3kmph, Elevation -20%, Upper limit on Tendon Force 1200N: (Top) Comparison between Tendon Force with and without assistance. (Bottom) Assistive Force

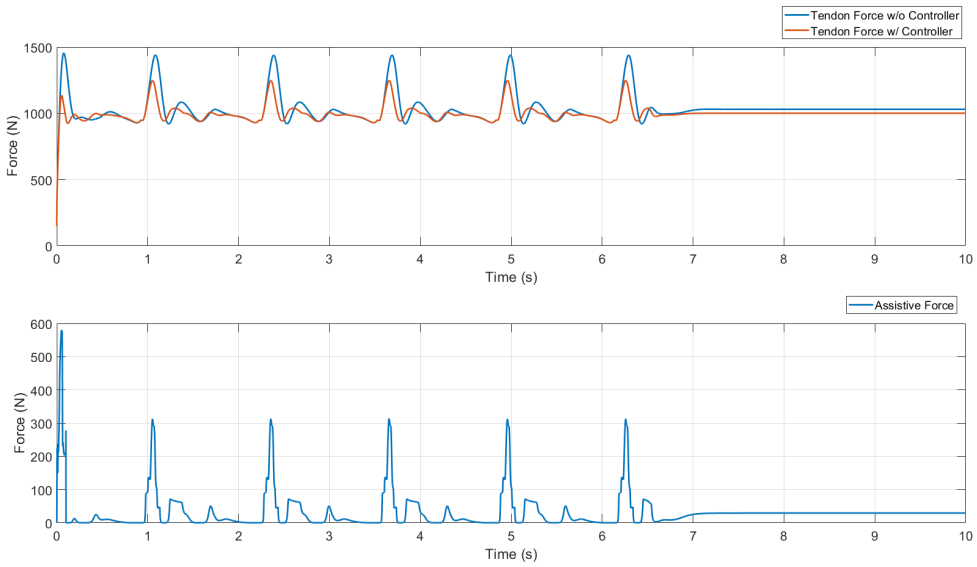

Figure B.18: NIFLC, Speed 3kmph, Elevation -20%, Upper limit on Tendon Force 1300N: (Top) Comparison between Tendon Force with and without assistance. (Bottom) Assistive Force

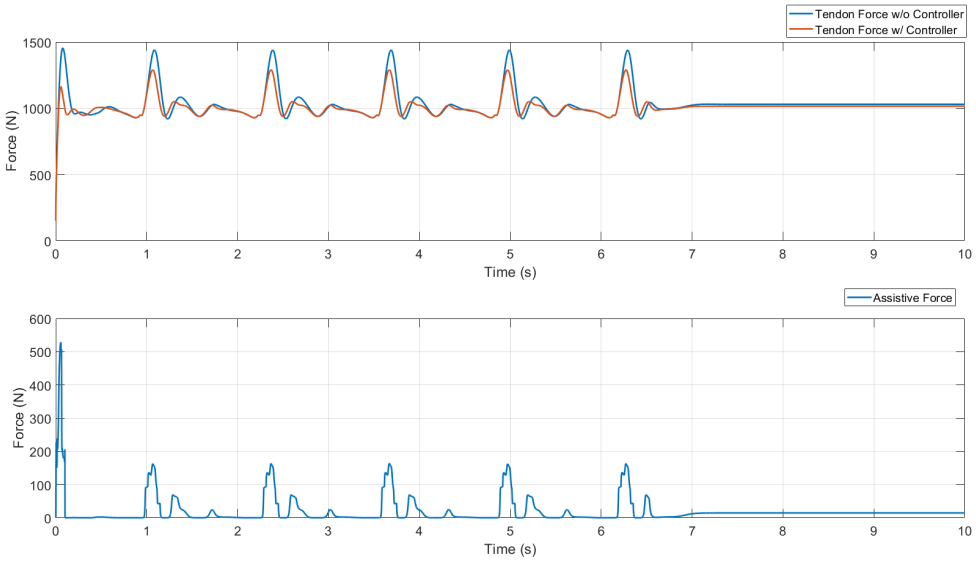

Figure B.19: NIFLC, Speed 3kmph, Elevation -20%, Upper limit on Tendon Force 1400N: (Top) Comparison between Tendon Force with and without assistance. (Bottom) Assistive Force

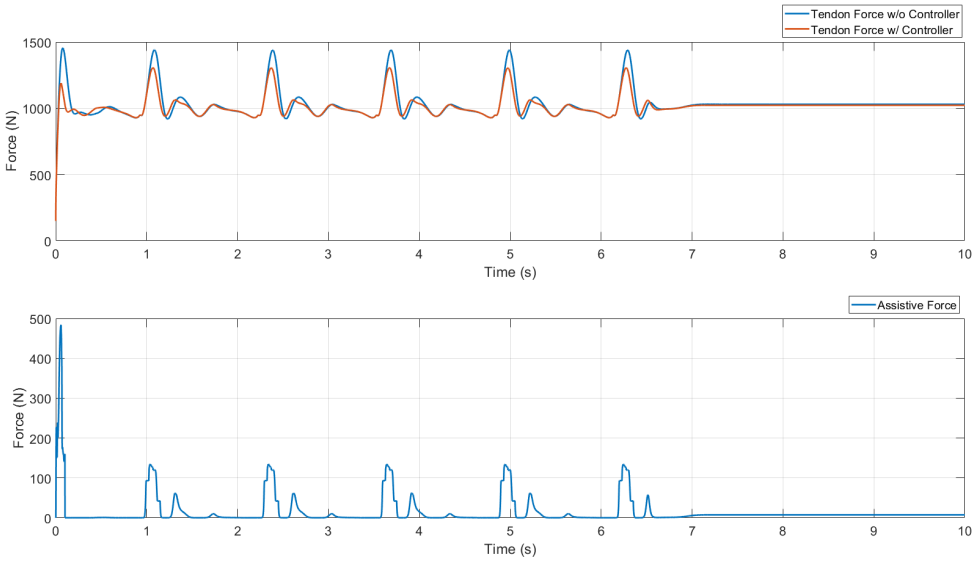

Figure B.20: NIFLC, Speed 3kmph, Elevation -20%, Upper limit on Tendon Force 1500N: (Top) Comparison between Tendon Force with and without assistance. (Bottom) Assistive Force

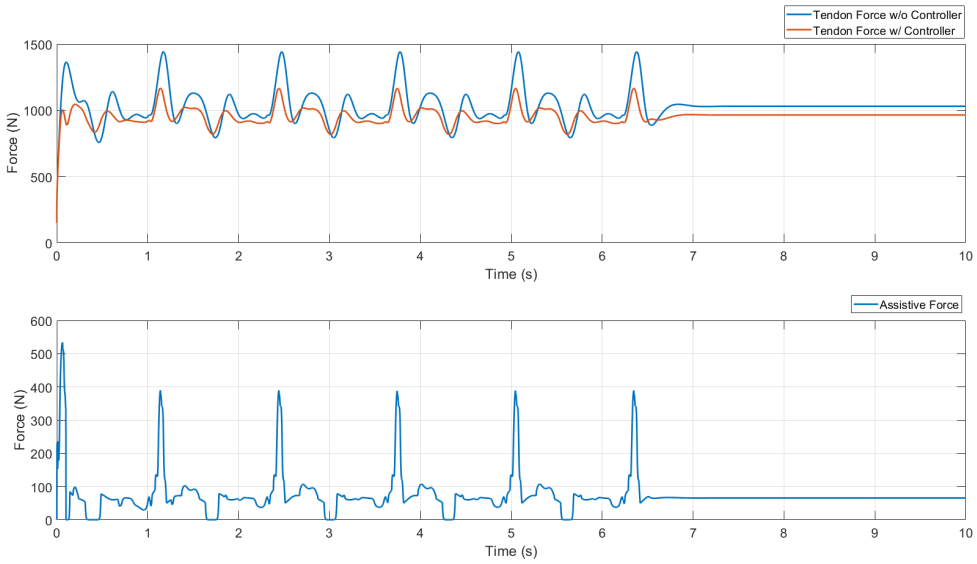

Figure B.21: NIFLC, Speed 3kmph, Elevation 0%, Upper limit on Tendon Force 1200N: (Top) Comparison between Tendon Force with and without assistance. (Bottom) Assistive Force

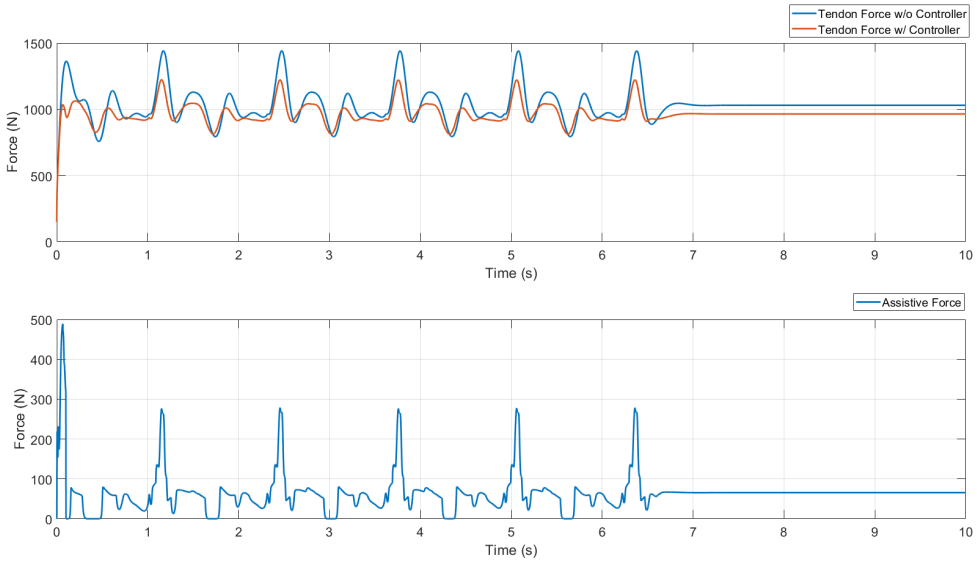

Figure B.22: NIFLC, Speed 3kmph, Elevation 0%, Upper limit on Tendon Force 1300N: (Top) Comparison between Tendon Force with and without assistance. (Bottom) Assistive Force

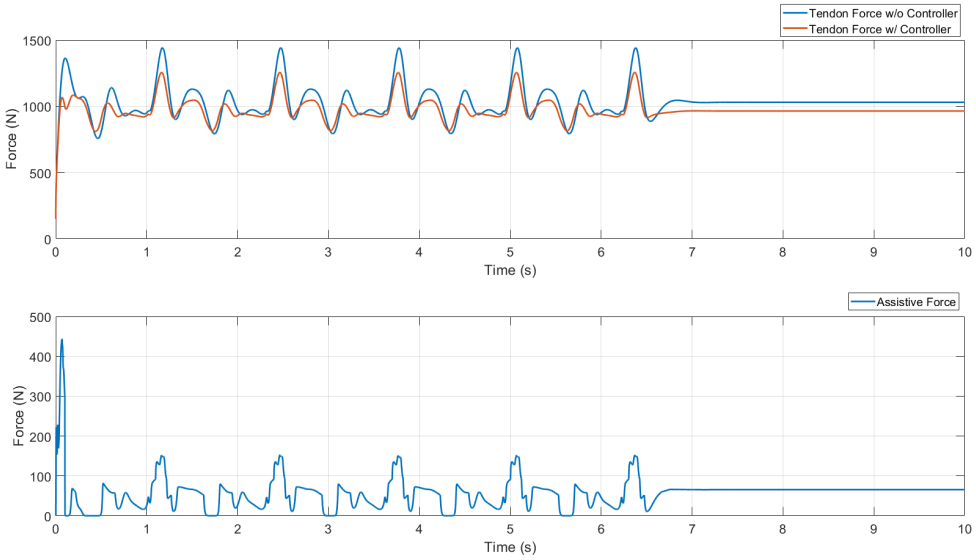

Figure B.23: NIFLC, Speed 3kmph, Elevation 0%, Upper limit on Tendon Force 1400N: (Top) Comparison between Tendon Force with and without assistance. (Bottom) Assistive Force

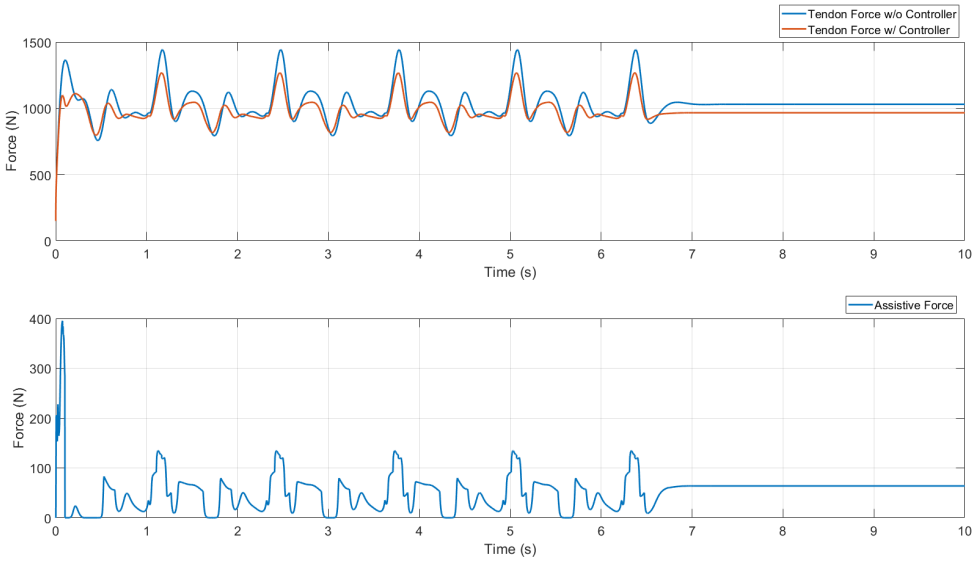

Figure B.24: NIFLC, Speed 3kmph, Elevation 0%, Upper limit on Tendon Force 1500N: (Top) Comparison between Tendon Force with and without assistance. (Bottom) Assistive Force

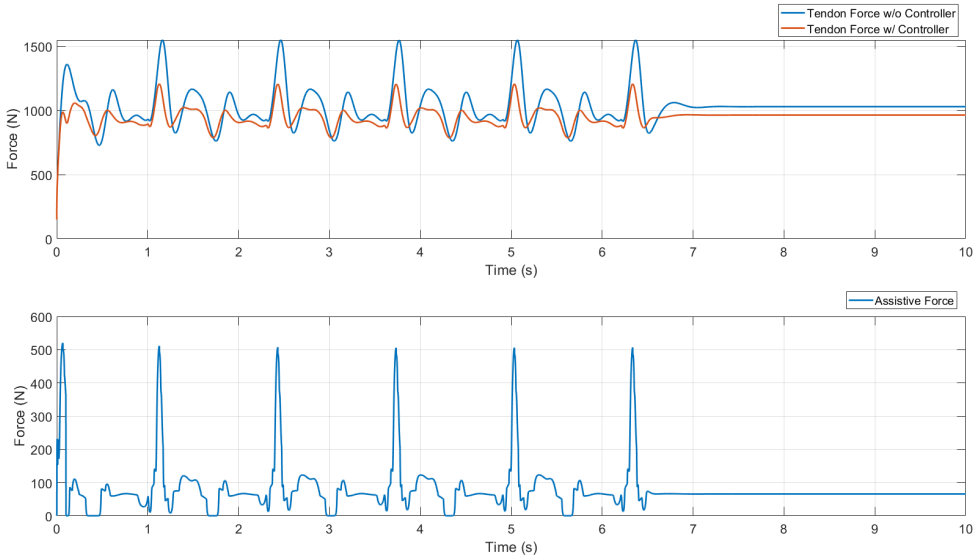

Figure B.25: NIFLC, Speed 3kmph, Elevation 20%, Upper limit on Tendon Force 1200N: (Top) Comparison between Tendon Force with and without assistance. (Bottom) Assistive Force

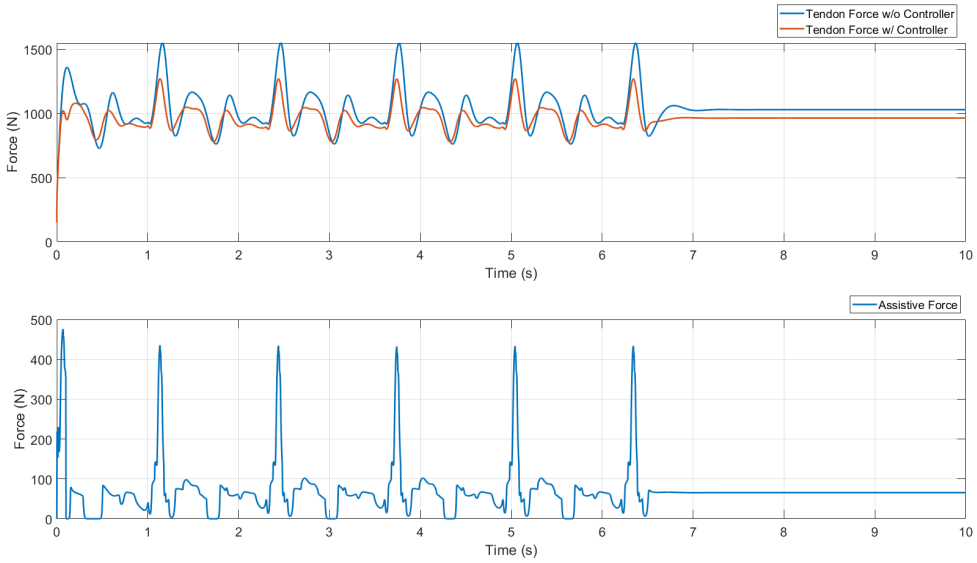

Figure B.26: NIFLC, Speed 3kmph, Elevation 20%, Upper limit on Tendon Force 1300N: (Top) Comparison between Tendon Force with and without assistance. (Bottom) Assistive Force

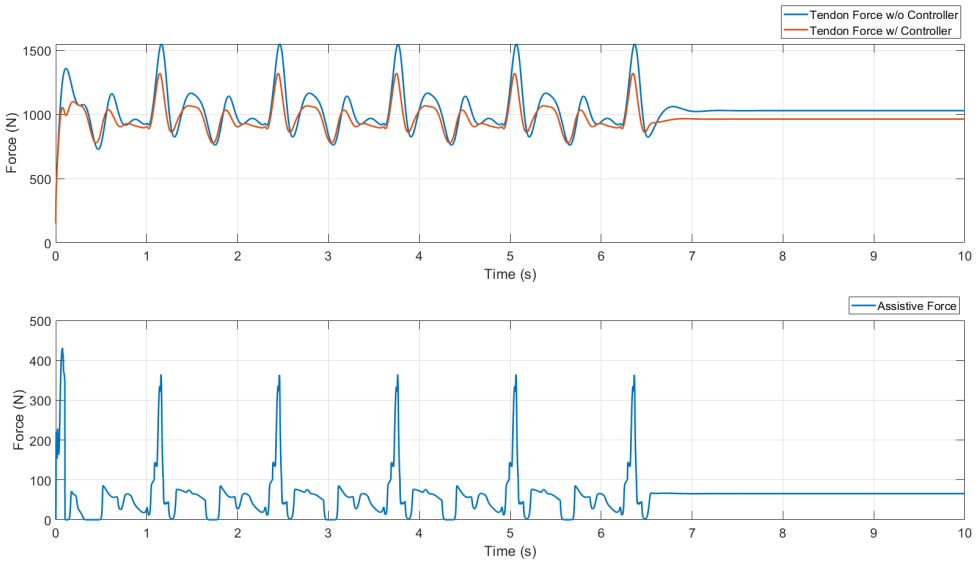

Figure B.27: NIFLC, Speed 3kmph, Elevation 20%, Upper limit on Tendon Force 1400N: (Top) Comparison between Tendon Force with and without assistance. (Bottom) Assistive Force

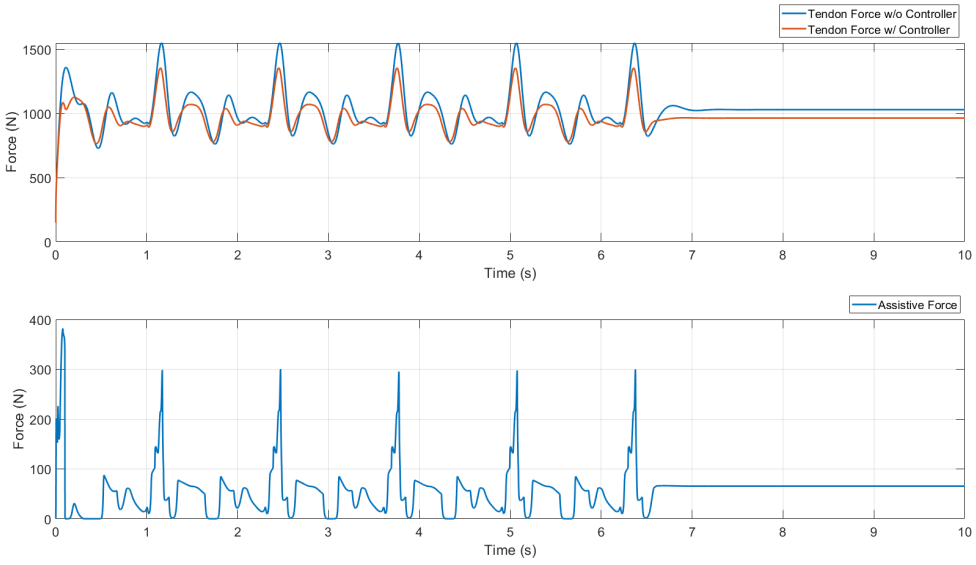

Figure B.28: NIFLC, Speed 3kmph, Elevation 20%, Upper limit on Tendon Force 1500N: (Top) Comparison between Tendon Force with and without assistance. (Bottom) Assistive Force

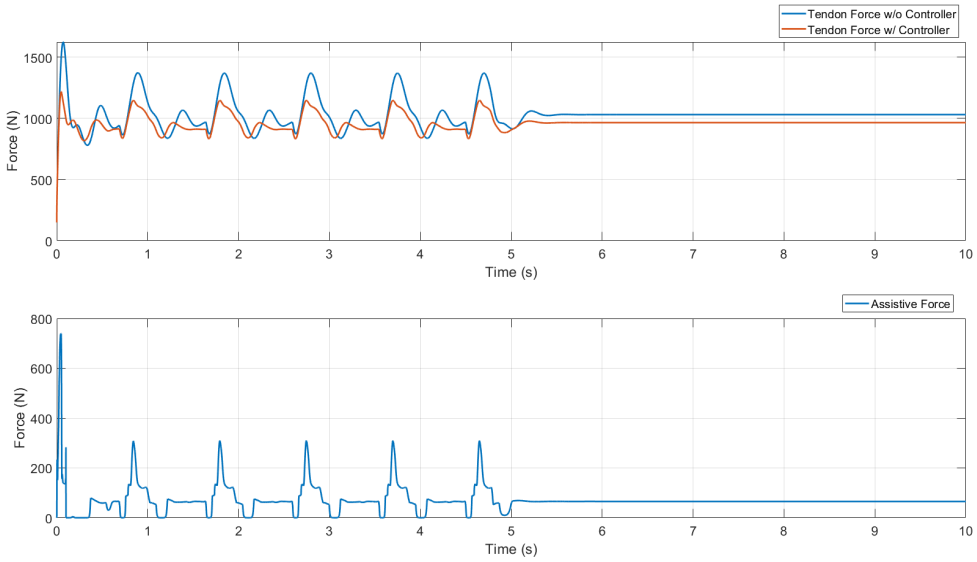

Figure B.29: NIFLC, Speed 5kmph, Elevation -20%, Upper limit on Tendon Force 1200N: (Top) Comparison between Tendon Force with and without assistance. (Bottom) Assistive Force

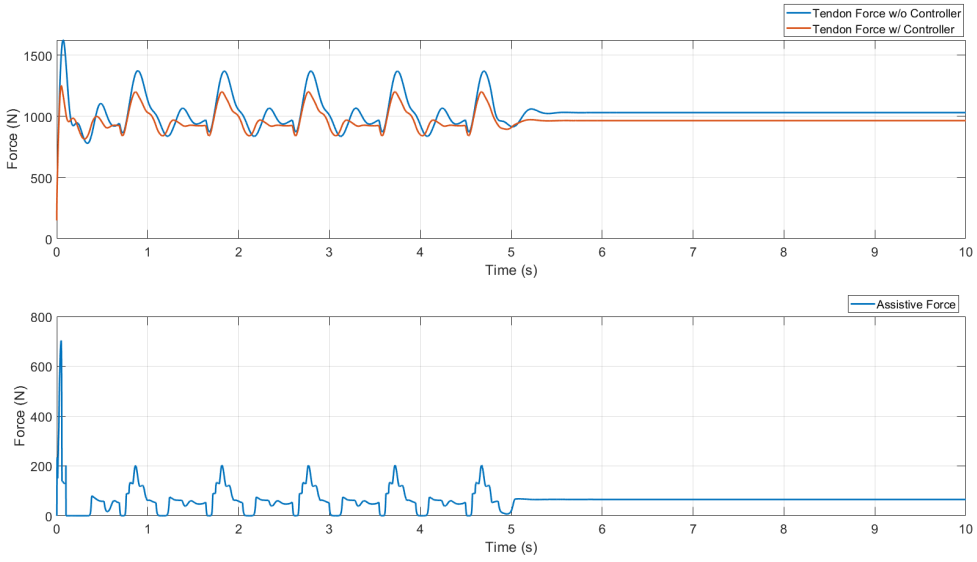

Figure B.30: NIFLC, Speed 5kmph, Elevation -20%, Upper limit on Tendon Force 1300N: (Top) Comparison between Tendon Force with and without assistance. (Bottom) Assistive Force

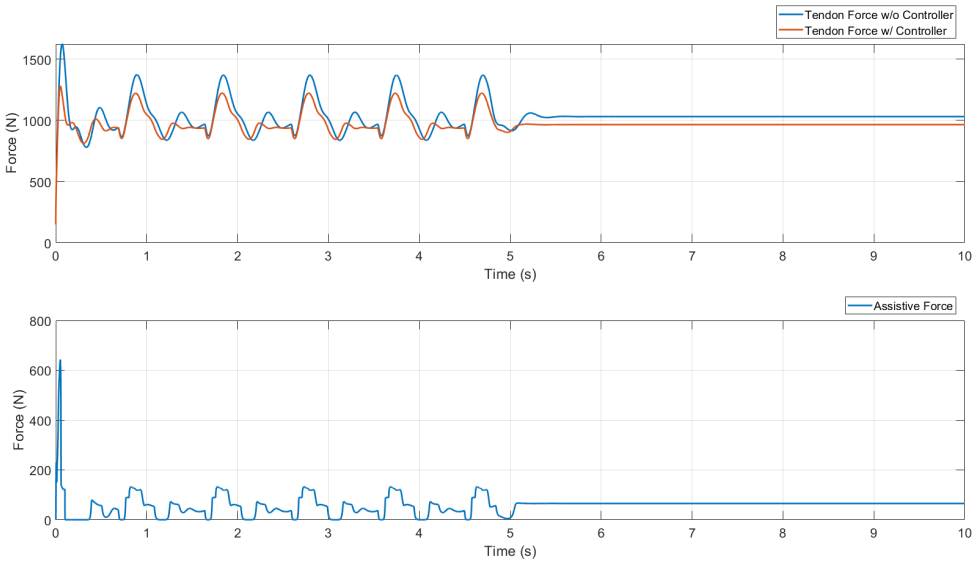

Figure B.31: NIFLC, Speed 5kmph, Elevation -20%, Upper limit on Tendon Force 1400N: (Top) Comparison between Tendon Force with and without assistance. (Bottom) Assistive Force

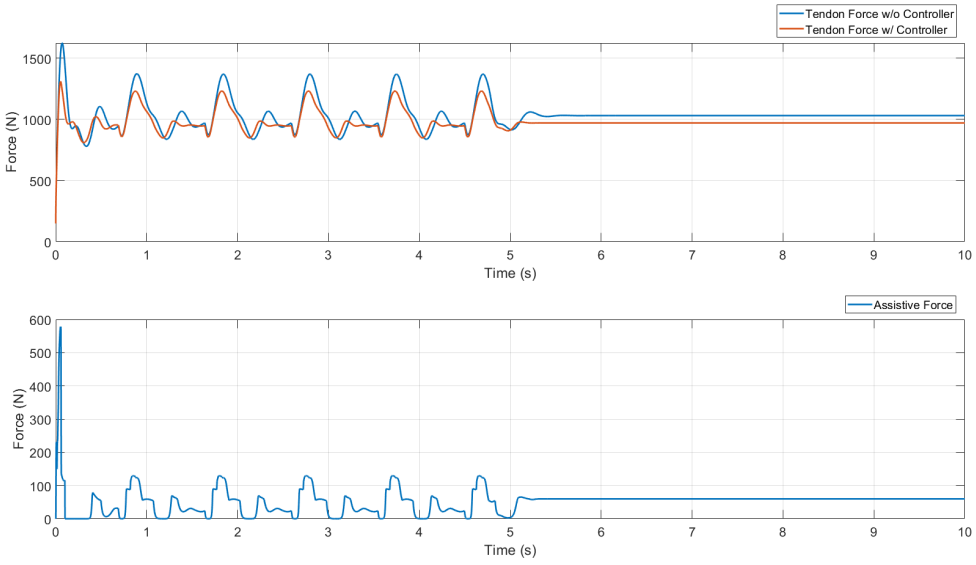

Figure B.32: NIFLC, Speed 5kmph, Elevation -20%, Upper limit on Tendon Force 1500N: (Top) Comparison between Tendon Force with and without assistance. (Bottom) Assistive Force

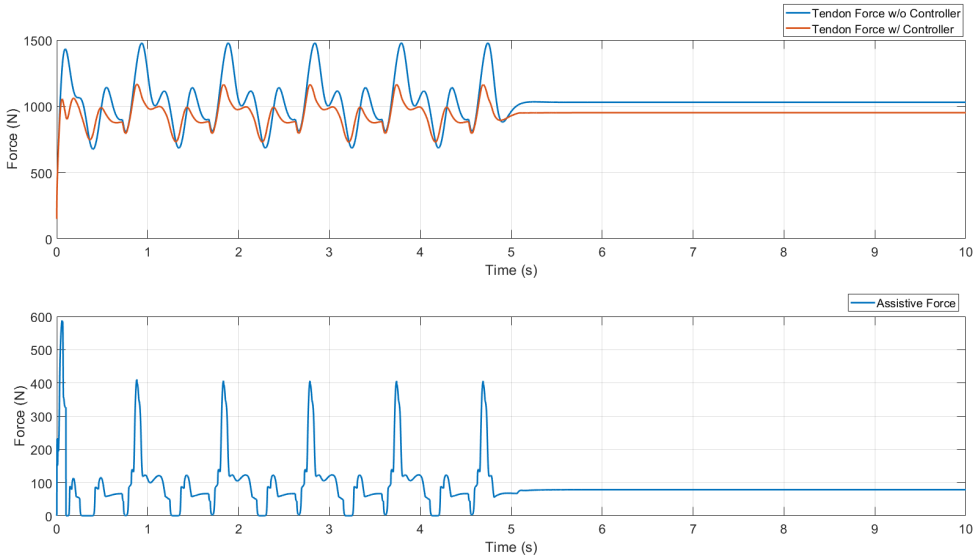

Figure B.33: NIFLC, Speed 5kmph, Elevation 0%, Upper limit on Tendon Force 1200N: (Top) Comparison between Tendon Force with and without assistance. (Bottom) Assistive Force

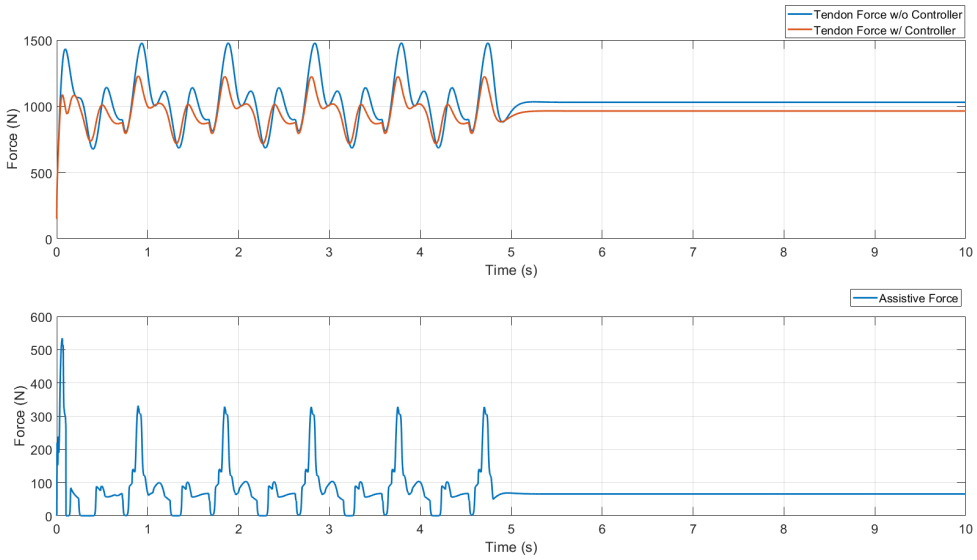

Figure B.34: NIFLC, Speed 5kmph, Elevation 0%, Upper limit on Tendon Force 1300N: (Top) Comparison between Tendon Force with and without assistance. (Bottom) Assistive Force

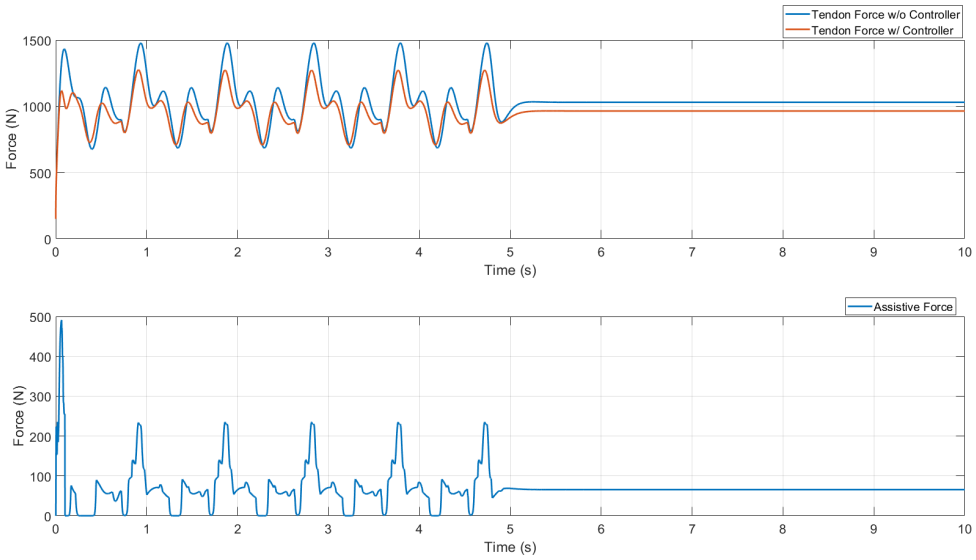

Figure B.35: NIFLC, Speed 5kmph, Elevation 0%, Upper limit on Tendon Force 1400N: (Top) Comparison between Tendon Force with and without assistance. (Bottom) Assistive Force

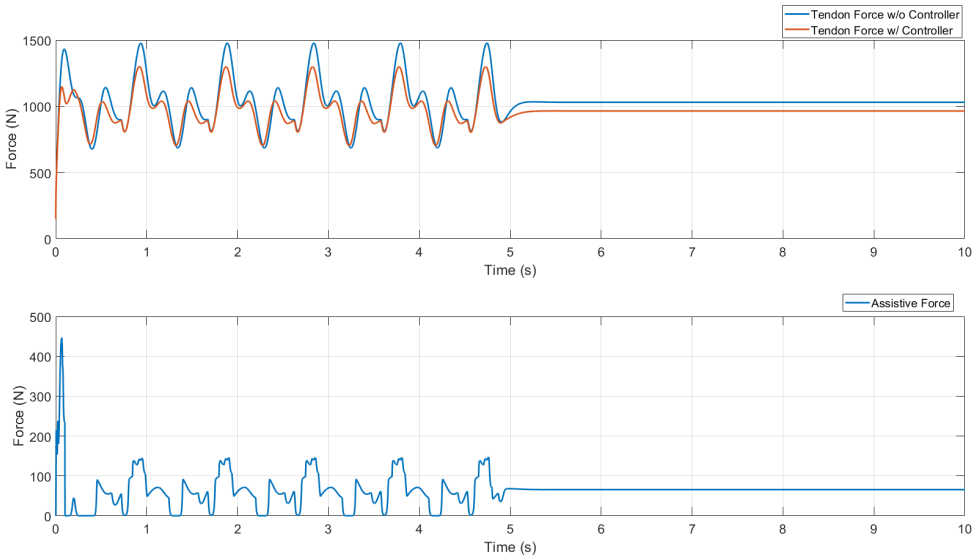

Figure B.36: NIFLC, Speed 5kmph, Elevation 0%, Upper limit on Tendon Force 1500N: (Top) Comparison between Tendon Force with and without assistance. (Bottom) Assistive Force

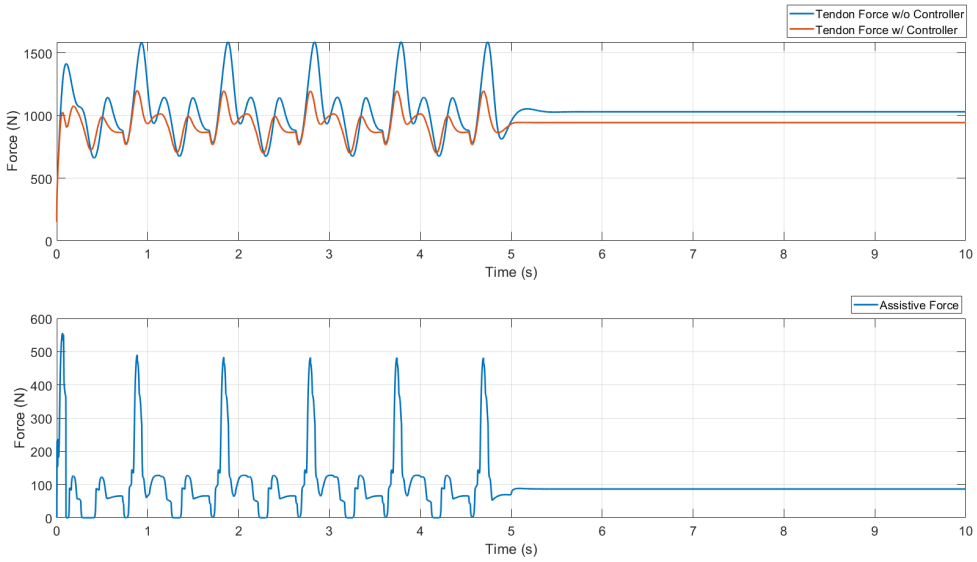

Figure B.37: NIFLC, Speed 5kmph, Elevation 20%, Upper limit on Tendon Force 1200N: (Top) Comparison between Tendon Force with and without assistance. (Bottom) Assistive Force

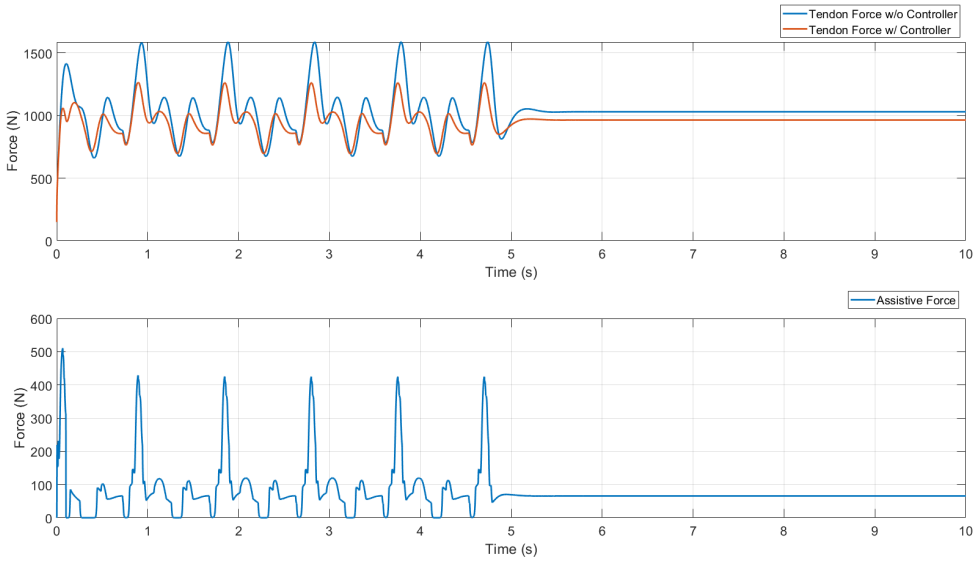

Figure B.38: NIFLC, Speed 5kmph, Elevation 20%, Upper limit on Tendon Force 1300N: (Top) Comparison between Tendon Force with and without assistance. (Bottom) Assistive Force

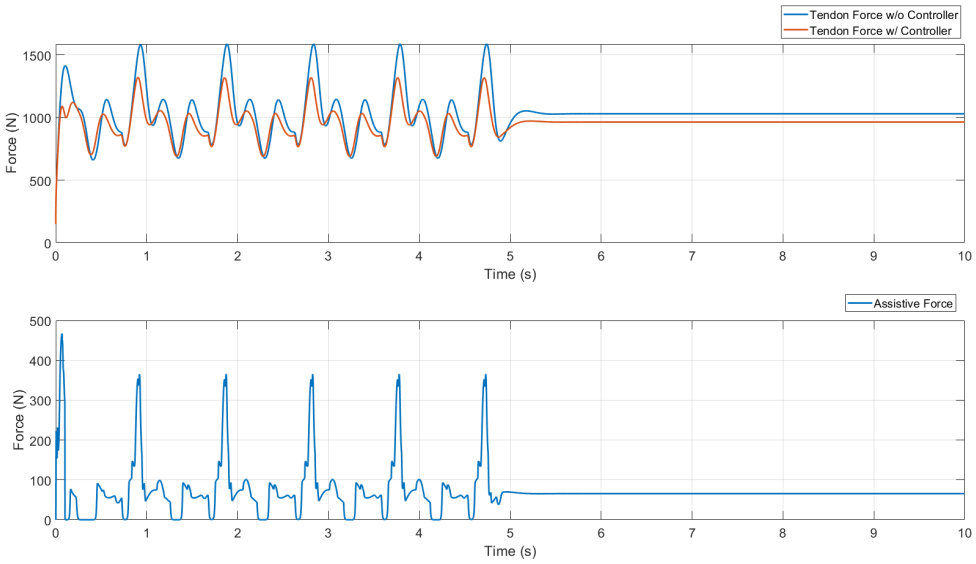

Figure B.39: NIFLC, Speed 5kmph, Elevation 20%, Upper limit on Tendon Force 1400N: (Top) Comparison between Tendon Force with and without assistance. (Bottom) Assistive Force

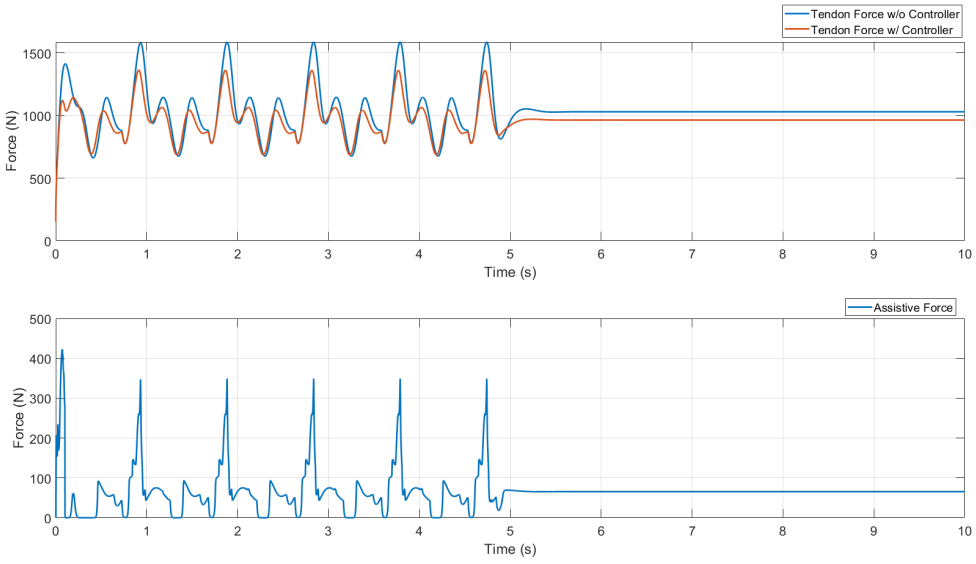

Figure B.40: NIFLC, Speed 5kmph, Elevation 20%, Upper limit on Tendon Force 1500N: (Top) Comparison between Tendon Force with and without assistance. (Bottom) Assistive Force